ARTIFICIAL NEURAL NETWORK BASED SCHEME FOR VOLTAGE AND HARMONIC COMPENSATION

BOLUO XIE

Your file Votre référence
ISBN: 978-0-494-33463-8
Our file Notre référence
ISBN: 978-0-494-33463-8

Artificial Neural Network Based Scheme for Voltage and Harmonic Compensation

By

© Boluo Xie, B. Eng (Hons.)

A thesis submitted to the School of Graduate

Studies in partial fulfilment of the

requirements for the degree of

Master of Engineering

Faculty of Engineering and Applied Science

Memorial University of Newfoundland

December 2006

St. John's Newfoundland Canada

Abstract

This thesis presents the analysis and design of the application of a novel hybrid active power filter (APF). The proposed APF scheme employs the recurrent artificial neural network (RANN) structure to determine each harmonic component in the distorted line voltage and the nonlinear line current. The compensation unit of the APF employs the multi-loop feedback control strategy to operate the PWM voltage source inverter to generate the replica of the harmonics and inject them into the system for compensation. The implementation of the proposed APF can maintain the utility supply current and the voltage at the point of common coupling (PCC) in a distribution network almost sinusoidal and minimize the total harmonic distortion (THD) levels in the network.

Applying the harmonics extraction method and inverter control scheme, three compensation topologies were investigated to examine the functionality of the system under different source-end disturbances and load-end conditions. The obtained simulation results showed that the compensation system is capable of mitigating the harmonic and distortion caused by the operation of two kinds of nonlinear loads.

In order to identify the contribution of design parameters and their interactions on the performance of the overall compensation system, the response surface method (RSM) was used to investigate the influence of the controlling parameters such as inverter controller gains and low-pass filter specification.

Acknowledgements

I would like to thank my supervisor Dr. J. E. Quaicoe for his invaluable guidance, constant understanding, financial support and help in preparing this manuscript. I would also like to extend my sincere thanks to Dr. H. Heys, Chair of Electrical and Computer Engineering for his valuable suggestions.

Appreciation is extended to Dr. R. Gosine, Dean of the Faculty of Engineering and Applied Science and Dr. R. Venkatesan, Associate Dean of the Faculty of Engineering and Applied Science for their support during the overall course of my study in Canada. I would like to extend my acknowledgement to Ms. M. Crocker, secretary to the Associate Dean for ensuring smooth and efficient operation of the associated administrative tasks of my graduate program. I am also thankful to Dr. B. Jeyasurya and Dr. T. Iqbal for their timely help during the course of the program. In anticipation of any oversight that remains, I wish to thank all those who contributed directly or indirectly to this work.

Finally, I would also like to express my profound gratitude to my parents and friends for their constant encouragement, understanding, guidance and support. I am also grateful to my fellow graduate students for their friendship during my study at Memorial University of Newfoundland.

Contents

List of Figures

List of Tables

List of Abbreviations

AC: Alternating Current

ANN: Artificial Neural Network

ANOVA: Analysis of Variance

APF: Active Power Filter

CAPF: Current Active Power Filter

CCD: Central Composite Design

CCS: Current Compensation Scheme

CRANN: Current Recurrent Artificial Neural Network

DC: Direct Current

DOE: Design of Experiments

DVR: Dynamic Voltage Restorer

EMI: Electromagnetic Interference

EPRI: Electric Power Research Institute

FFT: Fast Fourier Transform

FRFT: Fractional Fourier Transform

HPF: High Pass Filter

HVDC: High Voltage Direct Current

IAS: Industrial Applications Society

IEEE: Institute of Electrical and Electronics Engineers

IRP: Instantaneous Reactive Power

LPF: Low Pass Filter

MLP: Multilayer Perceptron

MSE: Mean Squared Error

PCC: Point of Common Coupling

PES: Power Engineering Society

PLL: Phase Locked Loop

PWM: Pulse Width Modulation

RANN: Recurrent Artificial Neural Network

RMS: Root Mean Square

RSM: Response Surface Methodology

SCR: Silicon Controlled Rectifier

STATCOM: Static Synchronous Compensator

SVC: Static VAR Compensator

TDD: Total Demand Distortion

THD: Total Harmonic Distortion

UPFC: Unified Power Flow Controller

UPQC: Unified Power Quality Conditioner

UPS: Uninterruptible Power Supply

VAPF: Voltage Active Power Filter

VCS: Voltage Compensation Scheme

VFD: Variable Frequency Drive

VRANN: Voltage Recurrent Artificial Neural Network

Chapter 1
Introduction and Literature Review

The growing use of power electronics devices in converters employed in applications such as adjustable speed drives, electric arc furnaces, electric welding machines, HVDC systems and widespread computer systems has led to huge concerns about power quality. The issues associated with power quality now become an indispensable consideration for electric utilities, electrical equipment companies and end users of electricity. Especially in today's digital economy, power quality and reliability are key competitive factors for our society's smooth operation. For example, according to a newly released study by the Electric Power Research Institute (EPRI), power quality disturbances and power outages cost the United States economy more than $119 billion annually.

In this chapter, the existing power quality scenario and issues are presented. Various active power filters classified by their topology and the existing harmonic extraction methods are reviewed.

1.1 Factors Related to Power Quality

Power quality is a term used to discuss events on electric power grids, which can damage or disrupt sensitive electronic devices. It refers to the degree to which the electric power received at some consumer terminal is distorted. Power quality is a comprehensive concept for many different types of power system disturbance. The voltage distortions and current harmonics are the main issues involved in the degradation of the power system. Certain sensitive loads such as highly automated production process and computer systems are particularly susceptible to the deterioration in the power quality of a distribution network. High power quality is generally desirable as it means the normal operation of the system and guarantees the functionality of the loads. On the other hand, low power quality may result in the poor performance or even the failure of some critical equipment such as microprocessor-based automation systems and power-electronics-based devices. The improvement of power quality would greatly increase the efficiency of the existing electric system, decrease the system downtime and operating cost, and postpone the avoidable large investment in new generation units, transmission units and distribution units.

1.1.1 Voltage and current harmonics

In general, harmonics are components of a periodic signal, which are integral multiples of the fundamental frequency. In North America's power system, the fundamental frequency

refers to the power line frequency of 60 Hz at which the supply system is designed to operate. Table 1.1 shows the harmonic order and how to determine the characteristic harmonics.

Table 1.1: Harmonic order and characteristic harmonics

Harmonic Order	Frequency (Hz)	Characteristic Harmonics
1st (Fundamental)	**60**	The characteristic harmonics are based on the number of rectifiers (pulse number) used in a circuit and can be determined by the following equation: $h = (n \times p) \pm 1$ Where: n = an integer (1, 2, 3, 4, 5...), p = number of pulses or rectifiers. For example, using a six pulse rectifier, the characteristic harmonics will be:
2nd	120	
3rd	**180**	
4th	240	
5th	**300**	
6th	360	
7th	**420**	
8th	480	
9th	**540**	
10th	600	
11th	**660**	
12th	720	$h = (1 \times 6) \pm 1 \Rightarrow 5^{th}$ and 7^{th} harmonics
13th	**780**	$h = (2 \times 6) \pm 1 \Rightarrow 11^{th}$ and 13^{th} harmonics
...	...	$h = (3 \times 6) \pm 1 \Rightarrow 17^{th}$ and 19^{th} harmonics
25th	**1500**	$h = (4 \times 6) \pm 1 \Rightarrow 23^{rd}$ and 25^{th} harmonics

According to the Fourier transform, any distorted signals could be decomposed into a sum of the fundamental component and all other harmonic components. In the single-phase power system, the dominant harmonics are the 3rd, 5th and 7th harmonics. In the balanced three-phase power system, the 120 degree phase shift between the three phases results in the cancellation of the 3rd and other triplens. Harmonics are the by-products of the modern solid-state electronic technology, which employs thyristors and other

semiconductor devices to feed the controlled AC power to electrical loads. These solid-state power switchers are widely applied in nonlinear loads such as isolated and networked computers, uninterruptible power supplies (UPSs), fluorescent lamps and variable frequency drives (VFDs), which draw the harmonic and reactive currents in abrupt short pulses from the main grid, rather than in a smooth sinusoidal manner. Figures 1.1(a) and 1.1(b) illustrate the distorted waveforms with and without triplen harmonics respectively. They are the typical distorted signals existing in the balanced and unbalanced three-phase power system.

In three-phase systems, these nonlinear loads cause imbalance and excessive neutral currents. The distorted current reflected through the distribution impedance causes the voltage drop, i.e. the harmonic voltage distortion. This relationship is proportional to the distribution system available fault current and to the industrial distribution system impedance design.

- High fault current (stiff system):

  Distribution system impedance and distortion is low.

  Harmonic current drawn is high.

- Low fault current (soft system):

  Distribution system impedance and distortion is high.

  Harmonic current drawn is low.

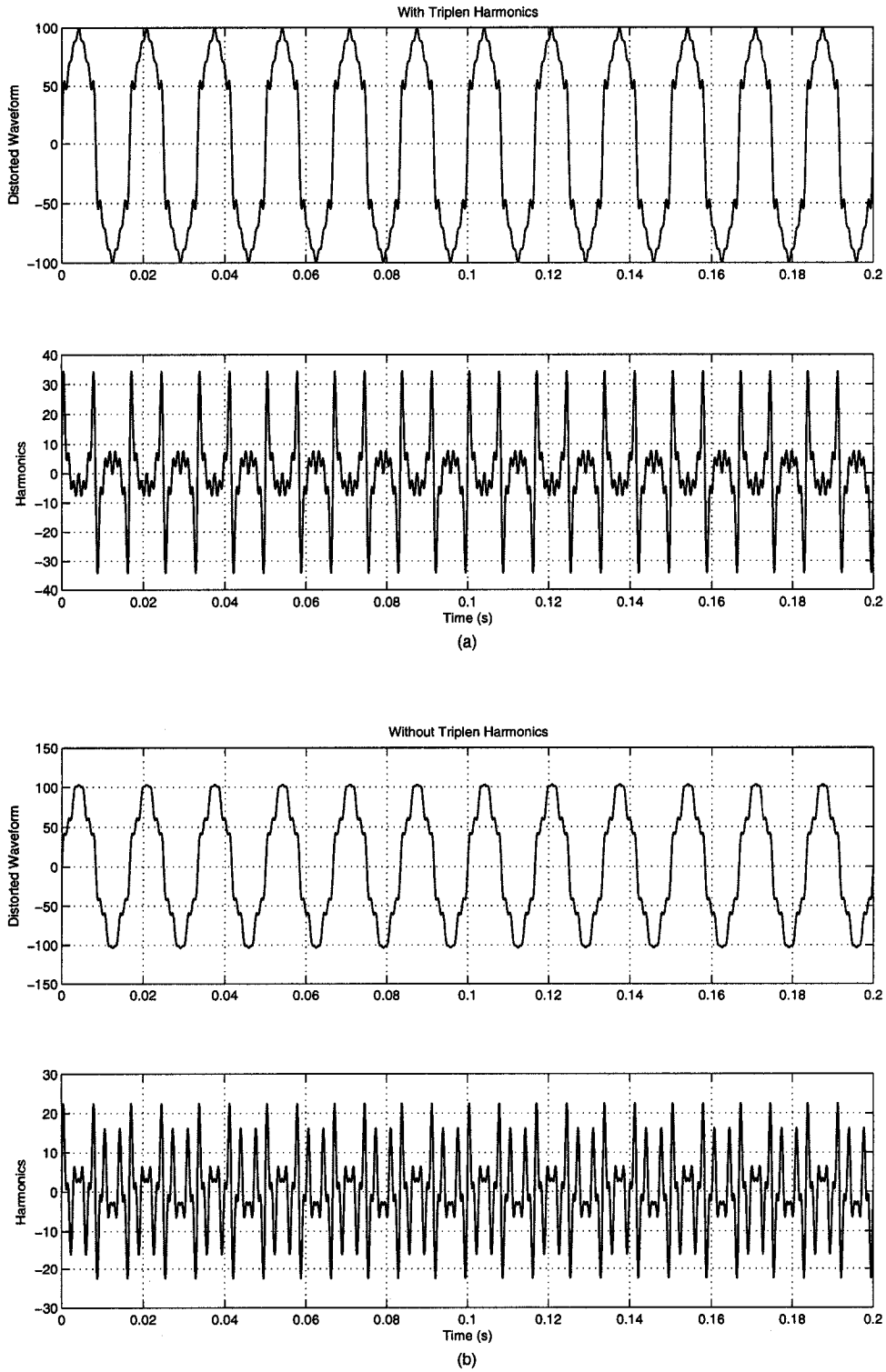

Figure 1.1: Distorted waveforms (a) with triplen harmonics; (b) without triplen harmonics

The excessive harmonics and reactive currents and imbalance in voltages and currents decrease the system efficiency and also reduce the power factor. High levels of harmonic distortion can lead to problems for the utility's distribution system, plant distribution system and any other equipment serviced by that distribution system. Effects can range from the spurious operation of equipment to the shutdown of important plant facilities, such as machines or assembly lines. Some of the negative ways that harmonics may affect plant equipments are listed below [1].

- Conductor Overheating: is a function of the square RMS current per unit volume of the conductor. Harmonic currents on undersized conductors or cables can cause the "skin effect", which increases with frequency and is similar to the centrifugal force.
- Capacitors: can be affected by the increased power loss which causes heat rise in the capacitors and hence reduces the life on the capacitors. If a capacitor is tuned to one of the characteristic harmonics such as the 5^{th} or 7^{th}, overvoltage and resonance can cause the dielectric failure or the rupture of the capacitor.
- Transformers: have increased iron and copper losses or eddy currents due to stray flux losses. This causes excessive overheating in the transformer windings.
- Generators: have similar problems to transformers. Sizing and coordination is critical to the operation of the voltage regulator and controls. Excessive harmonic

voltage distortion will cause multiple zero crossings of the current waveform. Multiple zero crossings affect the timing of the voltage regulator, causing interference and operation instability.

- Fuses and Circuit Breakers: harmonics can cause false or spurious operation and trips, and damage or blow components for no apparent reason.
- Drives and Power Supplies: can be affected by the misoperation due to multiple zero crossings. Harmonics can result in failure of the commutation circuits, which are found in DC drives and AC drives with silicon controlled rectifiers (SCRs).
- Utility Meters: may record measurements incorrectly, and may lead to higher billings to consumers.
- Computers and Telephones: may experience interference or failures.

IEEE 519-1981, "IEEE Guide for Harmonic Control and Reactive Compensation of Static Power Converters", originally established levels of voltage distortion acceptable to the distribution system for individual non-linear loads. With the greatly rising usage of industrial non-linear loads, such as variable frequency drives, it became necessary to revise the standard. The IEEE working groups of the Power Engineering Society (PES) and the Industrial Applications Society (IAS) prepared recommended guidelines for power quality that the utility must supply and the industrial user can inject back onto the power distribution system. The revised standard was issued on April 12, 1993 and titled

IEEE 519-1992, "IEEE Recommended Practices and Requirements for Harmonic Control in Electrical Power Systems" [1].

The revisions to IEEE 519-1992 establish recommended guidelines for harmonic voltages on the utility distribution system as well as harmonic currents within the industrial distribution system. According to the standard, the industrial system is responsible for controlling the harmonic currents created in the industrial workplace. Since harmonic currents reflected through distribution system impedances generate harmonic voltages on the utility distribution systems, the standard proposes guidelines based on industrial distribution system design. Table 1.2 defines the voltage distortion limits that can be reflected back onto the utility distribution system and Table 1.3 defines levels of harmonic currents that an industrial user can inject onto the utility distribution system [2]. Usually if the industrial user could control the overall combined current distortion according to Table 1.3, this would help them meet the limitations set forth in Table 1.2.

Table 1.2: Low-voltage system classification and voltage distortion limits

	Special Applications[1]	General System	Dedicated System[2]
Notch Depth	10%	20%	50%
THD (voltage)[3]	3%	5%	10%
Notch Area (A_N)[4]	16,400	22,800	36,500
NOTE: The value A_N for other than 480 V systems should be multiplied by V/480. 1 Special applications include hospitals and airports. 2 A dedicated system is exclusively dedicated to the converter load. 3 THD means total harmonic distortion. 4 In volt-microseconds at rated voltage and current			

Table 1.3: Current distortion limits for general distribution systems

120 V Through 69,000 V						
Maximum Harmonic Current Distortion in Percent of I_L						
Individual Harmonic Order (Odd Harmonics)						
I_{SC}/I_L	< 11	11 ≤ h < 17	17 ≤ h < 23	23 ≤ h < 35	35 ≤ h	TDD
< 20	4.0	2.0	1.5	0.6	0.3	5.0
20 < 50	7.0	3.5	2.5	1.0	0.5	8.0
50 < 100	10.0	4.5	4.0	1.5	0.7	12.0
100 < 1000	12.0	5.5	5.0	2.0	1.0	15.0
> 1000	15.0	7.0	6.0	2.5	1.4	20.0
Where: I_{SC} = Maximum Short Circuit Current at PCC (Point of Common Coupling) I_L = Maximum Demand Load Current (Fundamental Frequency Component) at PCC TDD = Total Demand Distortion						

1.1.2 Source-end disturbances

The causes of power quality deterioration also include the source-end disturbances such as voltage sags, voltage swells, voltage interruptions, voltage surges, voltage notches and voltage flicker.

As defined by IEEE Standard 1159-1995, "IEEE Recommended Practice for Monitoring Electric Power Quality" [3], a voltage sag or voltage swell is a decrease or increase respectively in the RMS voltage magnitude at the power line frequency. There are several different categories for voltage sag and voltage swell according to the time duration. The most frequently occurring disturbances in the distribution system are the short duration voltage variations, which could keep up from 0.5 cycles to 1.0 minute. The typical values of the reported remaining voltage are between 0.1 PU and 0.9 PU. Sags and swells lasting

more than 1.0 minute are classified as undervoltages and overvoltages respectively. Table 1.4 shows the detailed categories and typical characteristics of short duration variations [3]. Figure 1.2(a) illustrates some typical voltage sag and voltage swell, which are 30% and 20% respectively. Voltage sags are mainly caused by phenomena resulting in high currents, which in turn cause the voltage drops across the network impedances. The magnitude of the voltage drops decreases in proportion to the electrical distance of the observation point from the source of the disturbance in accordance with circuit laws. Such phenomena may include system faults, the switching of heavy loads and the starting of large motors. An induction motor will draw 2.5 times its full load current while starting with the soft-starter. Should the lagging current magnitude be large enough relative to the system available fault current, the resulting voltage sag may be significant.

Table 1.4: Categories and typical characteristics of electromagnetic phenomena

Categories	Typical Duration	Typical Voltage Magnitude
Short Duration Variations		
1 Instantaneous		
1.1 Sag	0.5 to 30 cycles	0.1 to 0.9 PU
1.2 Swell	0.5 to 30 cycles	1.1 to 1.8 PU
2 Momentary		
2.1 Interruption	0.5 cycles to 3 s	< 0.1 PU
2.2 Sag	30 cycles to 3 s	0.1 to 0.9 PU
2.3 Swell	30 cycles to 3 s	1.1 to 1.4 PU
3 Temporary		
3.1 Interruption	3 s to 1 min	< 0.1 PU
3.2 Sag	3 s to 1 min	0.1 to 0.9 PU
3.3 Swell	3 s to 1 min	1.1 to 1.2 PU

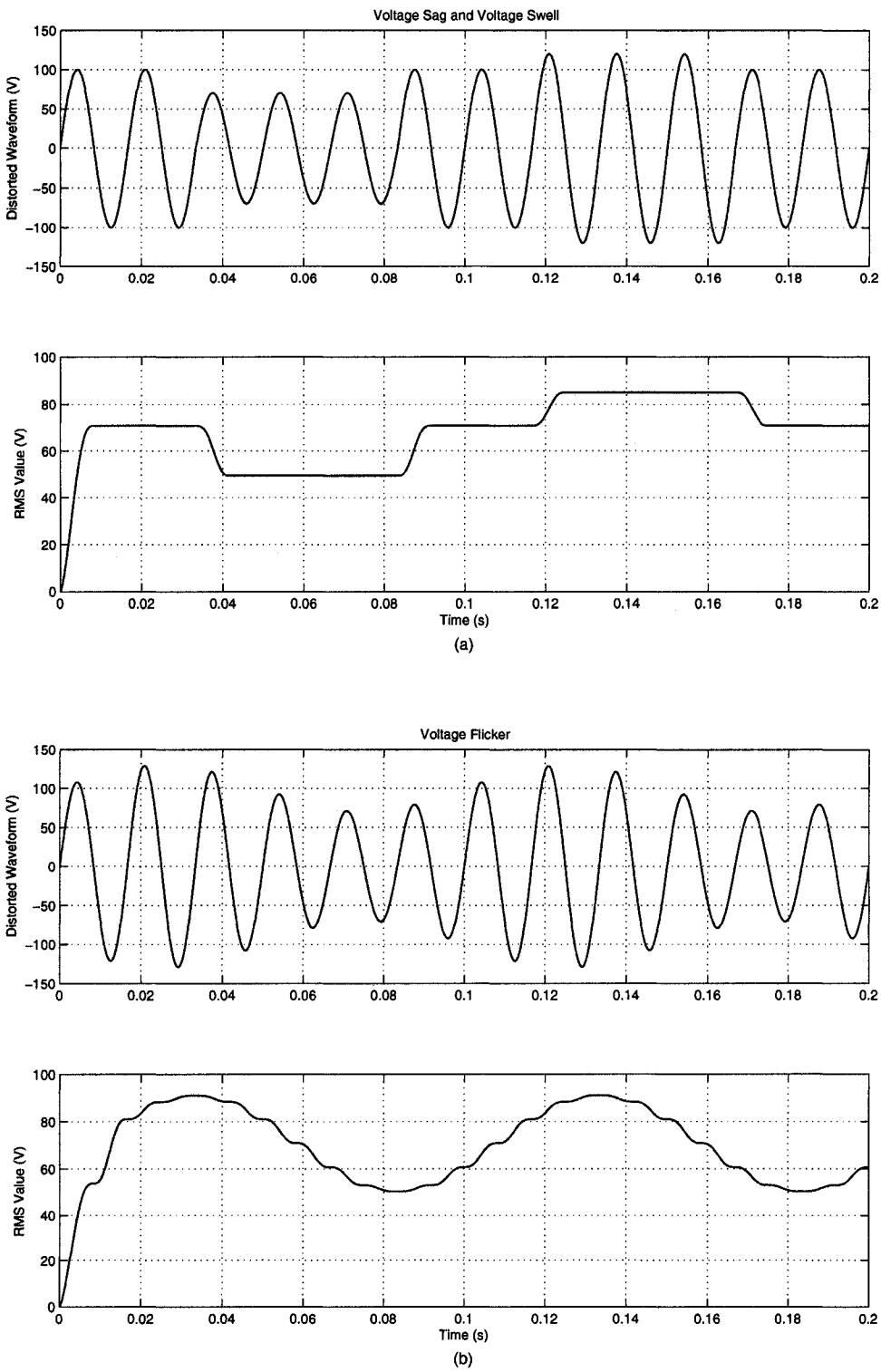

Figure 1.2: Distorted waveforms (a) Voltage sags and swells; (b) Voltage flicker

Voltage interruption is the complete loss of voltage to one or more customers. The industry defines the sustained interruptions as those lasting more than one minute. Voltage surges normally refer to transient overvoltages resulting from lightning and equipment switching, which usually last less than a few milliseconds. These surges can have a high enough voltage level to cause the insulation to break down leading to the failure of the equipment.

Voltage notches are periodic voltage disturbances caused by the normal operation of power electronic devices when the current is commutated from one rectifier leg to another. Voltage notches occur because the rectifier current goes from zero to peak in a few degrees rather than, as the sine wave does, in 90 degrees. This fast change is driven by a transient phase to phase short circuit at the rectifier and is called overlap. Because of the periodicity and continuity, voltage notch can be characterized and analyzed through the harmonic spectrum of the rectifier terminal voltage.

Another power quality problem is voltage flicker which is a repetitious variation in the luminance of a light source [4]. In general, voltage flicker is the amplitude modulation of the fundamental frequency voltage waveform by one or more frequencies, which are typically less than 30 Hz. These modulations, which could be quite small, can cause visible brightening and dimming of connected lights. The visibility of this fluctuation is a function of the repetition rate, the change in voltage and the type of the light source.

Voltage flicker is primarily a visual perception problem to human rather than a cause of equipment malfunction. Large, rapidly fluctuating loads such as arc furnaces and electric welding machines, especially during the period when the electric arc is being struck, are the main cause of the voltage flicker. Until recently, there were no generally accepted standards for voltage flicker measurements and the industry has almost universally employed the so-called "GE Flicker Curve" for the past 80 years. Figure 1.2(b) illustrates a typical voltage flicker, which has the 30% modulation depth in 10 Hz.

The influence of such disturbances at the terminal of the load depends on the distance to the origin of the disturbance, the level of interconnection and the impedance of the transmission line links. The terminal voltage of some critical loads is also affected by system faults such as single-phase to ground or three-phase to ground short circuit faults, and switching operations such as connection or disconnection of large loads, power factor correction equipments and static var compensators (SVCs). The increased severity of these interference on the power quality has prompted electrical engineers and researchers to develop feasible and flexible solutions to guarantee the normal operation of the power system.

Power quality is quantified technically on the basis of the following criteria [5].

- Waveform shape: should be constantly sinusoidal without any harmonics
- Waveform frequency: should be an unchanged nominal value such as 60 Hz

- Symmetry: three-phase voltages should be phase-shifted by 120 degrees
- Amplitude: three-phase voltages should have equal nominal RMS values which are unchanged all the time
- Stability: source-end voltages should be unaffected by load changes
- Reliability: electric energy should be available in required amounts at all time

The following section discusses some of the solutions that have been developed to achieve the above criteria.

1.2 Literature Review

In order to obtain clean power and reduce the unwanted loss, it is necessary to compensate for the current harmonics and voltage distortions in the system. Traditionally, passive filters including series and shunt filters are used to alleviate the harmonic problem. These tuned passive compensators consisting of LC filters and/or high-pass filters have been utilized to improve the power factor and absorb the harmonics in the power system for many years. Their inherent shortcomings render them unsuitable, especially since the emergence of the active power filter (APF) around 30 years ago. Due to the recent advancement in power semiconductor device technology , APFs have been widely used to compensate for current harmonics, reactive power and neutral current in the power industry [6] [7] [8]. APFs are also employed to mitigate voltage distortions, to regulate load-end voltage and to eliminate voltage imbalance in three-phase AC systems.

These objectives are achieved either individually or in cooperation with other compensation devices, depending on the task requirements, control strategies and system configurations [8].

1.2.1 Active power filter (APF)

There are some different approaches to utilize APF to solve power quality problem, including pure APF solution or hybrid filter solution. According to their topologies, APFs can be classified as series APFs, shunt APFs and series-shunt APFs. On the other hand, the effectiveness of each topology depends on the type of harmonic source [9].

1 Series APFs

The series APF is connected in series with the load between the main grid and the load using a coupling transformer. It is used to eliminate voltage harmonics, to compensate for voltage sags and swells in dynamic voltage restoration and to regulate the line voltages [10]. It can also be installed by electric utilities to damp out the harmonic propagation caused by resonance with line impedance and shunt passive filters [8]. The core part of the series APF is the voltage source inverter which is used to generate the compensating voltage injected into the system. The basic schematic of a stand-alone series APF is shown in Figure 1.3. The simplified model of the series APF is shown in Figure 1.4, where the series APF is modeled as a controllable voltage source which can inject any demanded voltage into the line to control the bus voltage profile and stem the harmonic

current flow.

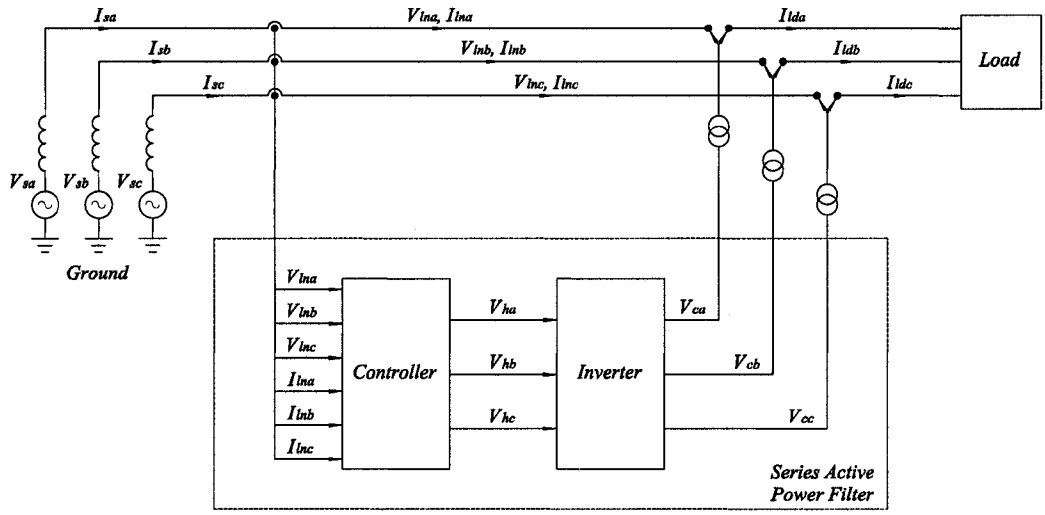

Figure 1.3: Basic system schematic of the series APF

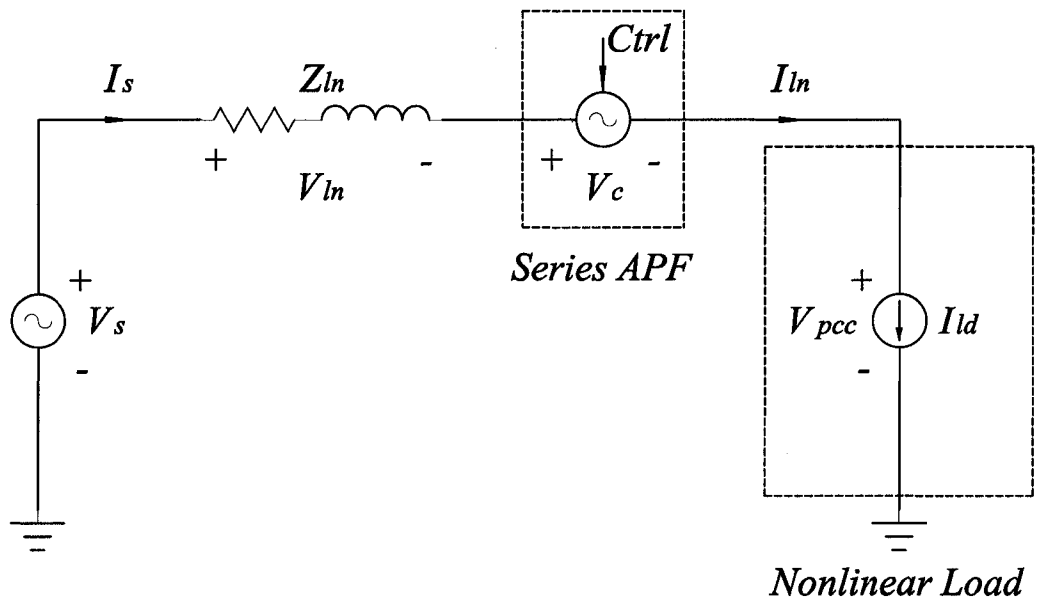

Figure 1.4: Simplified single-phase equivalent circuit model of the series APF

The series APF does not directly compensate for current harmonics, but it could be controlled to act as a high value impedance to the current harmonics drawn by the nonlinear loads [11]. When the primary function of the series APF is to regulate the load voltage, it is often referred to as the dynamic voltage restorer (DVR) [10]. Since the series APF is partially rated with respect to the load, it would be a better choice for voltage compensation and regulation due to its relatively lower cost. Some drawbacks of the series APF are listed below.

- Unable to directly compensate for current harmonics
- Unable to suppress neutral currents and to balance the load currents

2 Shunt APFs

The shunt APF is connected in shunt with the load using a coupling transformer, while the position of the injection point is varied between the source-end and the load-end in different application situations. It is primarily used to eliminate current harmonics, to provide reactive power compensation and to balance the unbalanced load currents. As the dual of the series APF, the shunt APF also utilizes the switch mode inverter to generate the replica of the reference signals, which are sensed and estimated from the line current by the harmonic extraction unit. If the injection point is at the load-end, the performance of the shunt APF would be independent of the utility system impedance. Since the shunt APF essentially acts as a controllable current source, it is not susceptible to the resonance

at dominant harmonic frequencies. The typical schematic of a stand-alone shunt APF is shown in Figure 1.5. The simplified single-phase equivalent circuit model of the shunt APF is shown in Figure 1.6, where the shunt APF is represented by a controllable current source which can inject any demanded current into the grid to compensate for current harmonics and improve the power factor.

The shunt APF can also be implemented as a SVC in the power system by utilities for stabilizing and improving the voltage profile. The shunt APF scheme is specially suitable for the compensation of voltage fluctuations, which are caused by high reactive current loads such as electric arc furnaces and large motors at the startup stage. In such application case, the shunt APF is often referred to as the static synchronous compensator (STATCOM) [12].

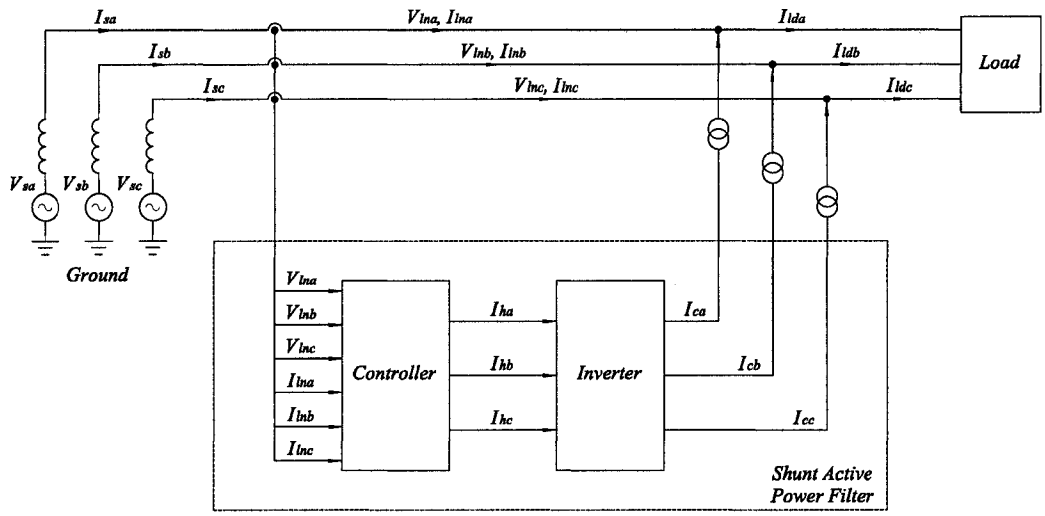

Figure 1.5: Basic system schematic of the shunt APF

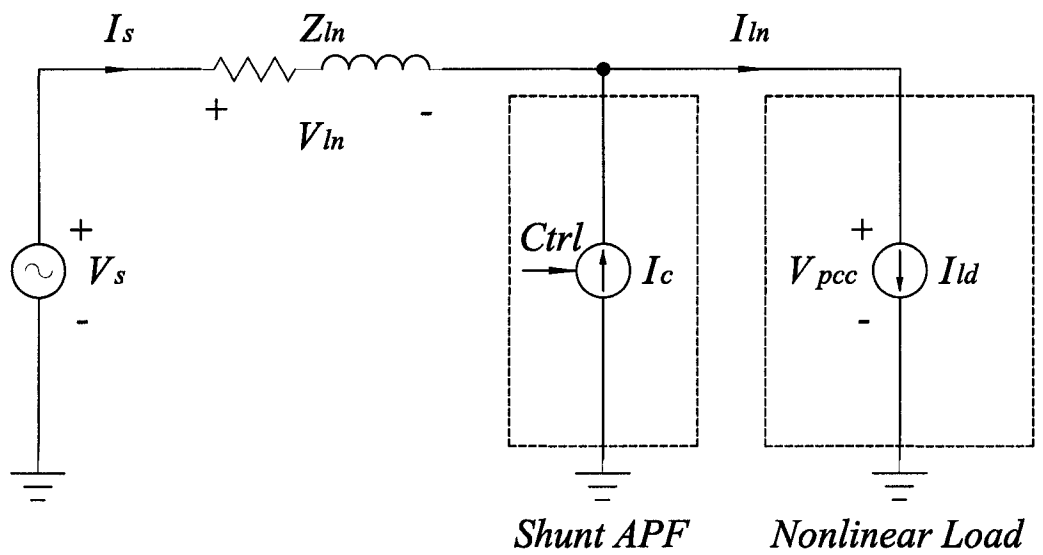

Figure 1.6: Simplified single-phase equivalent circuit model of the shunt APF

There are some drawbacks of the shunt APF as follows:

- High VA rating: the VA rating of the switch mode inverter could be quite high due to the fact that the shunt APF is connected in parallel with the load, which results in the converter having to withstand the line frequency utility voltage and supply the harmonic current. The negative influences coming with the high VA rating are higher cost, higher electromagnetic interference (EMI), higher power losses and lower efficiency.
- Susceptibility: the low-pass LC filter, which is allocated at the inverter's output end to eliminate most of the high frequency switching harmonics, is highly susceptible to utility line interactions and may require additional passive or active damping.
- The shunt APF could not compensate for the voltage harmonics and is less effective for voltage regulation in some systems with high short circuit current at the point of common coupling (PCC).

3 Series-shunt APFs

The series-shunt APF is a combination of the series APF and the shunt APF, which is also referred to as the unified power quality conditioner (UPQC) [13] or universal power line conditioner [14] [15] if both APFs are coupled via a common DC link storage element which could be DC bus capacitor or inductor. If the UPQC is used primarily for

fundamental power compensation such as power flow control, the device is also called the unified power flow controller (UPFC) [16] which allows bi-directional flow of real power between the series output terminals of the series APF and the shunt output terminals of the shunt APF. The more general structure of the series-shunt APF is to employ two independent DC links for the series APF and the shunt APF respectively. Figure 1.7 illustrates the basic schematic of the series-shunt APF and the single-phase equivalent circuit model of the series-shunt APF is shown in Figure 1.8.

The series-shunt APF is able to provide fast and simultaneous control of the system terminal voltage and active or reactive power flow. This compensation system is considered as an ideal active filtering system which is capable of eliminating voltage and current harmonics completely and providing qualified electric power to some critical and vulnerable loads such as hospital equipments and computer systems. The series APF acts as a controllable voltage source to provide the voltage compensation, while the shunt APF acts as a controllable current source to provide the current compensation. The relative position of both APFs in the whole system is determined by the designated control objective.

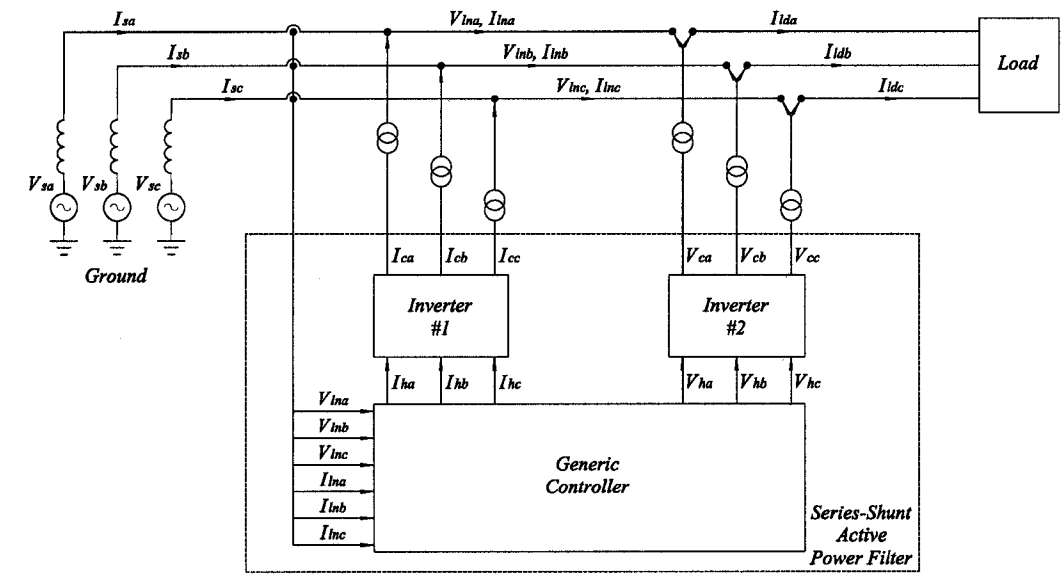

Figure 1.7: Basic system schematic of the series-shunt APF

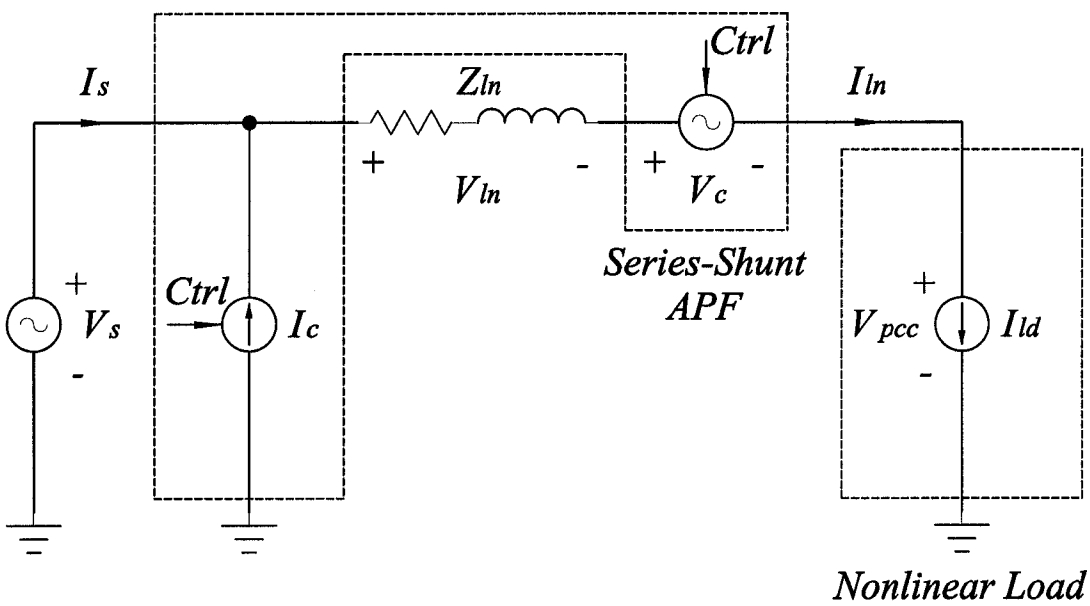

Figure 1.8: Simplified single-phase equivalent circuit model of the series-shunt APF

The series-shunt APFs has the cumulative functions and advantages of both APFs as follows.

- Compensate for voltage harmonics including the negative and zero sequence components at the fundamental line frequency
- Provide harmonics isolation to suppress the current harmonics from propagating through the line
- Control the active and reactive power flow by controlling the magnitude and phase angle of the injected voltage with respect to the line current
- Compensate for current harmonics including the negative and zero sequence components at the fundamental line frequency
- Fulfill the reactive power demand of the loads

The main drawback of the series-shunt APF is its high cost and control complexity resulting from the involved large number of solid state devices.

1.2.2 Harmonic extraction methods

The harmonic extraction is a critical issue to the APF, since it sets up the standard and reference to be followed by the power inverter. The inaccuracy and inefficiency of the harmonic extraction method would inevitably deteriorate the overall compensation performance. Several harmonic extraction methods have been presented in the literature, which are designed to perform the reconstruction of the current harmonics and voltage

distortions. A review of some of them is provided as following.

1 Classical Fourier transform based extraction method

This extraction method applies the classic Fourier transform theory to the analysis of the voltage and current. It is the most intuitional and basic method that can virtually solve any decomposition and recomposition problems from the mathematical point of view. In this method, the distorted voltage or current signal is firstly separated into the fundamental and harmonic components. The harmonic components are then treated as the reference signal for the switch mode inverter to generate the compensating voltage or current [17] [18]. There are some variants that apply the modified Fourier transform algorithms such as Fast Fourier transform (FFT) and Fractional Fourier transform (FRFT) [19]. The block diagram of this method is shown in Figure 1.9.

However the mathematically soluble method is not always equal to the practically feasible method. The harmonic estimation method that requires long time to solve the equations is meaningless to online power filtering, since the practical sensed signal is instantaneously varied and the tolerable time delay is quite small.

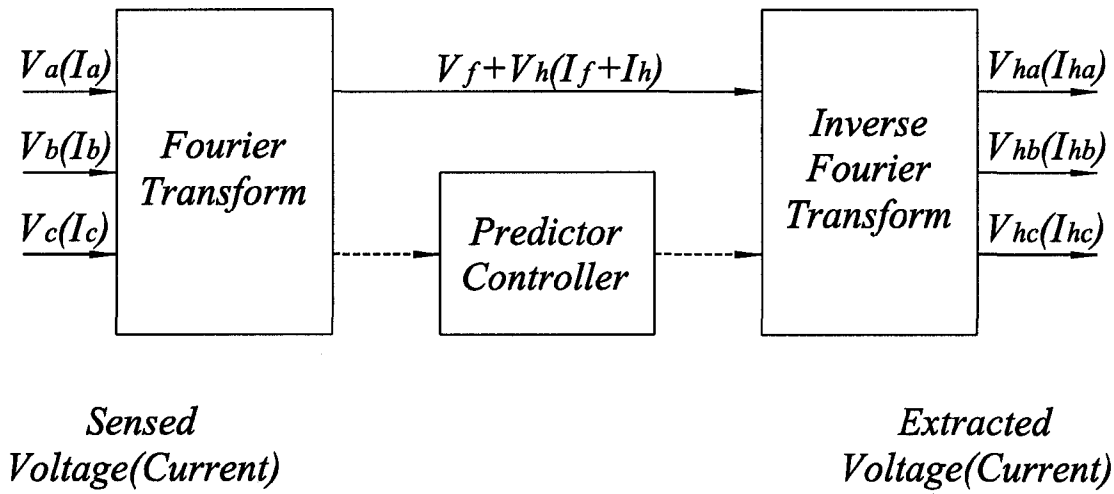

Figure 1.9: Classical Fourier transform based extraction method

The following inherent drawbacks make it unrealistic for the online power compensation.

- Laborious and complex computation results in the real-time application being cumbersome and generating unacceptable time delay.
- For loads with deterministic harmonic spectrum, the predictive control unit is necessary to be included in the APF control scheme. For those unpredictable loads, the main part of the system, this method is quite difficult to implement.

2 Synchronous reference frame based extraction method

The Park transformation plays a key role in this extraction method. Firstly, the voltage or current signal is switched into the rotating synchronous reference frame using the Park

transformation, where the fundamental component become DC component and all other harmonic components are translated downwards along the frequency axis [20]. The DC component in the synchronous reference frame is then removed from the signal by passing through a high-pass filter whose cut-off frequency is close to 1 Hz. The filtered signal is then switched back to the stationary three-phase reference frame using the inverse Park transformation. The phase of the variable vectors is locked in with source voltage V_{sa} using a phase locked loop (PLL) unit. The block diagram of this method is shown in Figure 1.10.

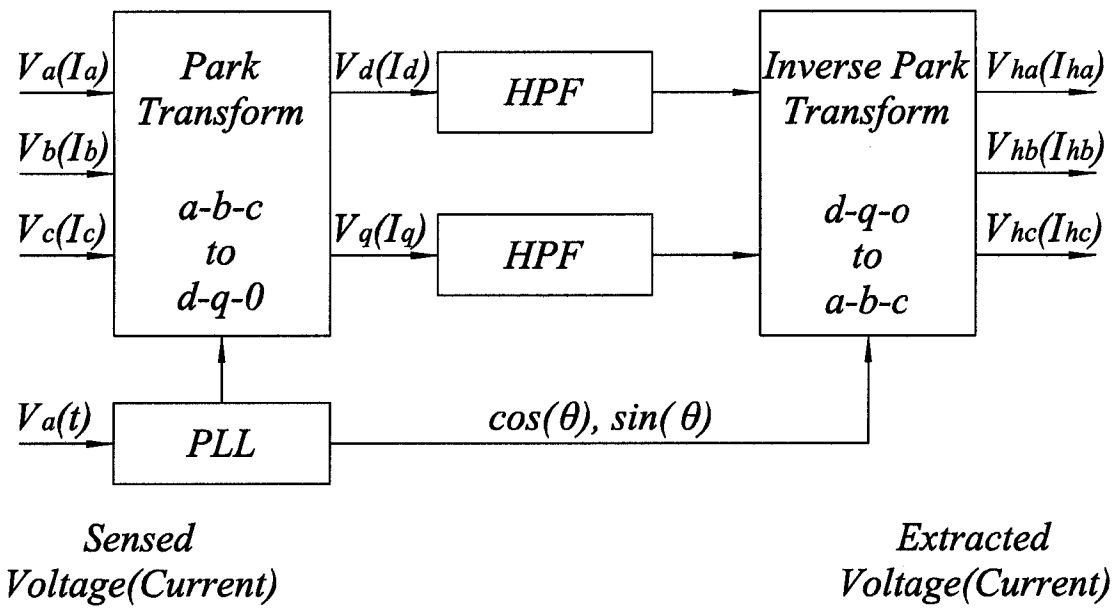

Figure 1.10: Synchronous reference frame based extraction method

Compared with the Fourier transform based method, this method has faster computation

speed and better implementing performance. However, its application is restricted in scope for the following reasons:

- It inherently requires that the processed signals are three-phase signals, which makes this method unsuitable to be used in the single-phase systems.
- The effectiveness of the extraction scheme is severely reduced in the presence of voltage imbalance, making it difficult to achieve the independent voltage compensation and voltage balancing.

3 Instantaneous reactive power (IRP) theory based extraction method

Proposed by Akagi et al. in 1984 [7], the IRP theory is based on the instantaneous voltages and currents in three-phase systems, with or without the neutral wire. The harmonic components can be estimated by determining the contributions of the harmonic components to p and q, where p and q are the instantaneous active and reactive power flow in the line respectively. For this reason, the IRP theory is also known as the p-q theory. Firstly, the voltage and current signals are transformed into the alpha-beta orthogonal coordinates using the transformation matrices respectively, which are then used to calculate the instantaneous active and reactive power. The DC components of p and q represent the conventional active and reactive power respectively. The contribution of the harmonics to p and q is determined by filtering out the DC component through a

high-pass filter. The filtered p and q are then transformed back to the three-phase reference harmonic currents using the inverse transformation matrices. The block diagram of this method is shown in Figure 1.11.

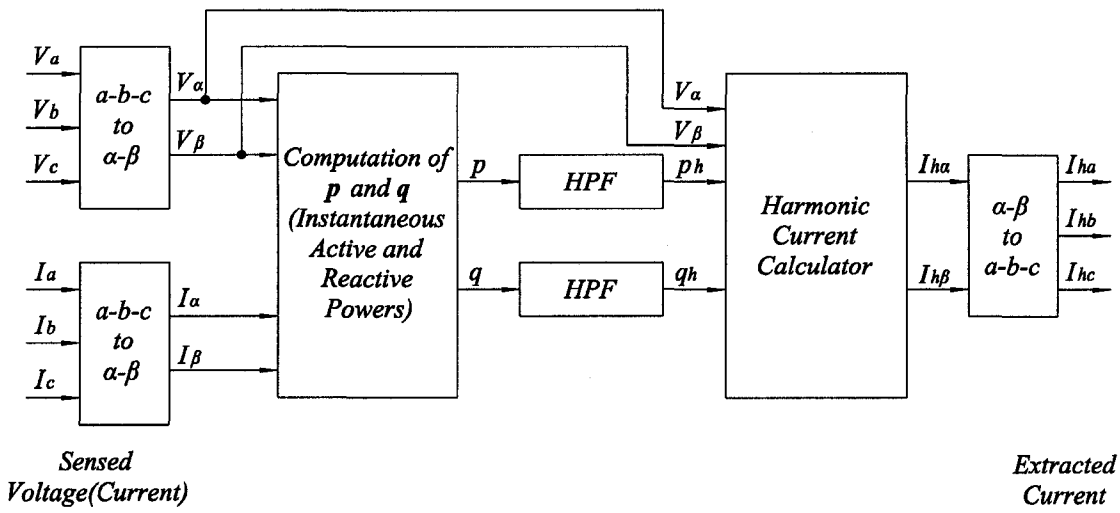

Figure 1.11: Instantaneous reactive power (IRP) theory based extraction method

The drawbacks of this approach are summarized as follows:

- The algorithm determines that the IRP method needs extra sensing of the line voltages in the current compensation, which means more cost, more computation and more complicated structure. It is also incapable of processing the single-phase signals.
- In the presence of voltage imbalance and zero sequence components, the unit

reference vectors derived from the alpha-beta coordinates may no longer be sinusoidal and orthogonal. This redundancy impedes the extraction of all the harmonics [21].

1.3 Objectives of the Thesis

The above mentioned harmonic extraction methods, i.e. synchronous reference frame based method and IRP theory based method, are incapable of effectively estimating harmonic components in the presence of imbalance and zero sequence components. Although the modified synchronous reference frame based method [21] could immunize the harmonic extraction technique to imbalance and zero sequence components, its more intensive computation complexity than the other two schemes becomes main problem. In terms of the number of floating point/integer multiplications, additions and divisions, the modified method overwhelmed the other two methods by a factor of 156% to 300%. This provides the motivation to implement a novel harmonic extraction strategy which could overcome this drawback without compromising the accuracy of harmonic detection.

The APF topologies including series APF, shunt APF and series-shunt APF are therefore chosen for detailed study in this thesis. The goal of the research is to develop a compensation approach that could effectively compensate for voltage distortions, current harmonics and source-end disturbances such as voltage sags, voltage swells and voltage flicker.

To this end the following investigations are undertaken in this research.

- Development of a reliable and high efficiency harmonic extraction scheme that provides an accurate measure of the harmonics in the presence of source-end disturbances
- Investigation of the decoupled voltage and current compensation processes that adopt the modified control strategy
- Investigation of the compensation system that incorporates voltage compensation and harmonic isolation together in both single-phase and three-phase systems in the case of voltage imbalance and more complicated non-linear loads
- Investigation of the influence of the controlling parameters such as inverter controller gains and low-pass filter specification on the performance of the overall system using the response surface methodology (RSM).

1.4 Organization of the Thesis

Chapter 1 presents the existing power quality scenario and introduces current issues and problems in the power industry. The current harmonics, voltage distortions and source-end disturbances such as voltage sags, voltage swells and voltage flicker are defined in detail, as well as their causes and effects. Various active power filters classified by their topology are presented and their advantages and disadvantages are highlighted. The existing harmonic extraction methods described in the literature are reviewed and their

strong points and weak points are identified. The objectives and the organization of the thesis are described in this chapter.

Chapter 2 introduces the recurrent artificial neural network (RANN) used in the harmonic extraction unit. Some applications of ANN in harmonic extraction are reviewed and the structure of proposed RANN is modeled and analyzed in detail. The multi-loop feedback control scheme is expanded from its original model to accommodate both voltage and current compensation. Its advantages for active power filtering are discussed. The models of the voltage compensation scheme (VCS) and the current compensation scheme (CCS) are described and analyzed. The performances of both the VCS and CCS with non-sinusoidal reference in normal and abnormal condition are demonstrated, while their limitations are also discussed.

Chapter 3 investigates the performance of whole compensation system, combining both the VCS and CCS, in single-phase and three-phase circumstances. The detailed description, modeling and analysis are carried out to determine the compensation characteristics of the systems. The preprocessing unit is introduced to mitigate the voltage imbalance and source-end disturbance. Simulation results with more complicated non-linear loads are presented to validate their functionalities.

Chapter 4 utilizes the response surface methodology (RSM) to determine the influence of the controlling parameters on the performance of the overall system. The optimized

design parameters and advantages of RSM are presented graphically.

Chapter 5 summarizes the thesis, highlighting the contribution of the research work and providing suggestions for carrying out future work along the lines of the approach proposed in the thesis.

Chapter 2
Active Power Filter Control Scheme

Control schemes play a very important role in the implementation of active power filtering. They are used to identify the harmonic contents, generate the desirable compensating components and maintain the system at the desirable voltage and current quality levels. The quality and performance of the active power filter (APF) depend on three considerations.

- The method used to extract the harmonic contents
- The design of the inverter
- The modulation and control method used to implement the compensation scheme.

The regeneration of the harmonic current and the distorted voltage is dependent on the following conditions:

- The effectiveness of the algorithm for extracting the harmonic current and the distorted voltage which are to be used as the reference signals for the power inverter

- The performance of the power inverter in regenerating the replica of the sensed harmonic current and distorted voltage which could comprise highly non-sinusoidal signals in different magnitudes, phases and frequencies.

Being an self-adaptive control strategy, the artificial neural network (ANN) is gaining more popularity in power electronics field for couple of years. Some developed applications employed the traditional training process to determine the current or voltage harmonic components [22] [23] [24] [25], while other applications used the modified ANN method to estimate the harmonic coefficients without the cumbersome learning process [26] [27]. There are myriad techniques for the control of the APF inverter. The multi-loop feedback control, originally used in the single-phase uninterruptible power supply (UPS) application [28], demonstrated its outstanding capability in the active filtering application [29].

The active power filter can be used in series or shunt configuration that leads to the series active power filter or shunt active power filter. In this chapter, the voltage compensation scheme (VCS) for the series active power filter and the current compensation scheme (CCS) for the shunt active power filter are investigated, separately.

2.1 Principle of the Recurrent Artificial Neural Network (RANN)

The artificial neural network (ANN) has been applied to many different engineering

fields, and has gained widespread use in the implementation of different control algorithms. The application of ANN in power electronics has grown in popularity for several years.

2.1.1 Review of ANN in harmonic extraction

When browsing the vast amount of literature on ANNs there does not seem to be one definition of ANN with which everyone agrees, but most types of ANNs can be covered by the following definition [30]:

> "A system of simple processing elements, neurons, that are connected into a network by a set of (synaptic) weights."

The function of the network is determined by the architecture of the network, the magnitude of the weights and the mode of operation of the processing elements.

The neuron or node, as it is also called, is the most elementary processing unit in the ANN that takes a number of inputs, applies weights to them, adds them up, and then sends the result as the argument to a singular valued function, the activation function. Figure 2.1 shows the typical structure of a neuron.

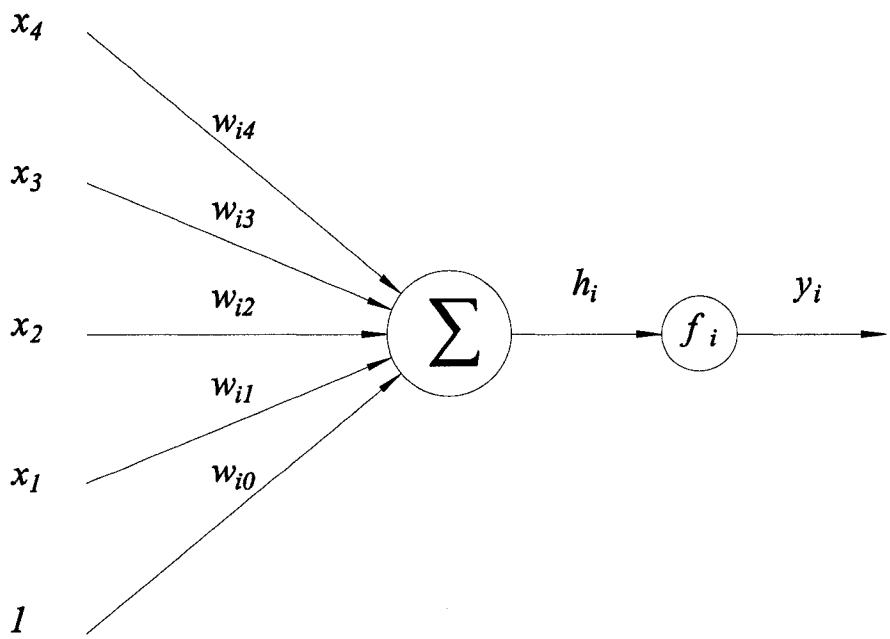

Figure 2.1: The structure of the neuron

The mathematical form of a neuron is [30]

$$y_i = f_i(h_i) = f_i\left(\sum_{j=1}^{n_x} w_{ij}x_j + w_{i0}\right). \tag{2.1}$$

The displacement w_{i0} is called the bias and can be interpreted as a weight applied to a pseudo input whose value is maintained at a constant value of 1.

Neurons can be united together into a network which could have many different structures. The most commonly used architecture is the multilayer perceptron (MLP) network which orders the neurons in layers and makes each neuron in one layer take as input only the outputs of neurons in the previous layer or the external inputs. Figure 2.2 illustrates a typical MLP network structure.

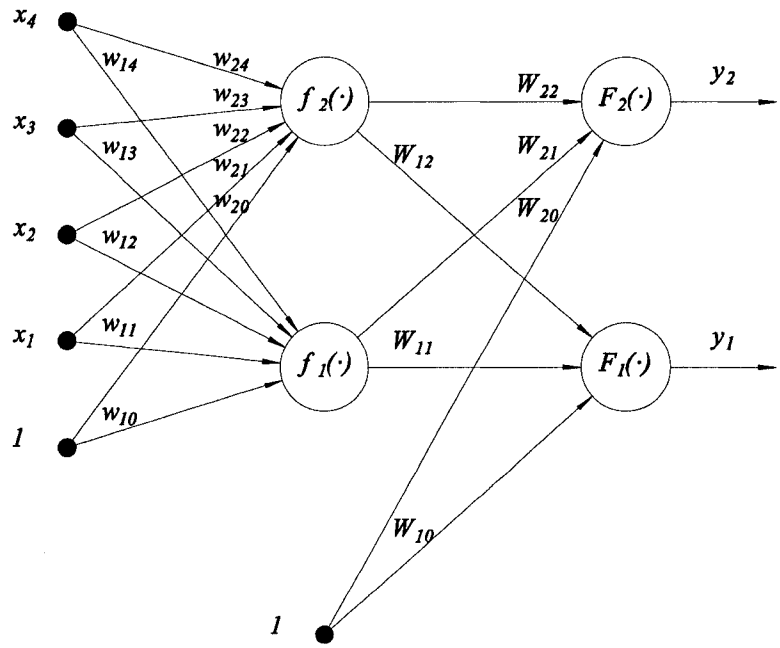

Figure 2.2: The structure of the MLP neural network

The MLP network has the following mathematical expression [30]

$$\hat{y}_i(t) = g_i[x,\theta] = F_i\left[\sum_{j=1}^{n_f} W_{ij} f_j\left(\sum_{l=1}^{n_x} w_{jl} x_l + w_{j0}\right) + W_{i0}\right]. \qquad (2.2)$$

The determination of the values of the weights from a set of given examples which show how the outputs are related to the inputs is called training or learning. The following issues need to be considered carefully before employing the conventional training process.

- The kind of relationships between the outputs and inputs that can be described accurately by a MLP network using the training process
- The number of hidden layers in the MLP network and the number of neurons in

each layer

- The activation function that should be used

The MLP network has been applied in harmonic component extraction strategies. Most of the methods are based on the cumbersome and time consuming training process using different patterns and algorithms. Round and Mohan [25] have proposed ANN active filter controllers which are able to learn to improve the compensation of utility current or voltage harmonic distortion. In a comparison between two types of controllers, frequency and time domain neural network controllers, based on steady state and transient performance, it was found that the computational delay of the former is very high due to the bulky ANN structure, and the latter is difficult to implement in practice. A compromise between transient performance and practical implementation is the use of a frequency domain ANN controller in parallel with a traditional active filter controller [25]. A self-adaptive noise countervailing method based on the MLP network has been shown to detect the fundamental and harmonic reactive currents of nonlinear loads [22]. This method requires the training of the neuron based upon the least mean square (LMS) algorithm and the magnitude of the training step is chosen such that neither the ANN become unstable nor the speed of the ANN declines too much. An ANN harmonic extraction scheme proposed by Gao and Sun [23] is based on the extraction of the fundamental component of the distorted load current in a single-phase shunt active power

filter. In this case, the fundamental component is calculated from the load current with the assistance of the ANN where the weights of the ANN are determined by the learning process. Tazune et al. [24] implement an interconnected inverter which suppresses the harmonic current components with an ANN controller. The harmonic voltage in the AC line is cancelled by generating the identical harmonic voltage portion in the inverter output. The ANN controller in this scheme employs a three-layer feedforward structure to train the neurons.

All of the above harmonic extraction strategies using ANN method are based on the cumbersome learning process from which the weights of each neuron are determined by training the ANN with suitable input and output patterns.

2.1.2 Introduction to RANN

The use of the feedforward MLP structure in harmonic extraction techniques requires an approach that relies on the training process to determine the appropriate number of hidden layers and the number of neurons in each hidden layer after the activation functions have been determined. The procedure can be reversed by constructing the desired objective functions first. From the objective functions, the structure of the ANN, the activation functions, the number of the hidden layers and the number of neurons in each hidden layer can be determined. In the harmonic extraction scheme, the objective functions are the harmonic components of the distorted currents and voltages. This

backward construction procedure avoids the cumbersome and time consuming learning process which is mandatory for the determination of the ANN's structure in the normal forward construction procedure.

The ANN in this backward procedure is used in an iterative computational mode. However, in order to exploit the iterative computational feature of the ANN, feedback loops are added to the outputs and inputs, or between hidden layers. This type of network is referred to as a recurrent artificial neural network (RANN) [30]. As shown in Figure 2.3, this network contains algebraic loops between hidden layers. The RANN is a dynamic system that has time-delayed memory of the previous status.

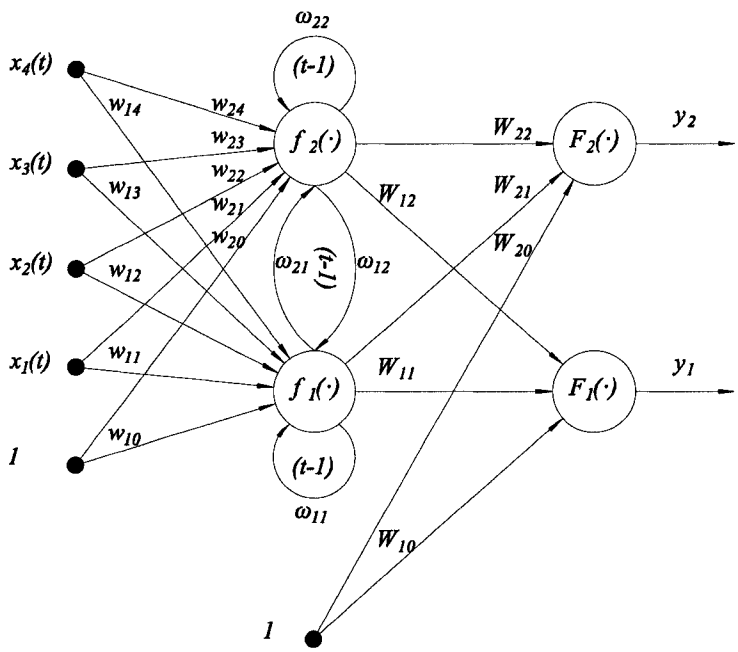

Figure 2.3: The structure of the RANN

In the harmonic extraction scheme, the RANN can be used to obtain the instantaneous harmonic component coefficients, from which the magnitude and phase angle of the fundamental and each of the harmonic currents and voltages can be determined. Consequently, the resultant of harmonic components can be separated from the load current and line voltage.

Compared to the basic feedforward MLP network, the RANN provides the inherent capacity of eliminating the steady state error by adding the integral feedback path between outputs and inputs. As long as the sampling frequency is high enough, the returned previous instant outputs can be used to predict the current instant inputs. In the harmonic extraction scheme, the internal feedback feature of the RANN avoids the necessity of installation of any extra sensors in the main grid used to monitor the error between the sensed harmonic current and regenerated harmonic current. It guarantees the accuracy of the reference signal of the power inverter, which is fundamental for the overall performance of the active power filter.

2.1.3 Development of a RANN-based harmonic estimator

The RANN-based signal processing technique is applied to the estimation of harmonic components in a typical nonlinear load in real-time. For the purpose of the following discussion, a three-phase diode bridge rectifier with an inductive load is assumed.

A balanced three-phase six-pulse diode bridge rectifier generates 5^{th}, 7^{th}, 11^{th}, 13^{th} ....

harmonics in the load current while the unbalanced case has 3^{rd}, 9^{th}, 15^{th} and additional harmonic components. In general, the load current can be expressed as

$$i(t) = \sum_{n=1,3,5,7...}^{N} I_n \cos(n\omega t - \phi_n) \tag{2.3}$$

where, I_n is the magnitude and φ_n is the phase angle of the n^{th} harmonic component (n = 1, 3, 5, 7...) and ω is the fundamental electrical angular frequency. Equation (2.3) can be rewritten as follows:

$$i(t) = \sum_{n=1,3,5,7...}^{N} \left(A_n \cos n\omega t + B_n \sin n\omega t\right) \tag{2.4}$$

where $A_n = I_n \cos\phi_n$ and $B_n = I_n \sin\phi_n$. The magnitude and phase angle can be determined as

$$I_n = \sqrt{A_n^2 + B_n^2} \tag{2.5}$$

$$\phi_n = \arctan\left(B_n / A_n\right) \tag{2.6}$$

If the fundamental and harmonic components are separated, (2.4) can be written as

$$i(t) = A_1 \cos\omega t + B_1 \sin\omega t + \sum_{m=1}^{M} \left(A_{(4m\pm1)} \cos(4m \pm 1)\omega t + B_{(4m\pm1)} \sin(4m \pm 1)\omega t\right) \tag{2.7}$$

where m = 1, 2, 3, ... M.

The RANN estimation algorithm samples the load current uniformly and uses the sampled signal to determine the magnitude and phase angle of the fundamental and each harmonic component by minimizing the objective function of the RANN. The objective

function of the RANN is the error between the calculated output of the RANN $i(t_k)$ and the sensed load current samples $s(t_k)$ at time t_k. This approach guarantees that the harmonic regeneration can be accomplished within one time period of the operating fundamental component.

The instantaneous mean squared error (MSE) at the k^{th} sample is evaluated by the objective function as follows [31]

$$\xi_k = \frac{1}{2}\left(i(t_k) - s(t_k)\right)^2 \tag{2.8}$$

After substituting (2.7) into (2.8),

$$\xi_k = \frac{1}{2}\left(A_1 \cos\omega t_k + B_1 \sin\omega t_k + \sum_{m=1}^{M}\left(A_{(4m\pm1)} \cos(4m \pm 1)\omega t_k + B_{(4m\pm1)} \sin(4m \pm 1)\omega t_k\right) - s(t_k)\right)^2 \tag{2.9}$$

The variables in (2.9) can be rewritten in vector forms as follows:

$$X_k = \left[\cos\omega t_k \quad \sin\omega t_k \quad \cos 3\omega t_k \quad \sin 3\omega t_k \quad \ldots \quad \cos N\omega t_k \quad \sin N\omega t_k\right]^T \tag{2.10}$$

$$Y_k = \left[A_1 \quad B_1 \quad A_3 \quad B_3 \quad \ldots \quad A_N \quad B_N\right]^T \tag{2.11}$$

where X_k is the known input variables and Y_k is the unknown output variables.

Equation (2.8) can then be expressed in vector notation form as [32]

$$\xi_k = \frac{1}{2}\left(s^2(t_k) - 2s(t_k)X_k^T Y_k + Y_k^T X_k X_k^T Y_k\right) \tag{2.12}$$

The optimum value of the object function is obtained by solving the differential equation [33] [34]

$$\frac{dY_k}{dt} = -K_1 \Delta\xi_k \tag{2.13}$$

Where K_1 is the integration constant and

$$\Delta\xi_k = \left[\frac{\delta\xi_k}{\delta A_1} \quad \frac{\delta\xi_k}{\delta B_1} \quad \frac{\delta\xi_k}{\delta A_3} \quad \frac{\delta\xi_k}{\delta B_3} \quad \cdots \quad \frac{\delta\xi_k}{\delta A_N} \quad \frac{\delta\xi_k}{\delta B_N}\right]^T \tag{2.14}$$

From (2.9), the partial derivatives in (2.14) are obtained as

$$\frac{\delta\xi_k}{\delta A_n} = \left(A_1 \cos\omega t_k + B_1 \sin\omega t_k + \sum_{m=1}^{M} \begin{pmatrix} A_{(4m\pm1)} \cos(4m\pm1)\omega t_k \\ + B_{(4m\pm1)} \sin(4m\pm1)\omega t_k \end{pmatrix} - s(t_k) \right) \cos n\omega t_k \tag{2.15}$$

$$\frac{\delta\xi_k}{\delta B_n} = \left(A_1 \cos\omega t_k + B_1 \sin\omega t_k + \sum_{m=1}^{M} \begin{pmatrix} A_{(4m\pm1)} \cos(4m\pm1)\omega t_k \\ + B_{(4m\pm1)} \sin(4m\pm1)\omega t_k \end{pmatrix} - s(t_k) \right) \sin n\omega t_k \tag{2.16}$$

From (2.11), (2.13), (2.15) and (2.16), the harmonic coefficients are obtained as

$$A_n = -K \int \left(A_1 \cos\omega t_k + B_1 \sin\omega t_k + \sum_{m=1}^{M} \begin{pmatrix} A_{(4m\pm1)} \cos(4m\pm1)\omega t_k \\ + B_{(4m\pm1)} \sin(4m\pm1)\omega t_k \end{pmatrix} - s(t_k) \right) \cos n\omega t_k dt \tag{2.17}$$

$$B_n = -K \int \left(A_1 \cos\omega t_k + B_1 \sin\omega t_k + \sum_{m=1}^{M} \begin{pmatrix} A_{(4m\pm1)} \cos(4m\pm1)\omega t_k \\ + B_{(4m\pm1)} \sin(4m\pm1)\omega t_k \end{pmatrix} - s(t_k) \right) \sin n\omega t_k dt \tag{2.18}$$

The proposed RANN is a feedback neural network that utilizes the previous output X_{k-1} at time t_{k-1} to calculate the current output X_k at time t_k. The structure of the proposed RANN method is shown in Figure 2.4. The determination of the harmonic coefficients A_n and B_n will reproduce the magnitude and phase angle of the fundamental and each current harmonic component at the sampling frequency using (2.5) and (2.6).

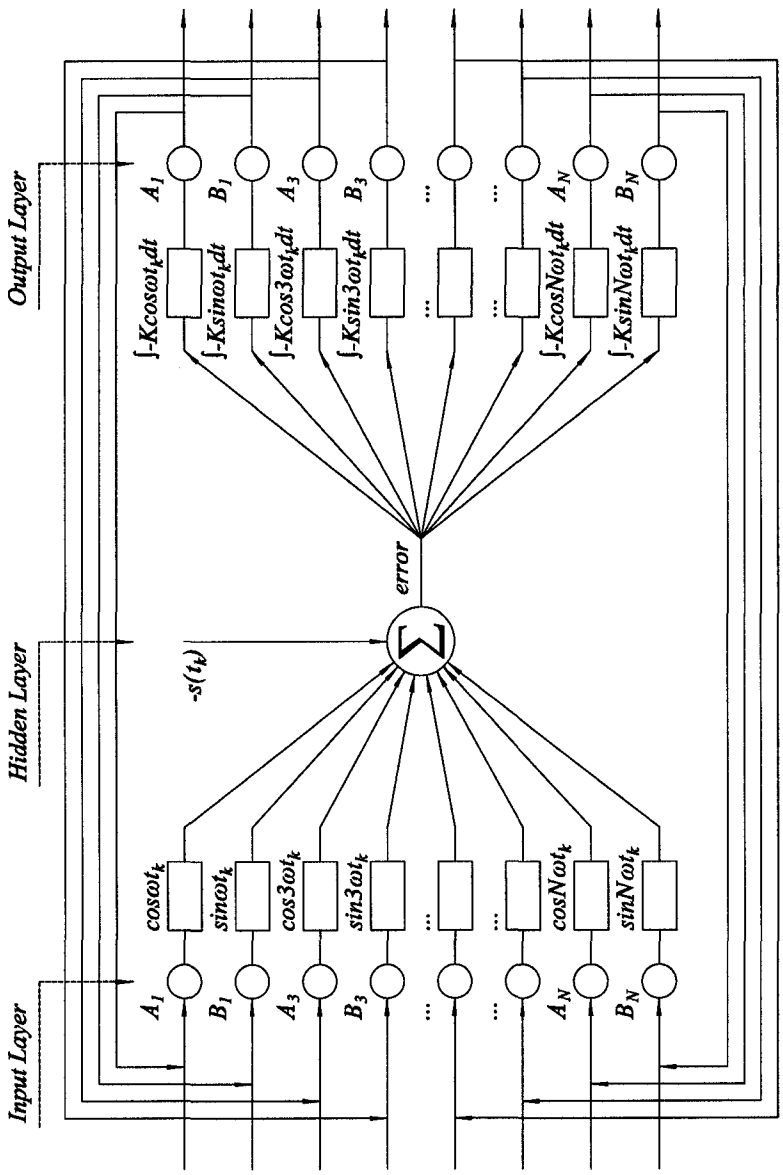

Figure 2.4: The structure of the proposed RANN harmonic extraction method

Although the current quantities are used as the variables in the derivation of (2.3) to (2.18), the expressions of the harmonic coefficients are applicable to the voltage quantities as well. In order to verify the capability of the proposed RANN harmonic extraction method, one known distorted voltage signal is introduced as the input signal of the RANN and is compared with the output signal of the RANN, which is designed to follow the reference signal and identify the harmonic components. The specifications of the distorted voltage and the used RANN are listed in Table 2.1. The simulation results are presented in Figure 2.5(a) and Figure 2.5(b).

Table 2.1: Specification of the distorted voltage and the RANN

Distorted Voltage				RANN	
	Magnitude	Frequency	Phase	Highest Order	25
Fundamental	100 V	60 Hz	0		
5^{th} Harmonic	100/3 V	300 Hz	0	With Triplen	Yes
7^{th} Harmonic	100/6 V	420 Hz	0		
11^{th} Harmonic	100/6 V	660 Hz	0	Sampling Frequency	76,800 Hz
13^{th} Harmonic	100/12 V	780 Hz	0		

From the shown figures, the proposed RANN harmonic extraction method is capable of extracting desired harmonic components from the input voltage or current signal, efficiently and accurately. This RANN method has very fast dynamic response which reaches the steady state in around half cycle of the sensed signal. The steady state error is close to zero due to the recurrent feedback structure which guarantees the accuracy of the system.

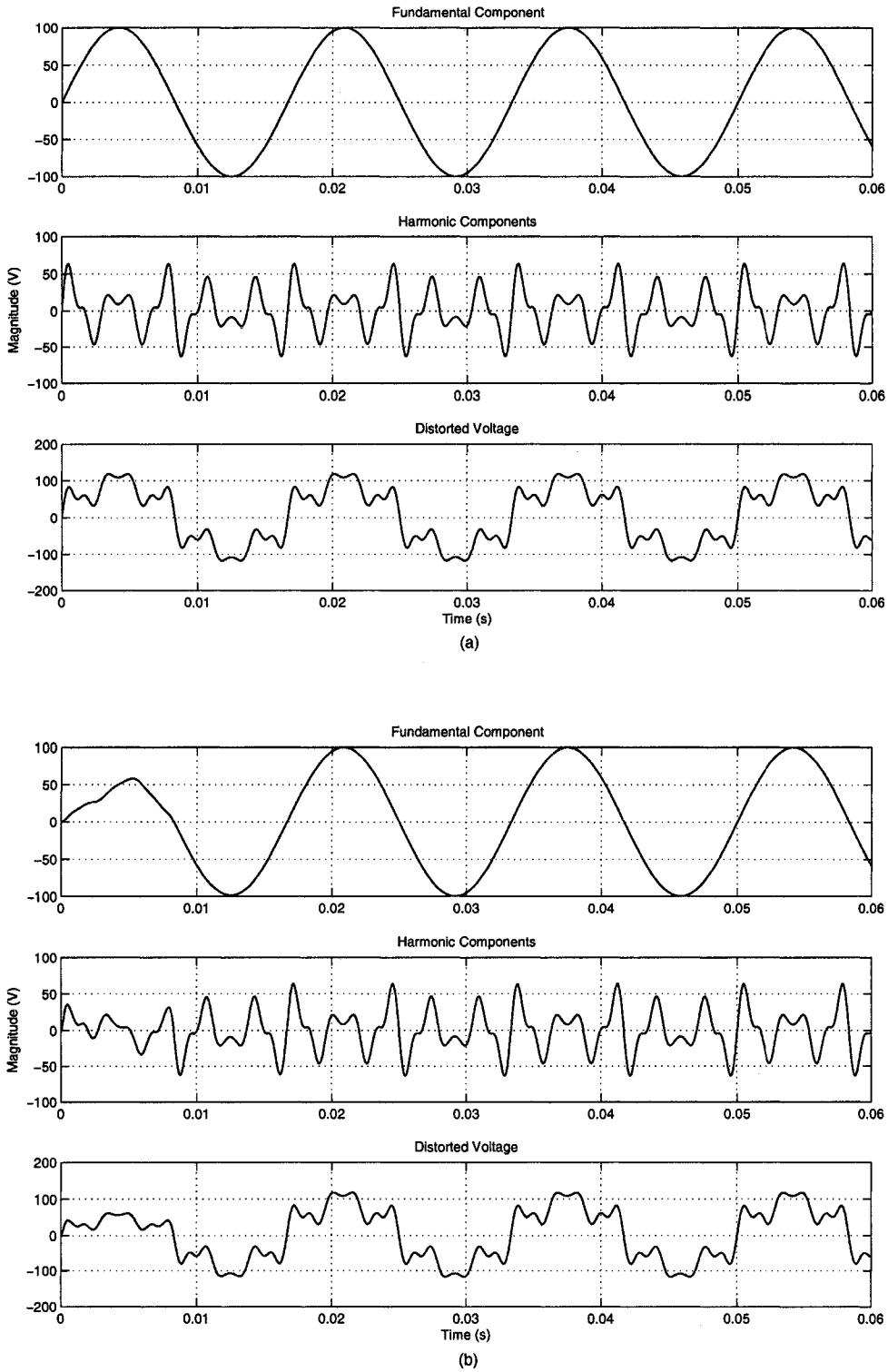

Figure 2.5: Performance of the RANN (a) Input signal; (b) Output signal

This RANN method can calculate any harmonic component which is used to construct the RANN regardless of its appearance in the original input signal. However the total harmonics is much more important than any single harmonic in voltage and current compensations. In this comparison, the total harmonics is achieved by adding all single harmonic component together to demonstrate the performance of the RANN method. In practical implementation, the total harmonics can be obtained by subtracting the fundamental component from the sensed input signal.

2.2 Multi-Loop Feedback Control in Active Power Filter Schemes

The multi-loop feedback control method is used to implement the compensation scheme in this active power filter (APF) design. Figure 2.6 shows the scheme proposed by Abdel-Rahim and Quaicoe [28] for regenerating a replica of a reference signal. It consists of a single-phase voltage-source half-bridge inverter, a second-order low-pass filter $R_f L_f C_f$, an inner current feedback loop and an outer voltage feedback loop. Proportional controllers are used in the feedforward paths of both inner and outer loops to increase the loop bandwidth.

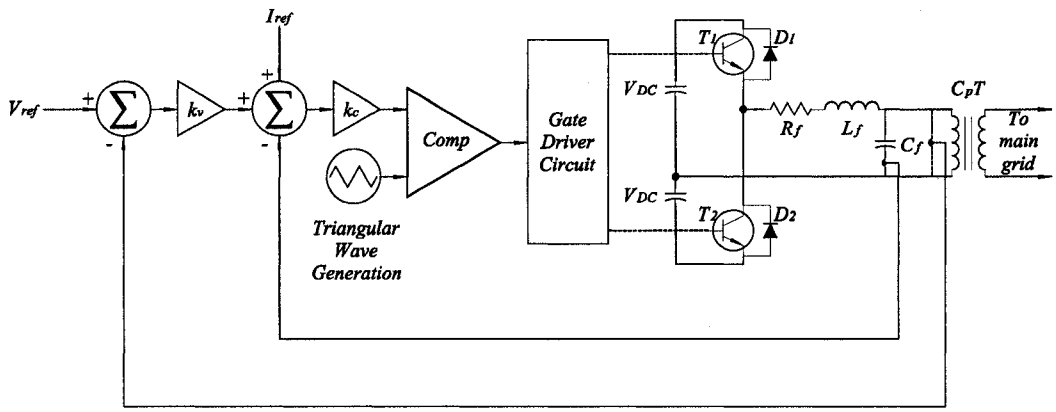

Figure 2.6: The structure of multi-loop feedback control based on capacitor

2.2.1 Multi-loop feedback control based on capacitor current: voltage compensation

In the case of voltage compensation in the APF design, the voltage reference V_{ref} is the voltage distortion i.e. the deviation of the actual voltage from the desired value. The APF operates to regenerate the voltage distortion and then to inject the generated voltage in opposite phase into the main grid so as to cancel the distortion in the actual voltage. The generated voltage signal is fed back and compared with its reference. The resulting error signal is passed through a proportional controller k_v and the output of the controller is then summed with the error signal obtained from comparing the capacitor current with its

reference. The resulting signal is passed through another proportional controller k_c in the inner control loop and the output of the controller is compared with a fixed switching frequency triangular waveform in a standard sinusoidal pulse width modulation (PWM). The pulse width modulated signals are then used to control the inverter switches after they have been appropriately processed by the gate drive circuit.

The inverter control scheme adopted for this work offers many advantages that are attractive for active filter operation. In addition to the basic features of most feedback control systems, such as insensitivity to parameter variations and robustness, it is simple to implement and capable of producing nearly perfect replica of the reference signal at moderate switching frequency and reasonable size of filter parameters. The inner current control loop provides an inherent peak current limit in the capacitor of the output filter which serves to limit the high current surges at the capacitor output especially during the system startup. Also, since the capacitor current represents the rate of change of the inverter output voltage, the control scheme is capable of predicting and correcting near future variations in the output voltage, thus providing the fast dynamic response of the overall system and lending itself to both linear and nonlinear load applications. The outer voltage control loop regulates the inverter output voltage and ensures that the inverter output closely follows its reference.

In order to verify the functionality of the capacitor based multi-loop feedback control

scheme, one test is carried out to demonstrate its validity and effectivity. Virtually, the converter which utilizes the multi-loop feedback control scheme can regenerate any input signal regardless of its shape, as long as the parameters of the converter are finely tuned. Since voltage and current harmonics are the main concern of this research, the sample input signal would be one segment of some harmonics as shown in Figure 2.7. The given results illustrate that the proposed control scheme can follow and reproduce the reference signal synchronously and accurately.

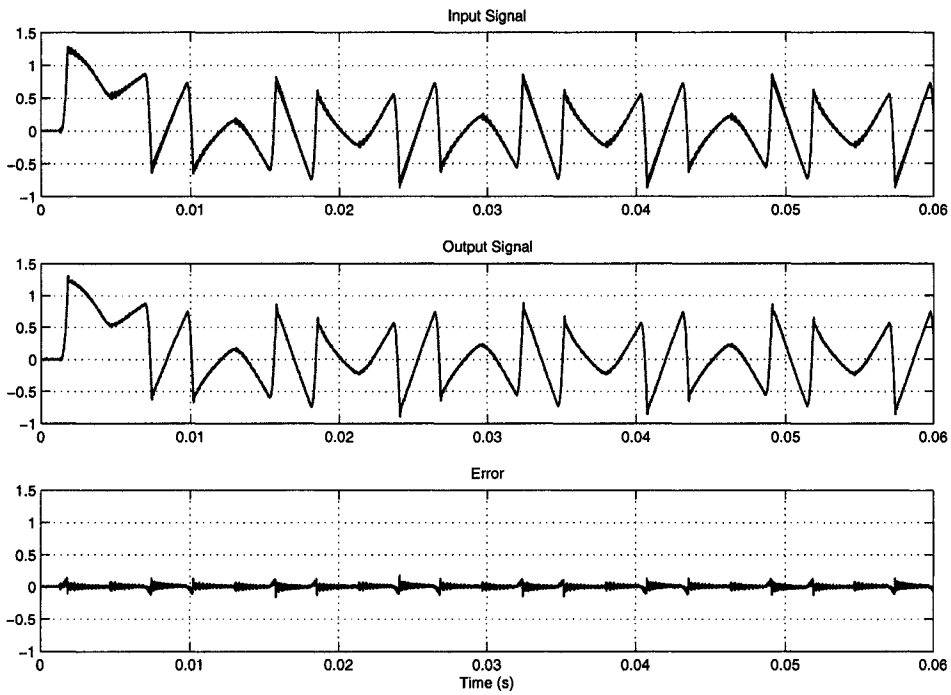

Figure 2.7: Performance of the capacitor based multi-loop feedback control scheme

The parameter tuning plays an important role in the converter design, which determines

the performance of the converter. For example, the effect of the capacitor is reflected not only in the output end low-pass filter, which is designed to let the compensating signal pass and filter out the high frequency switching harmonics, but also in the outer loop feedback gain that influences the closed loop response. The selection and adjustment of the parameters are interconnected and complicated and one method called response surface method (RSM) is introduced in Chapter 4.

2.2.2 Multi-loop feedback control based on inductor voltage: current compensation

The original multi-loop feedback control scheme was designed to regenerate a replica of the reference voltage. In this thesis, the concept is extended to current compensation.

In general, the reference signal of the multi-loop feedback control method could be any type of electric quantity such as voltage, current or power. The useful information carried by the signal is its wave shape rather than the place where it comes from. Hence the control scheme can be used to replicate a reference current signal. However the capacitor based multi-loop feedback control structure has some practical problem when dealing with current replication for current compensation. Firstly, the capacitor voltage could not be used as a feedback signal to track the reference current signal any longer since the required injection of the coupling transformer is the current signal rather than the voltage signal. If the topology of the output filter were changed to use the capacitor current to

track the reference current signal, this multi-loop feedback control strategy will lose the capability of predicting and correcting near future variations in the APF output and lead to a deterioration of the dynamic response of the whole system. This is due to the fact that the capacitor current would no longer represent the rate of change of the inverter output. A dual model which is based on inductor voltage sensing and control for current compensation is proposed in this thesis. The structure of the inductor based multi-loop feedback controller is shown in Figure 2.8.

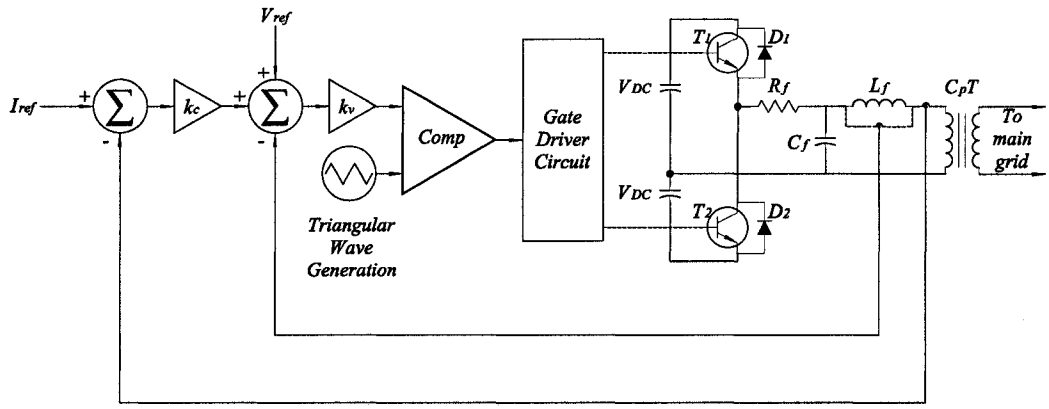

Figure 2.8: The structure of multi-loop feedback control based on inductor

As a dual of the original control scheme, the structure also consists of an inverter, an output filter, an inner voltage feedback loop, an outer current feedback loop and two

proportional controllers. The current reference I_{ref} is the current distortion i.e. the deviation of the actual current from the desired value. The APF operates to regenerate the current distortion and then to inject the generated current in phase into the main grid so as to cancel the distortion in the actual current. The generated current signal is fed back and compared with its reference. The resulting error signal is passed through a proportional controller k_c and the output of the controller is then summed with the error signal obtained from comparing the inductor voltage with its reference. The resulting signal is passed through another proportional controller k_v in the inner control loop and the output of the controller is compared with a fixed switching frequency triangular waveform in a standard sinusoidal PWM. The pulse width modulated signals are then used to control the inverter switches after they have been appropriately processed by the gate drive circuit. The structure of the output filter has some change to facilitate the dual model. This dual model has the same advantages as well as its prototype.

It is necessary to validate the function of the inductor based multi-loop feedback control scheme as well as the capacitor based one. The same sample input signal is used as the reference signal that the converter is designed to track down. The test results are shown in Figure 2.9 which is similar to Figure 2.7. Due to the different structure used in these two kinds of control methods, the parameters are chosen in dissimilar values and result in minor difference in the output signal. The simulation confirms that the proposed inductor

based method has the same advantages the original one has and can be utilized to achieve the satisfactory current compensation result. This method also have to deal with the parameter tuning, such as the value choosing in the output end second order Butterworth low-pass filter.

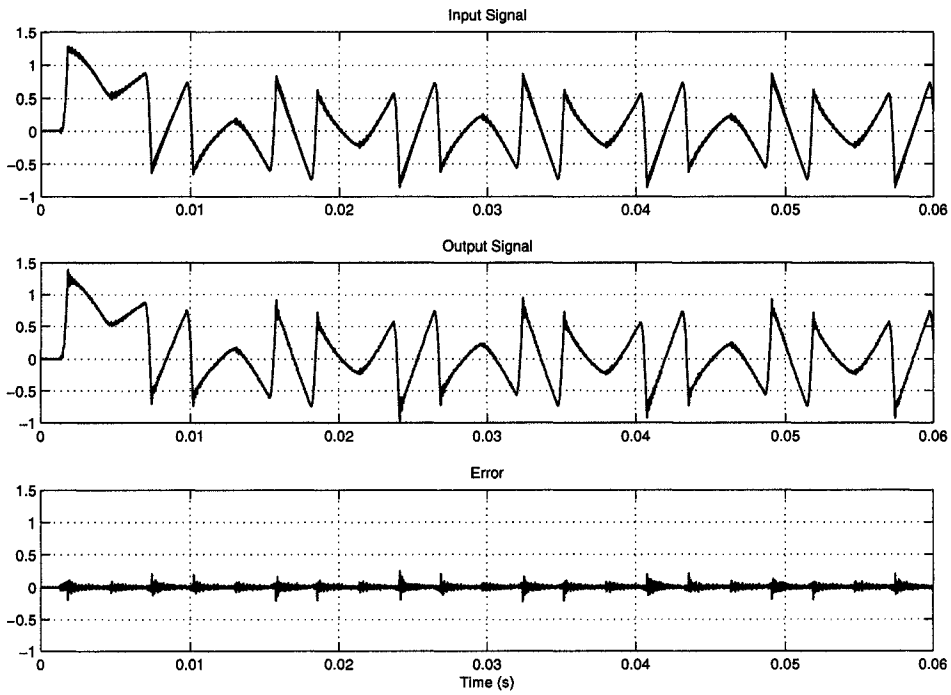

Figure 2.9: Performance of the inductor based multi-loop feedback control scheme

2.3 The Voltage Compensation Scheme (VCS)

The purpose of the voltage compensation scheme (VCS) is to maintain the voltage at the point of common coupling (PCC) almost sinusoidal and to minimize the total harmonic distortion (THD) level. In a three-phase system, voltage compensation can be achieved

by utilizing three single-phase compensation units as opposed to a single three-phase unit. This approach enables the voltages of the phases to be compensated separately so as to accommodate unbalanced voltages and differences in phase parameters.

2.3.1 Principle of the VCS

Figure 2.10 shows the block diagram of the VCS.

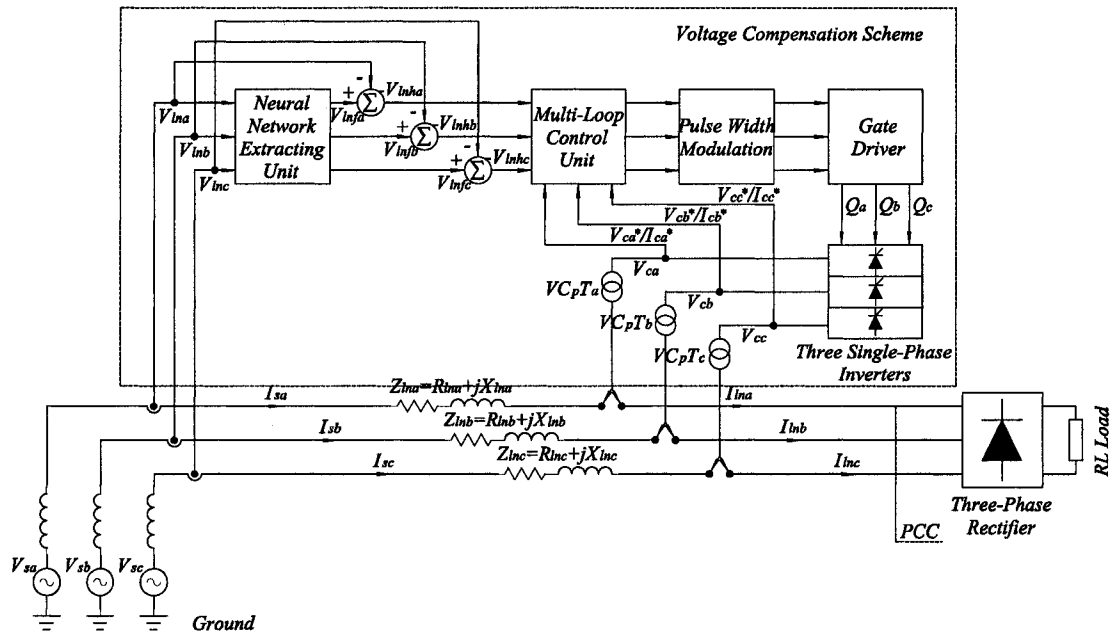

Figure 2.10: The block diagram of the three-phase VCS

The sensing module detects the voltage drops (V_{lna}, V_{lnb}, V_{lnc}) across the line impedances (Z_{lna}, Z_{lnb}, Z_{lnc}) and then passes the sensed signals into the extracting module which employs the RANN structure to determine each harmonic component in the distorted voltages. The extracted harmonic signals (V_{lnha}, V_{lnhb}, V_{lnhc}) are then sent into the

generating module which applies the active filtering concept discussed in section 2.2 to produce the compensation voltages (V_{ca}, V_{cb}, V_{cc}), which have the identical magnitude and the antiphase phase angle as the reference signals. The compensation signals are injected into the main grid by using the coupling transformers (VC_pT_a, VC_pT_b, VC_pT_c) at the PCC.

2.3.2 Analysis of the VCS

Figure 2.11 shows the single-phase equivalent circuit representation of the voltage compensation scheme. The utility supply is modeled as an ideal voltage source V_s and the voltage drop across the line impedance Z_{ln} is V_{ln}. In order to maintain the voltage at the PCC V_{pcc} almost sinusoidal, a compensation voltage V_c is injected in series with the line voltage to cancel the harmonic component V_{lnh} in the line voltage. The current source nonlinear load is modeled by a harmonic current source I_{ld}. The single-phase steady state analysis is a reasonable choice since the compensation of the three-phase system is achieved via independent compensation of each phase.

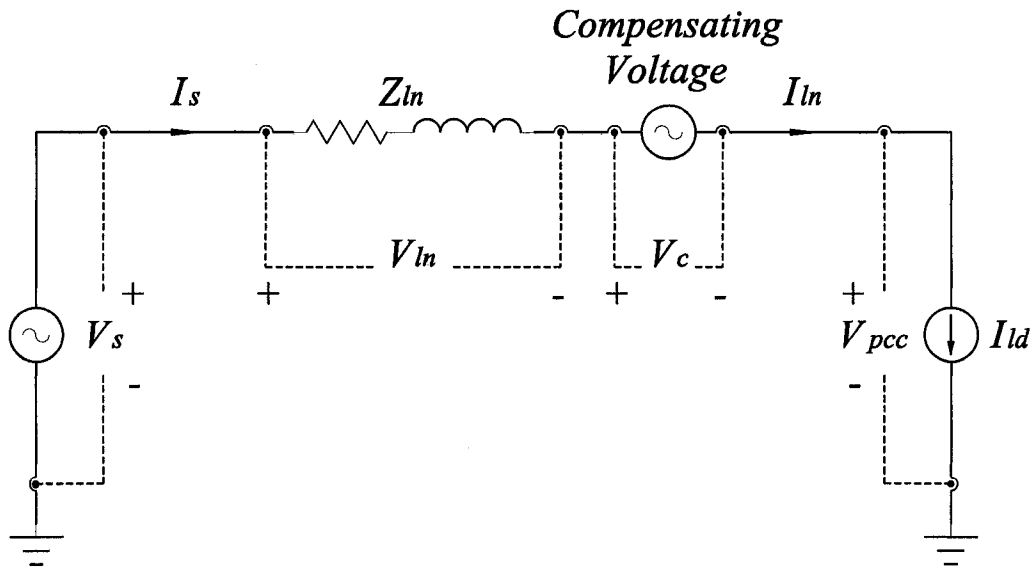

Figure 2.11: The single-phase equivalent circuit of the VCS

The voltage source V_s is treated as ideal.

$$V_s = V_{s1} \tag{2.19}$$

where V_{s1} is the fundamental component of the source.

Since the nonlinear load draws harmonic current from the source, the nonlinear current will generate voltage distortion across the line.

$$V_{ln} = V_{ln1} + V_{lnh} \tag{2.20}$$

where V_{ln1} and V_{lnh} are the fundamental and harmonic component of the line voltage respectively.

The voltage at the PCC without the compensating voltage is given by

$$V_{pcc} = V_s - V_{ln} = V_{s1} - (V_{ln1} + V_{lnh}) = (V_{s1} - V_{ln1}) - V_{lnh} \quad (2.21)$$

In (2.21), V_{ln1} causes a drop in the fundamental component of the voltage at the PCC and V_{lnh} introduces harmonics in the voltage at the PCC.

With the compensating voltage, the voltage at the PCC is given by

$$V_{pcc} = V_s - V_{ln} - V_c = V_{s1} - (V_{ln1} + V_{lnh}) - V_c = (V_{s1} - V_{ln1}) - (V_{lnh} + V_c) \quad (2.22)$$

where V_c is the compensating voltage.

In order for the voltage at the PCC to be free of harmonic, V_c must be opposite to V_{lnh}.

2.3.3 Performance of the VCS

A computer simulation model of the VCS is constructed in MATLAB using SIMULINK and SimPowerSystems blockset (see Appendix A) to verify its performance under various operating conditions. The nonlinear harmonic source is a current source three-phase diode bridge rectifier with an inductive load. The system specification and circuit parameters used in the simulation are presented in Table 2.2.

Table 2.2: System specification and circuit parameters (One phase)

AC Source Voltage, V_s	100 V (Peak)
DC Inverter Voltage, V_{DC}	250 V
Fundamental Frequency	60 Hz
Sampling Frequency	76,800 Hz
PWM Carrier Frequency	50 kHz
Load Resistance, R_L	100 Ω
Load Inductance, L_L	95 mH
Line Resistance, R_l	100 Ω
Line Inductance, L_l	2 mH
Outer Loop Gain for the Controller, k_{1V}	4
Inner Loop Gain for the Controller, k_{2V}	2

2.3.3.1 Normal operation

Under normal operation i.e. when there is no system disturbance of any form, and with the system loaded by the nonlinear load, Figures 2.12 and 2.13 show the waveforms and harmonic spectra of the three-phase voltage at the PCC, with and without the VCS, respectively. The given spectra results in Figures 2.12(b) and 2.13(b) by SIMULINK include the interharmonics and subharmonics.

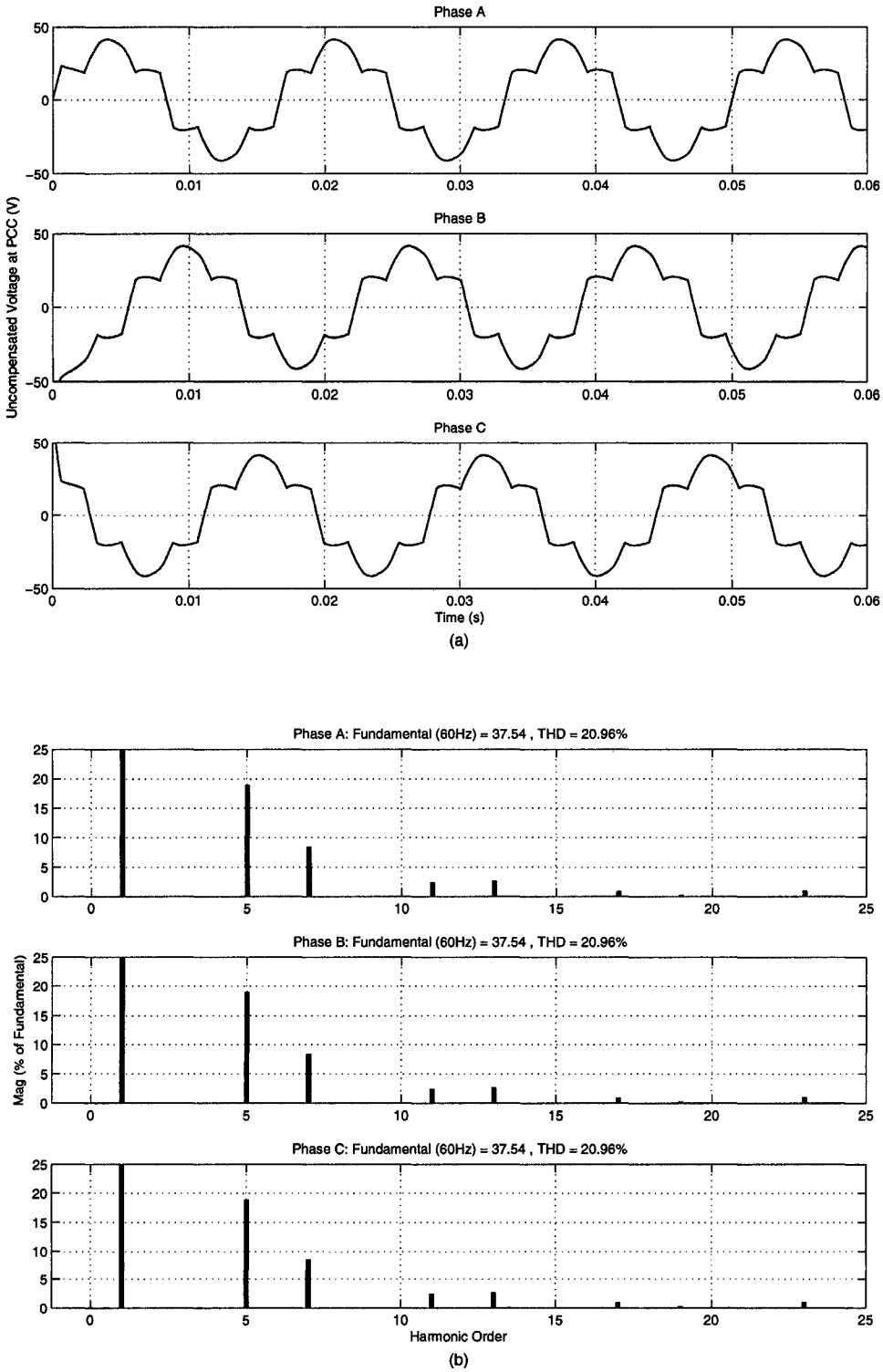

Figure 2.12: Performance without the VCS (a) Voltage at PCC; (b) Harmonic spectra

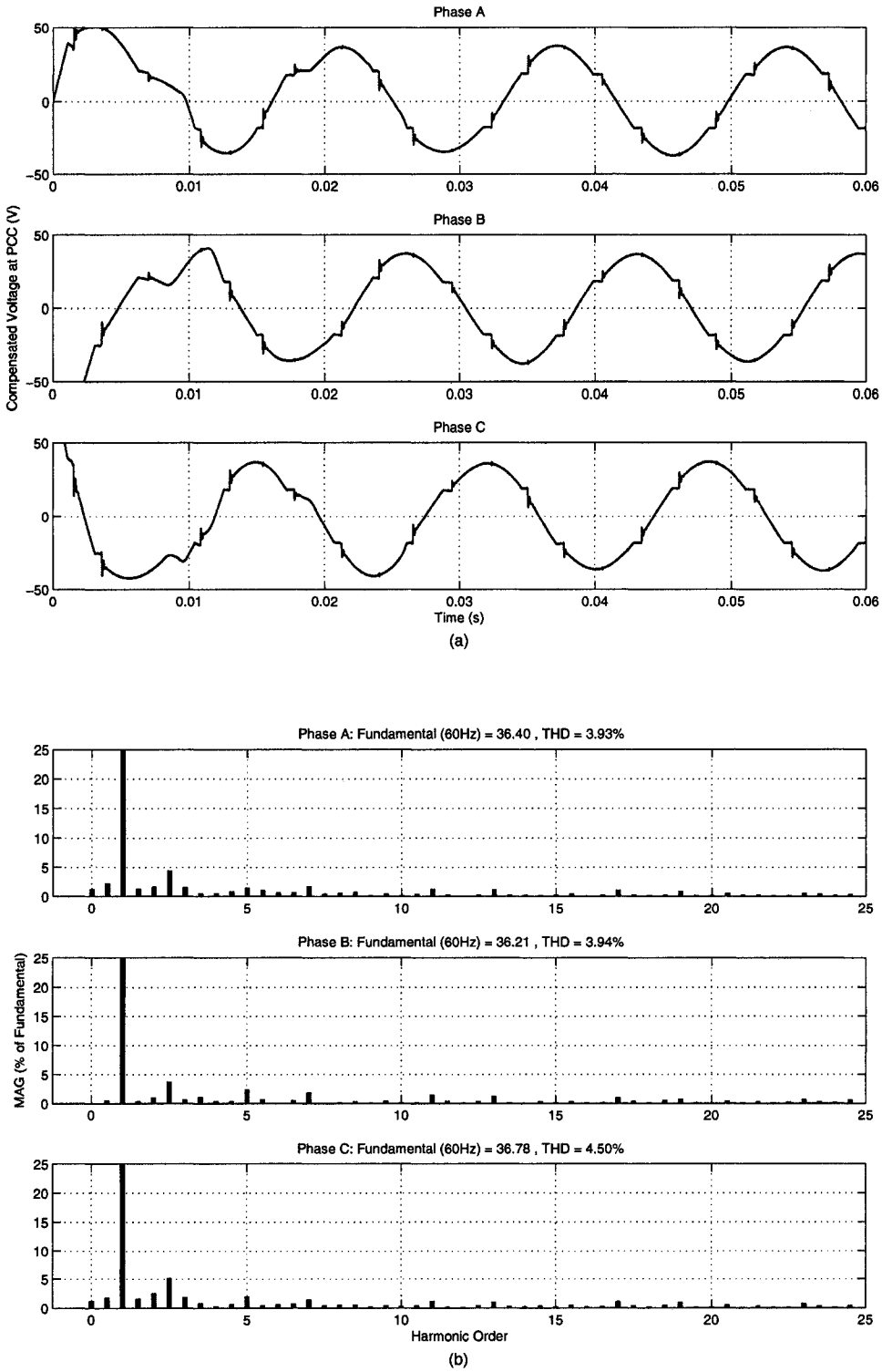

Figure 2.13: Performance with the VCS (a) Voltage at PCC; (b) Harmonic spectra

For phase A, the total harmonic distortion (THD) of the voltage at the PCC without the VCS is determined from Figure 2.12(b) as 20.96% while the THD of the voltage at the PCC with VCS is obtained from Figure 2.13(b) as 3.93%, a figure which meets the recommended harmonic specifications of IEEE Standard 519-1992 [2]. The results of phase B and phase C also fulfill the requirements as well. Figure 2.13(a) shows the VCS can remove the harmonics of the voltage at the PCC successfully within about one fundamental cycle.

From the obtained results, the system with the VCS has the capability of compensating for nonlinear line voltage distortion and maintaining the voltage at the PCC almost sinusoidal. Its weakness is its inability to mitigate the source current harmonics. The system is thus able to prevent the voltage harmonic distortion from spreading beyond the point of common coupling, but unable to keep the source current free of the harmonic components. Figure 2.14(a) shows the compensating voltage reference signals generated by the RANN harmonic extraction unit while Figure 2.14(b) is the regenerated compensation voltage by the active power filter which is then injected into the main grid via the coupling transformer. Figure 2.15 is the error signal between the reference voltage and output voltage of the VCS.

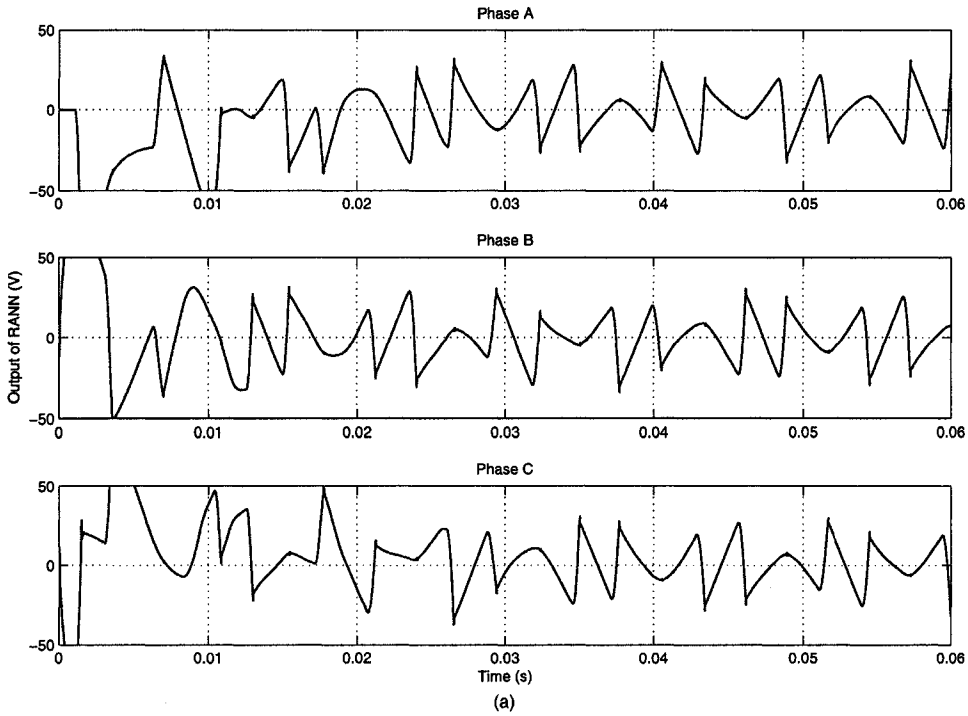

Figure 2.14: Performance of the VCS (a) Output of RANN; (b) Output of APF

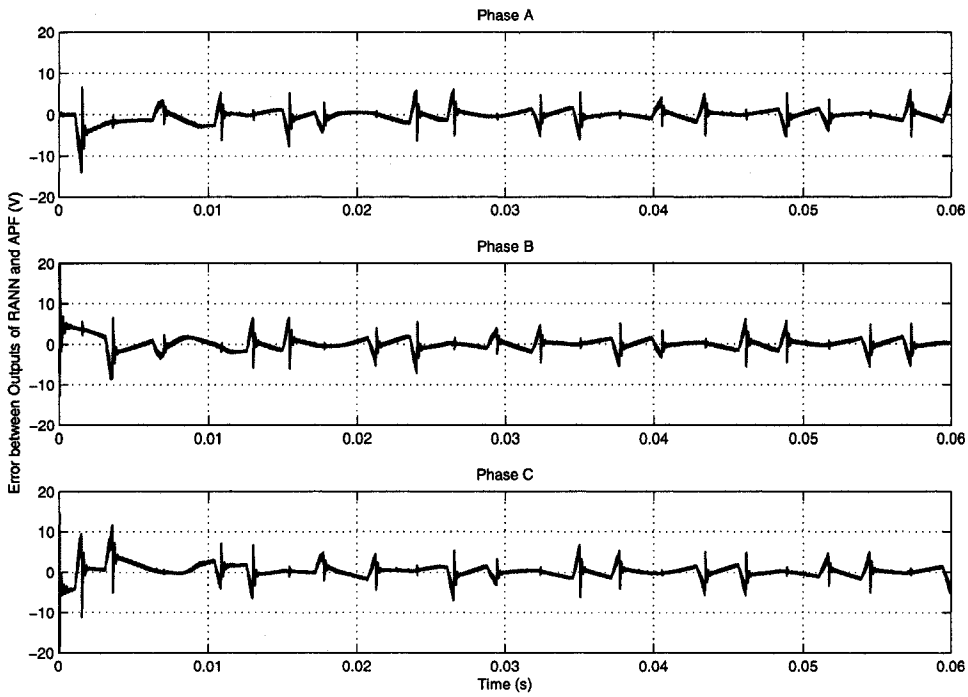

Figure 2.15: Error between the outputs of RANN and APF

The inductive nonlinear load causes the saltation of the line voltage, which subsequently generates a high impulse in the format of the derivative of the voltage in the inner loop of the VCS. This transient leads to a temporary large error between the reference voltage and output voltage of the VCS.

2.3.3.2 Abnormal operation

The algorithm of the VCS assumes that the source supply is a pure ideal sinusoidal voltage source. The objective then is to cancel the voltage distortion across the line impedance to maintain the voltage at the PCC free of harmonics. If there are some

source-end disturbance such as voltage sag, voltage swell or voltage flicker, the VCS is unable to compensate for the voltage at the PCC to the desired voltage level directly due to the absence of the valid fundamental reference signal. Figure 2.16 shows the performance of the system undergoing the voltage sag and voltage swell without the VCS. Figure 2.16(a) shows a 30% sag at 1/15 second and a 20% swell at 2/15 second respectively at the source-end [3]. Figure 2.16(b) shows the sensed line voltage which is influenced by the voltage sag and voltage swell accordingly. Figure 2.16(c) shows the voltage at the PCC which is suffering not only the harmonics but also the source-end disturbance. Figure 2.17 shows the performance of the system with the VCS. Figure 2.17(a) shows the same source-end conditions as Figure 2.16(a). Figure 2.17(b) shows the sensed line voltage is unaffected by the adding of the VCS. Figure 2.17(c) shows the voltage at the PCC removes most of the harmonics by using the active power filter while its fundamental wave shape is still deteriorated by the abnormal supply conditions. Figure 2.17 illustrates that the output of the VCS can follow the step change of the source voltage instantaneously, in other words, which is unable to maintain a constant output in the case of the varied source supply.

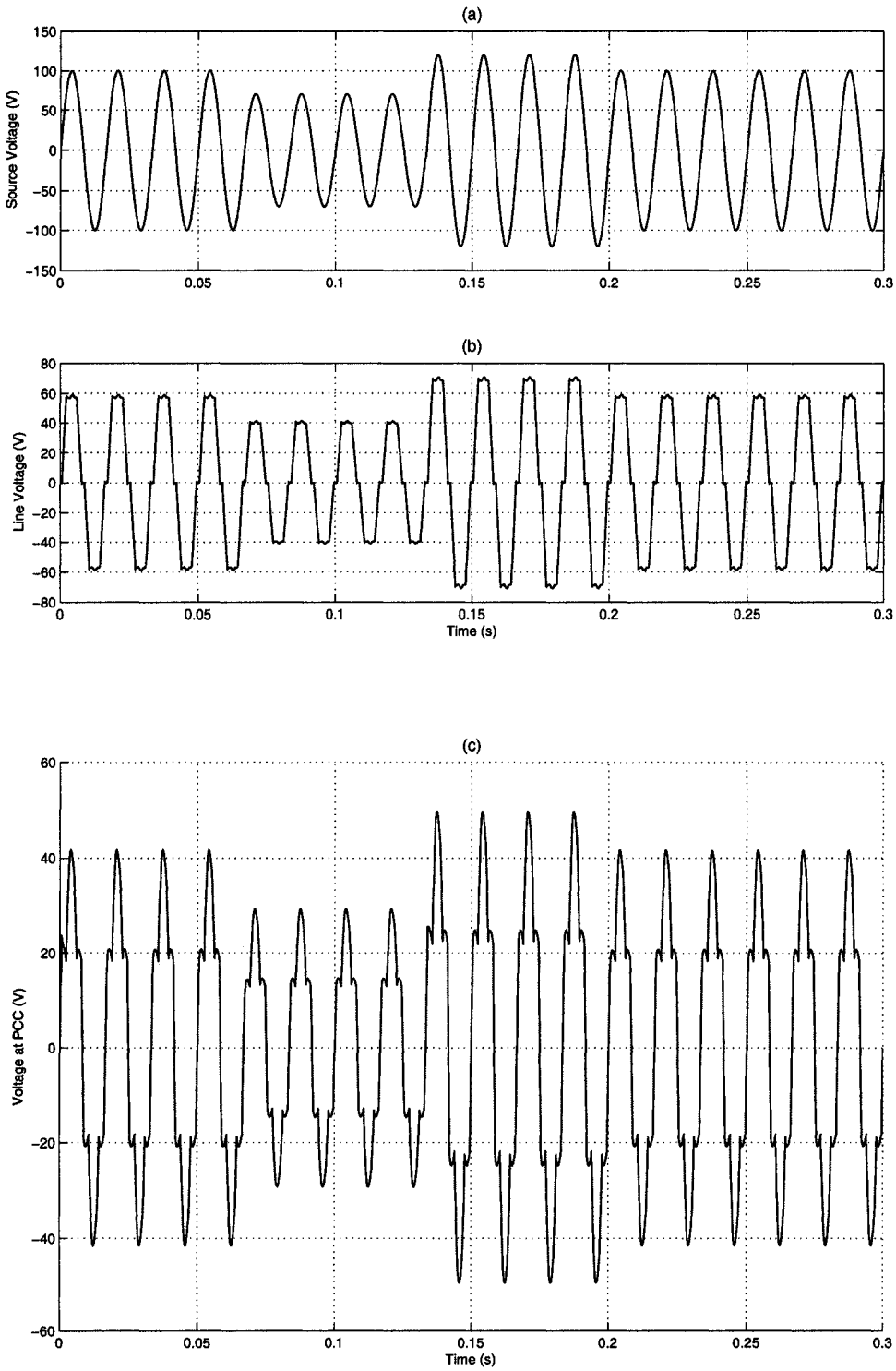

Figure 2.16: Performance without the VCS under voltage sag and voltage swell

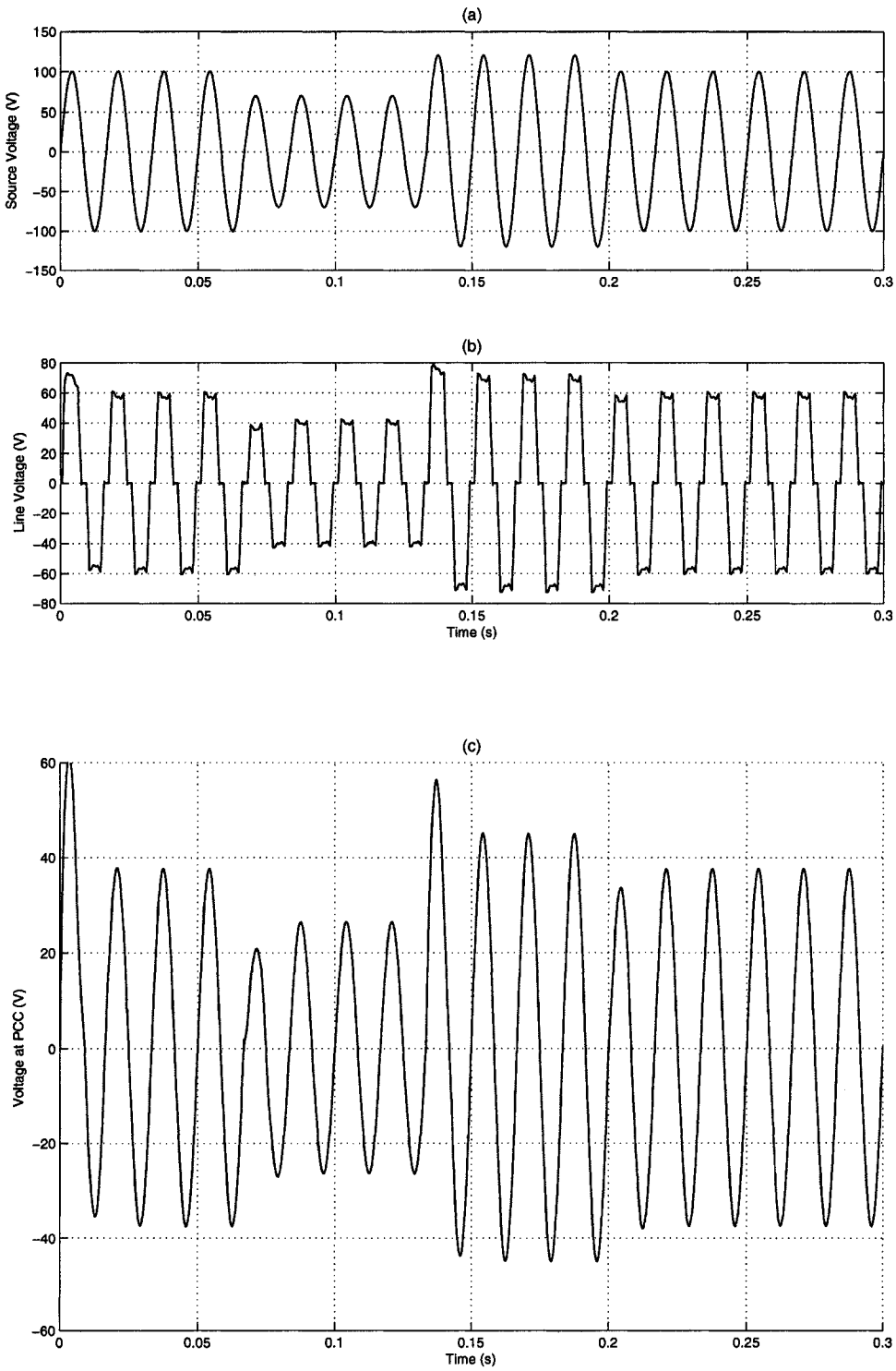

Figure 2.17: Performance with the VCS under voltage sag and voltage swell

The effect of voltage flicker on the performance of the VCS is shown in Figures 2.18 and 2.19. Figure 2.18(a) shows the source voltage with its amplitude modulated by a 10 Hz sinusoidal signal with a 30% modulation depth. This amplitude modulation results in the voltage flicker at the load-end shown in Figure 2.18(c) and could produce extremely annoying fluctuations at the PCC. Figure 2.19 shows the performance of the compensation system with the VCS. Similar to the previous case, the VCS can eliminate most of the harmonics of the voltage at the PCC while the distorted fundamental component still remains. The voltage flicker could be treated as the slower amplitude variation in the source voltage, which combines the voltage sag and voltage swell together. The proposed VCS is unable to eliminate the voltage fluctuation in the voltage at the PCC.

In Chapter 3, a preprocessing scheme is proposed to mitigate the effect of the various disturbances on the voltage at the PCC. This preprocessing unit is also capable of solving the problem of unbalanced power supply.

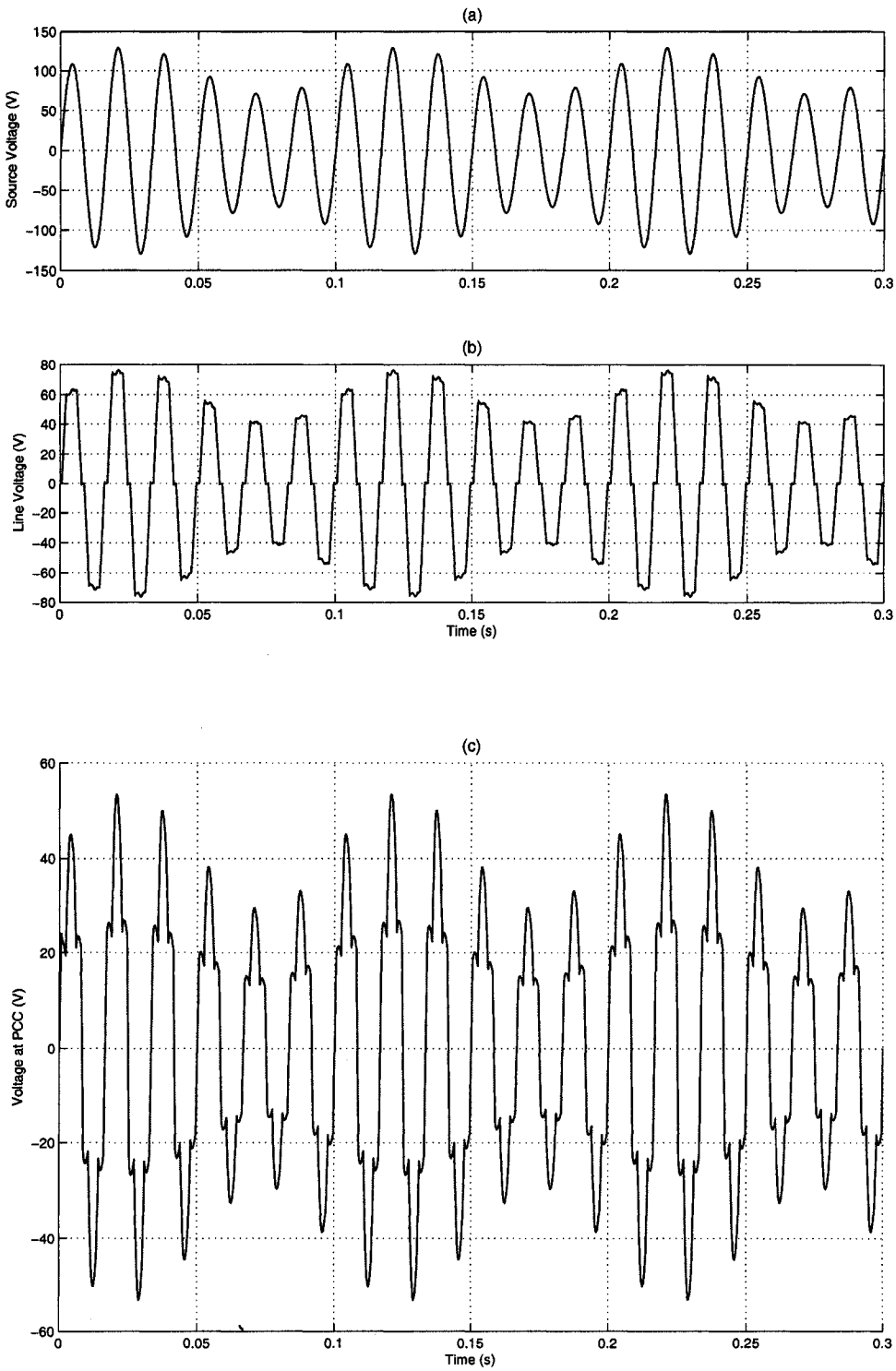

Figure 2.18: Performance without the VCS under voltage flicker

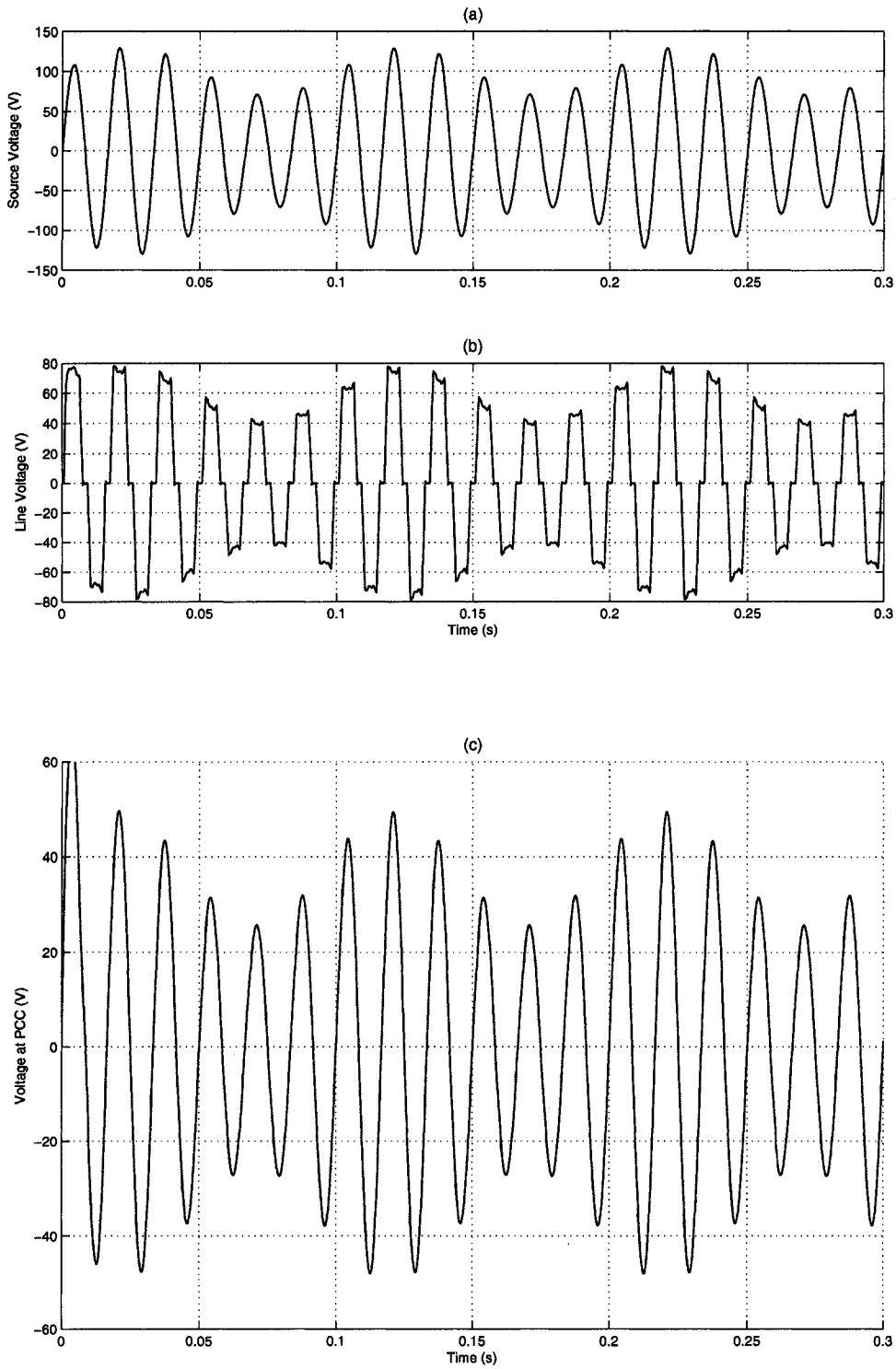

Figure 2.19: Performance with the VCS under voltage flicker

2.4 The Current Compensation Scheme (CCS)

The purpose of the current compensation scheme (CCS) is to cancel the harmonic components of the source current which is caused by the nonlinear loads and to minimize the total harmonic distortion (THD) level. In a three-phase system, current compensation can be achieved by utilizing three single-phase compensation units as opposed to a single three-phase unit. This approach enables the currents of the phases to be compensated separately so as to accommodate unbalanced currents and differences in phase parameters.

2.4.1 Principle of the CCS

Figure 2.20 shows the block diagram of the CCS.

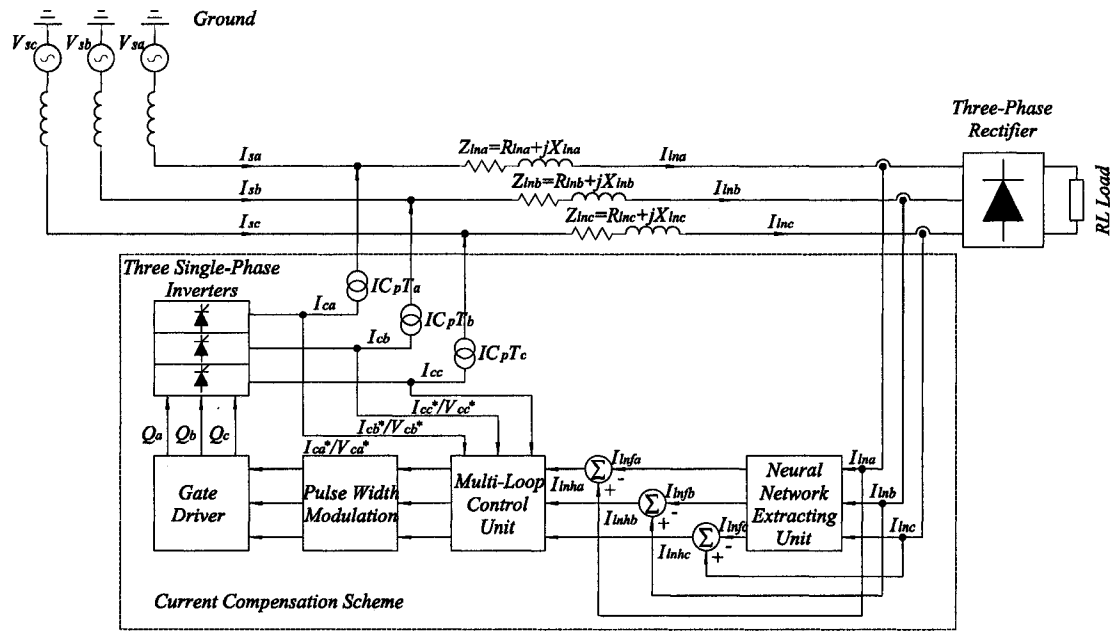

Figure 2.20: The block diagram of the three-phase CCS

The sensing module detects the line currents (I_{lna}, I_{lnb}, I_{lnc}) along the line impedances (Z_{lna}, Z_{lnb}, Z_{lnc}) and then passes the sensed signals into the extracting module which employs the RANN structure to determine each harmonic component in the distorted currents. The extracted harmonic signals (I_{lnha}, I_{lnhb}, I_{lnhc}) are then sent into the generating module which applies the active filtering concept discussed in section 2.2 to produce the compensation currents (I_{ca}, I_{cb}, I_{cc}), which have the identical magnitude and the inphase phase angle as the reference signals. The compensation signals are injected into the main grid by using the coupling transformer (IC_pT_a, IC_pT_b, IC_pT_c) at the source-end.

2.4.2 Analysis of the CCS

Figure 2.21 shows the single-phase equivalent circuit representation of the current compensation scheme. The utility supply is modeled as an ideal voltage source V_s and the current flowing along the line impedance Z_{ln} is I_{ln}. In order to prevent the source current I_s from being contaminated by the harmonic currents drawn by the nonlinear loads, a compensation current I_c is injected in shunt with the line current to supply the harmonic component I_{lnh} in the line current which is originally provided by the source current. The current source nonlinear load is modeled by a harmonic current source I_{ld} as before. The single-phase steady state analysis is a reasonable choice since the compensation of the three-phase system is achieved via independent compensation of each phase.

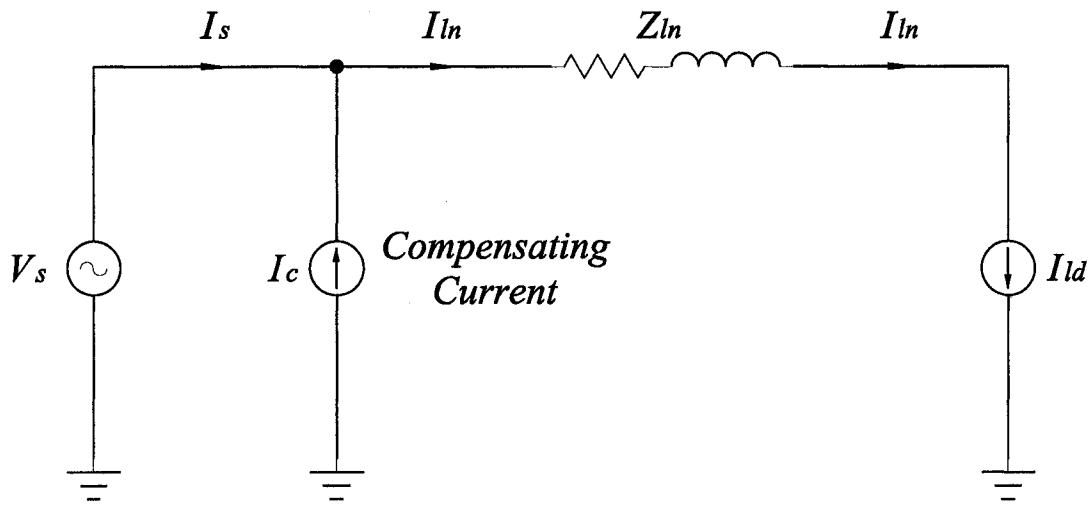

Figure 2.21: The single-phase equivalent circuit of the system with the CCS

The source current I_s could be expressed as

$$I_s = I_{s1} + I_{sh} \tag{2.23}$$

where I_{s1} and I_{sh} are the fundamental and harmonic component of the source current respectively.

Since the nonlinear load draws harmonic current from the source, the nonlinear current will flow over the line impedance as well.

$$I_{ln} = I_{ln1} + I_{lnh} \tag{2.24}$$

where I_{ln1} and I_{lnh} are the fundamental and harmonic component of the line current respectively.

The source current without the compensating current is given by

$$I_s = I_{ln} = I_{ld} = I_{ln1} + I_{lnh} = I_{ld1} + I_{ldh} \tag{2.25}$$

In (2.25), I_{ln1} is the same with the fundamental component of the source current and I_{lnh} introduces harmonics in the source current.

With the compensating current, the source current is given by

$$I_s = I_{ln} - I_c = (I_{ln1} + I_{lnh}) - I_c = I_{ln1} + (I_{lnh} - I_c) \tag{2.26}$$

where I_c is the compensating current.

In order for the source current to be almost sinusoidal, I_c must be equal to I_{lnh}.

2.4.3 Performance of the CCS

A computer simulation model of the CCS is constructed in MATLAB using SIMULINK and SimPowerSystems blockset (see Appendix A) to verify its performance under various operating conditions. The nonlinear harmonic source is a current source three-phase diode bridge rectifier with an inductive load. The system specification and circuit parameters used in the simulation are presented in Table 2.3.

Table 2.3: System specification and circuit parameters (One phase)

AC Source Voltage, V_s	100 V (Peak)
DC Inverter Voltage, V_{DC}	250 V
Fundamental Frequency	60 Hz
Sampling Frequency	76,800 Hz
PWM Carrier Frequency	50 kHz
Load Resistance, R_L	100 Ω
Load Inductance, L_L	95 mH
Line Resistance, R_l	100 Ω
Line Inductance, L_l	2 mH
Outer Loop Gain for the Controller, k_{1C}	100
Inner Loop Gain for the Controller, k_{2C}	10

2.4.3.1 Normal operation

Under normal operation i.e. when there is no system disturbance of any form and with the system is loaded by the nonlinear load, Figures 2.22 and 2.23 show the waveforms and harmonic spectra of the three-phase line currents and the source currents, respectively. The given spectra results in Figures 2.22(b) and 2.23(b) by SIMULINK include the interharmonics and subharmonics.

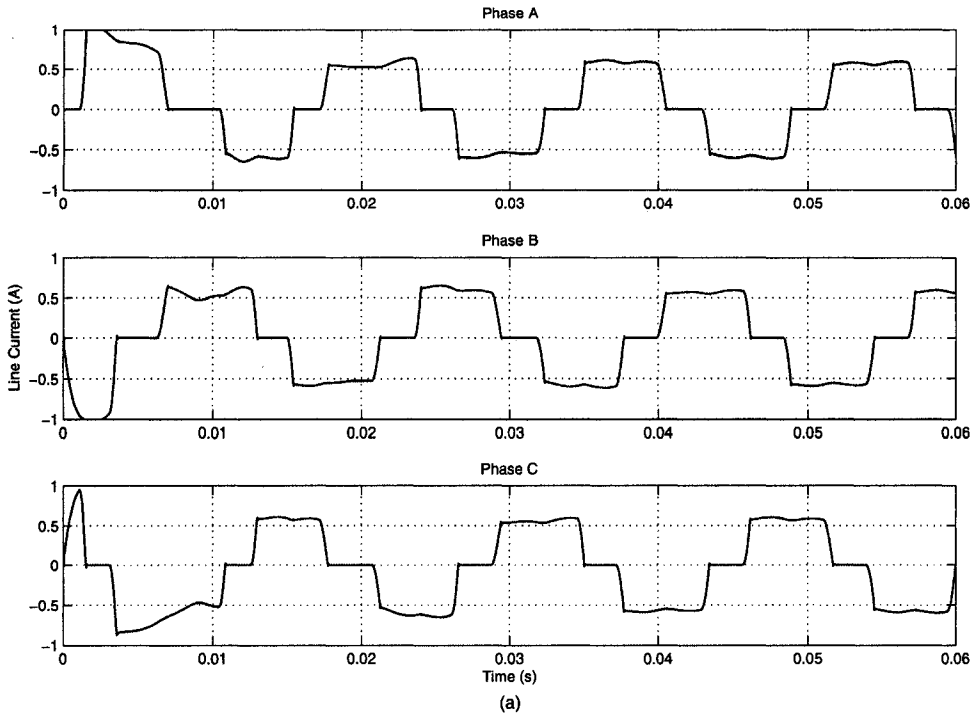

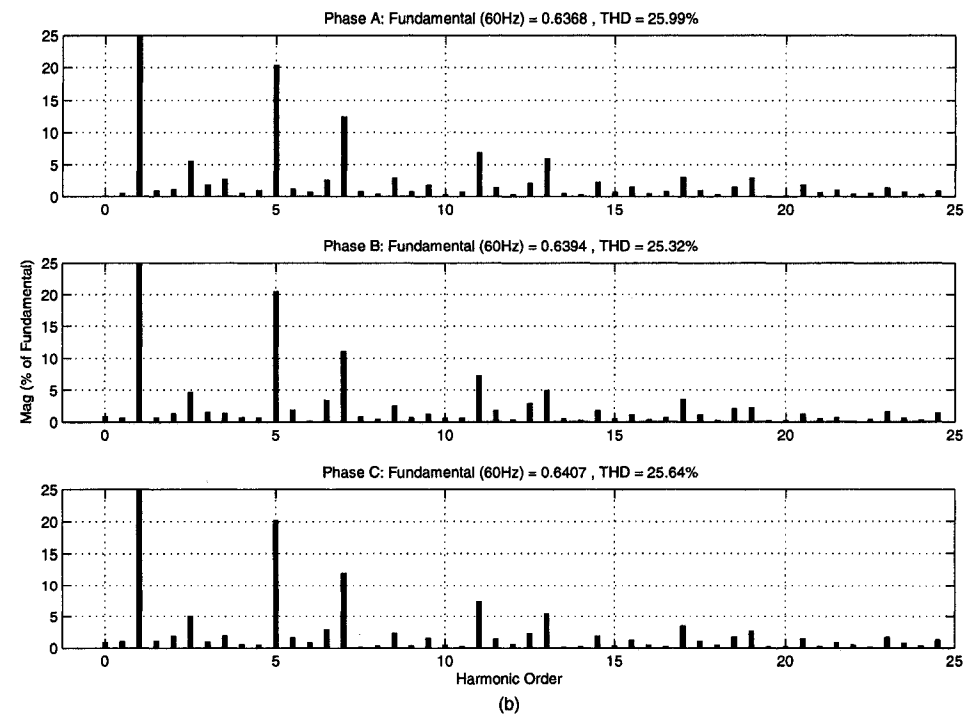

Figure 2.22: Performance of the CCS (a) Line current; (b) Harmonic spectra

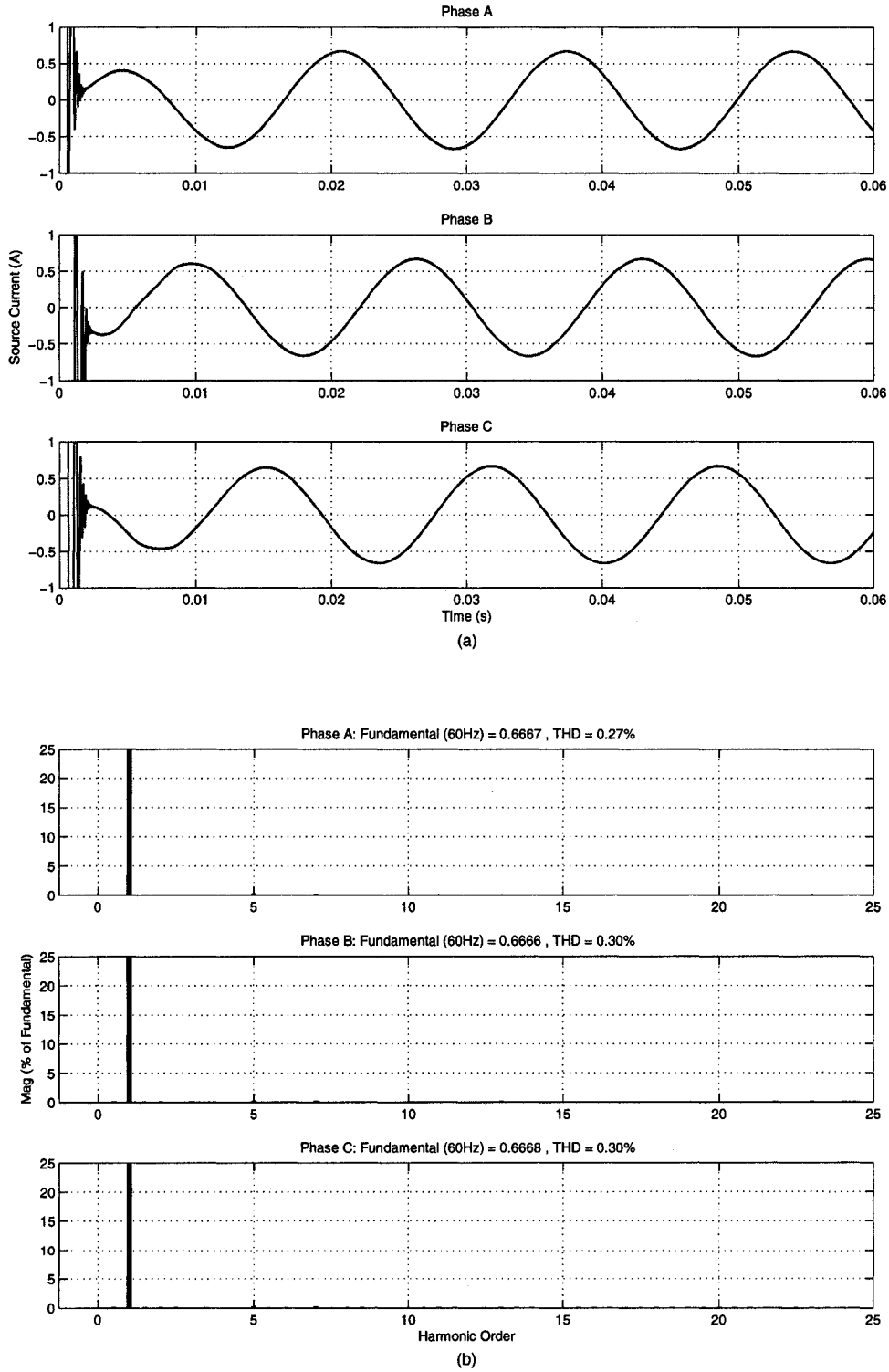

Figure 2.23: Performance of the CCS (a) Source current; (b) Harmonic spectra

For phase A, the total line current harmonic distortion is determined from Figure 2.22(b) as 25.99% while the THD of the source current is obtained from Figure 2.23(b) as 0.27%, a figure which greatly meets the recommended harmonic specifications of IEEE Standard 519-1992 [2]. The results of phase B and phase C also reach the standards as well. Figure 2.23(a) shows that the CCS can remove the harmonics from the source current successfully within about one fundamental cycle.

From the results obtained, the system with CCS has the capability of compensating for nonlinear line current distortion and maintaining the source current almost sinusoidal. The shunt APF provides a low-impedance byway for the harmonic components generated by the nonlinear loads, which prevents the source current from being contaminated. Its weakness is its inability to mitigate the line voltage distortions. The system is thus able to maintain the source current free of the harmonic components, but unable to prevent voltage harmonic distortion from spreading beyond the point of common coupling. Figure 2.24(a) shows the compensating current reference signals generated by the RANN harmonic extraction unit while Figure 2.24(b) is the regenerated compensation current by the active power filter which is then injected into the main grid via the coupling transformer. Figure 2.25 is the error signal between the reference current and output current of the CCS.

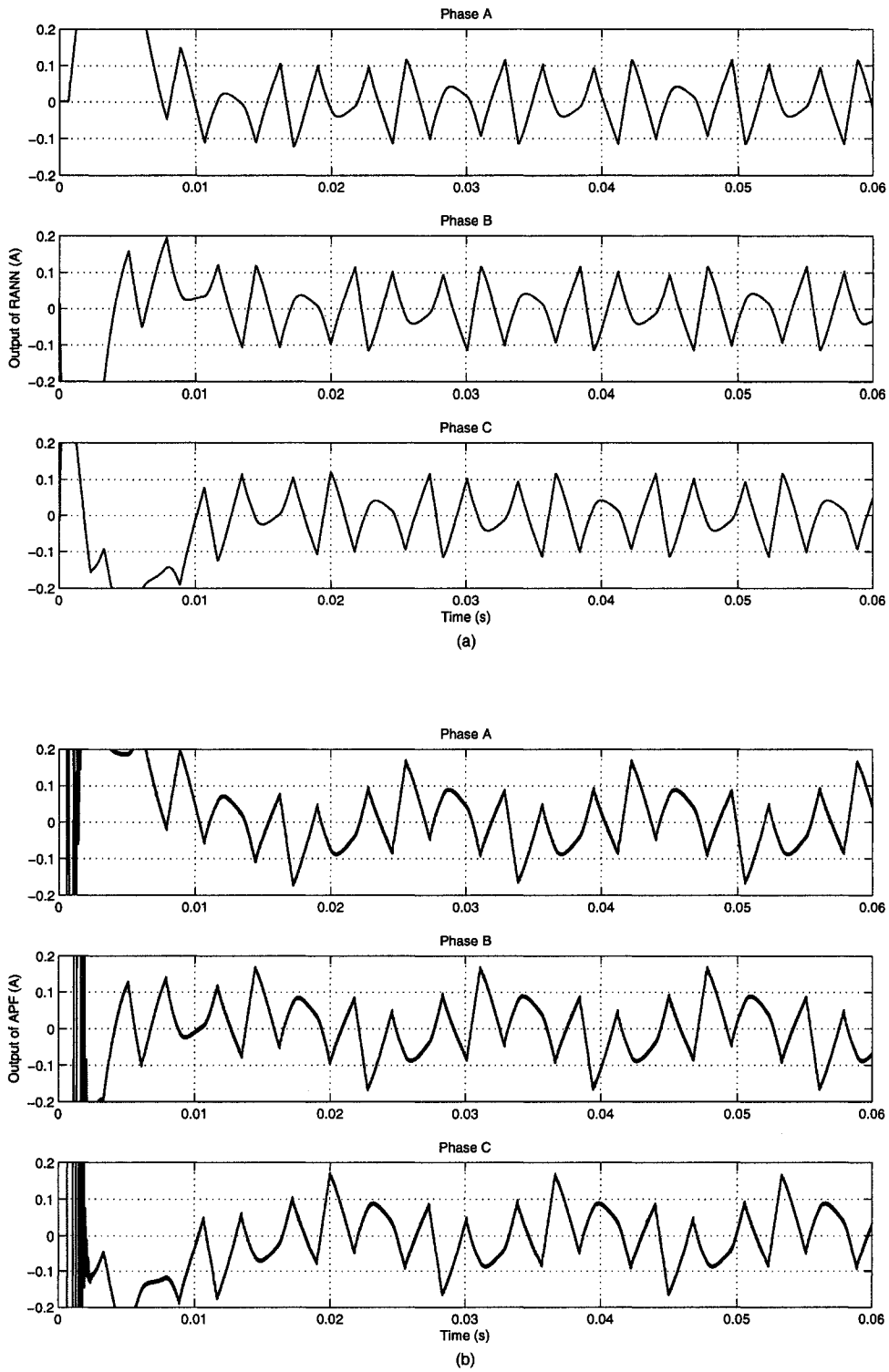

Figure 2.24: Performance of the CCS (a) Output of RANN; (b) Output of APF

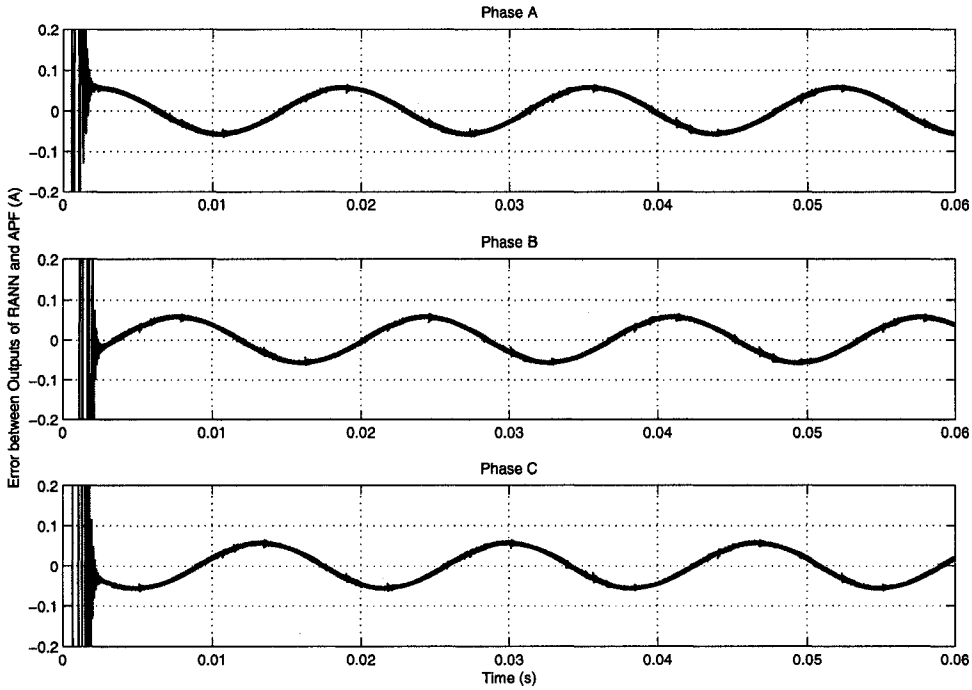

Figure 2.25: Three-phase error between outputs of RANN and APF

2.4.3.2 Abnormal operation

Being similar to the application of the VCS, the structure of the CCS determines that the shunt active power filter is capable of compensating for the harmonic components of the source current by tracking the line current as the reference signal. However the source-end distortion such as voltage sags, voltage swells or voltage flicker would result in the lost of the valid fundamental voltage information which would cause the lost of the valid fundamental current information consequently. Under the abnormal conditions, the fundamental magnitude of the compensated source current would deviate from the

standard value even though the CCS removes most of harmonic components from it. The proposed preprocessing unit in Chapter 3 is capable of eliminating the influences of the various disturbance on the source current.

2.5 Summary

In this chapter, the principle of the recurrent artificial neural network (RANN) and the algorithm of the multi-loop feedback control were introduced and discussed. Two compensation schemes which are suitable for voltage and current compensations of both linear and nonlinear loads were investigated. The voltage compensation scheme (VCS) utilized the series active power filters using the multi-loop feedback control scheme to regenerate the harmonic replicas. The current compensation scheme (CCS) employed the shunt active power filters which utilized an extended dual multi-loop feedback control scheme to operate the power inverters. Both the VCS and CCS applied the RANN algorithm for the voltage and current harmonic extraction. The performance of the VCS and CCS was investigated under various source conditions. Under the normal operating condition, the VCS was effective in minimizing the total harmonic distortion (THD) level of the line voltage and in maintaining the voltage at the point of common coupling (PCC) almost sinusoidal. The CCS was capable of supplying a low-impedance harmonic component bypass for the nonlinear loads and of keeping the source current from being contaminated. Due to the inherent limitations of the algorithm, the VCS and CCS were

unable to sufficiently compensate for the voltages at the PCC and the source currents under abnormal source conditions such as voltage sags, voltage swells and voltage flicker.

The combination of VCS and CCS into one compensation system is capable of implementing the voltage and current compensations simultaneously and the introduction of one preprocessing unit would solve the problems resulting from the abnormal source conditions, including the unbalanced case.

Chapter 3
Balanced and Unbalanced Voltage and Harmonic Compensation in the Series-Shunt Compensation System

In Chapter 2, the single VCS and the single CCS were used to compensate for the voltage at the PCC and the source current respectively. The successful compensation results verified the feasibilities and the performances of the RANN harmonic extraction algorithm and the multi-loop feedback control scheme.

In general, the simultaneous voltage and current compensation are the basic demand for the distribution power system so that the application of combining the VCS and the CCS together should be investigated. Due to the flexibility of the RANN algorithm, it could be implemented in either single-phase or three-phase system. The effects of harmonic order and sampling frequency on the compensation results are investigated to fulfill the parameter tuning in the RANN. The performance of the series-shunt compensation system under different load conditions is also investigated.

The functions of the VCS and the CCS are limited while there are some source-end distortions such as voltage sags, voltage swells or voltage flicker. In some worse situation, the source supply may sustain the unbalanced disturbance that could result in severe damages to the electrical equipments. One possible solution is to implant one preprocessing unit into the power system, which could compensate for any distortion and disturbance caused by the source supply. The structure and performance of the preprocessing unit are analyzed and discussed. The application of the series-shunt compensation system with the preprocessing unit is then investigated.

3.1 The Series-Shunt Compensation System

The series-shunt compensation system which utilizes both the VCS and the CCS can provide online voltage and harmonic compensation simultaneously. The proper topology of the hybrid compensation system should be chosen for the specific demands.

3.1.1 Model of the series-shunt compensation system

The purpose of the series-shunt compensation system is to maintain the voltage at the PCC sinusoidal and to keep the source current free of the harmonics at the same time. The injection point of the compensating current generated by the shunt APF should be placed in front of the grid line impedance, otherwise the CCS would lose track of the reference signal sampled from the line current. In a single-load case, the sensing of the load current could be used as the replacement of the reference signal; however,

cumbersome sensing and calculation of the load current would be impractical in multiple-load cases. The complete series-shunt APFs configuration is illustrated in Figure 3.1 with the reproduction of compensating signals achieved by using the multi-loop feedback control strategy. Figure 3.1 illustrates the three-phase series-shunt compensation system whose structure and topology can be easily transplanted to the single-phase series-shunt compensation system.

For the VCS section, the RANN extracts the fundamental components (V_{lnfa}, V_{lnfb}, V_{lnfc}) from the nonlinear line voltages (V_{lna}, V_{lnb}, V_{lnc}). The desired harmonic components (V_{lnha}, V_{lnhb}, V_{lnhc}) are obtained by subtracting the fundamental components from the sensed line voltages. Compared with the method of detecting and summing each voltage harmonic component to obtain the total voltage harmonics, the proposed method results in less complicated structure and less computation efforts. The harmonic component in the RANN is computed up to the 25^{th} order which is a compromise between the precision of the calculation and the complexity of the RANN. The lower order harmonics such as 3^{rd}, 5^{th} and 7^{th} harmonic components contribute the most portions of the total voltage harmonics. However, the interdependence of harmonic coefficients always produces errors in the calculation of the fundamental component, for any finite maximum harmonic order.

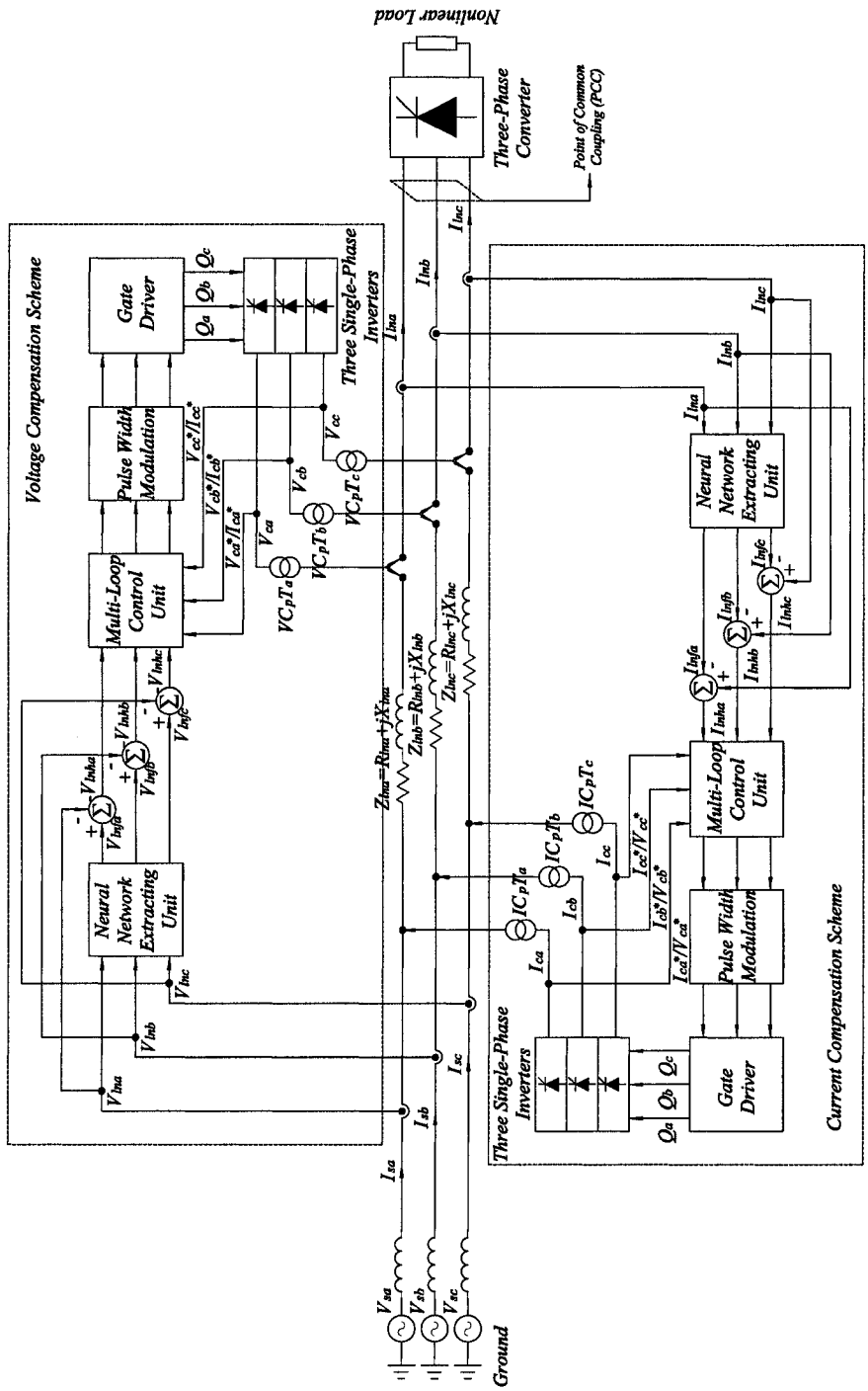

Figure 3.1: The block diagram of the three-phase series-shunt compensation system

The harmonic reference signals are then sent to the regeneration unit which is controlled by the multi-loop feedback scheme to generate the PWM gating signals (Q_a, Q_b, Q_c) required to drive the voltage source inverters. The outputs of the inverter (V_{ca}, V_{cb}, V_{cc}) which have the identical magnitude and the antiphase phase angle with the reference signal (V_{lnha}, V_{lnhb}, V_{lnhc}) are injected into the main power grid by using the coupling transformers (VC_pT_a, VC_pT_b, VC_pT_c) at the point of common coupling (PCC).

The CCS is a dual of the VCS, which senses the line currents (I_{lna}, I_{lnb}, I_{lnc}) and separates the harmonic components (I_{lnha}, I_{lnhb}, I_{lnhc}) from the distorted currents using the same method as the VCS. By applying the multi-loop feedback control strategy to operate the PWM voltage source inverter to generate the compensation signals (I_{ca}, I_{cb}, I_{cc}) which are identical with the reference signals (I_{lnha}, I_{lnhb}, I_{lnhc}) in magnitude and phase angle. The CCS accomplishes the shunt current compensation by using the coupling transformers (IC_pT_a, IC_pT_b, IC_pT_c) at the source-end point. In order to perform the parameter adjustment independently to accommodate unbalanced cases, three single-phase RANNs and inverters are utilized instead of one three-phase inverter in both the VCS and the CCS.

3.1.2 Analysis of the series-shunt compensation system

Figure 3.2 shows the single-phase equivalent circuit representation of the series-shunt compensation system. The insertion point of the CCS is chosen to be at the source-end to guarantee the previous derived models could be directly applied. The source-end CCS

acts as a harmonic current generator to make the source current sinusoidal, while the load-end VCS filters out the voltage harmonics, which is caused by the harmonic current flowing through the line impedance, to regulate the voltage at the PCC.

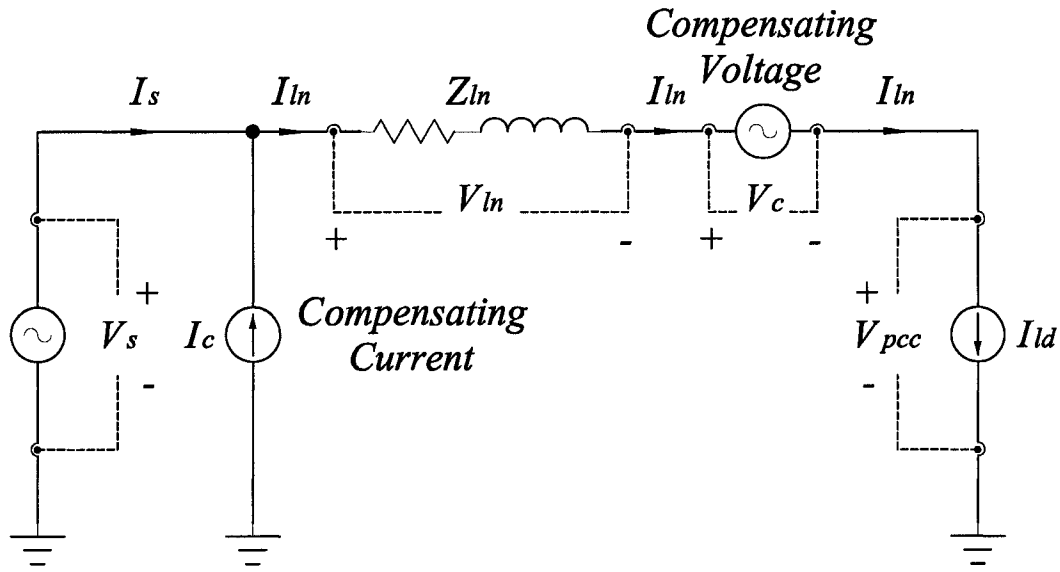

Figure 3.2: The single-phase equivalent circuit of the series-shunt compensation system

As usual, the utility supply is modeled as an ideal voltage source V_s. The current flowing along the line impedance Z_{ln} is I_{ln} and the voltage drop across Z_{ln} is V_{ln}. In order to prevent the source current I_s from being contaminated by the harmonic current drawn by the nonlinear loads, the shunt compensation current I_c has to be injected to supply the harmonic component I_{lnh} of the line current which is originally provided by the source current. In order to maintain the voltage at the PCC (V_{pcc}) almost sinusoidal, the series

compensation voltage V_c has to be injected to cancel the harmonic component V_{lnh} in the line voltage. The current source nonlinear load is modeled as a harmonic current source I_{ld} as before. The single-phase steady state analysis is a reasonable choice since the compensation of the three-phase system is achieved via independent compensation of each phase.

The voltage source V_s is treated as an ideal source supply which is expressed in (3.1) and the source current I_s could be represented by (3.2).

$$V_s = V_{s1} \tag{3.1}$$

$$I_s = I_{s1} + I_{sh} \tag{3.2}$$

where V_{s1} is the fundamental component of the voltage source, I_{s1} and I_{sh} are the fundamental and harmonic component of the source current respectively.

Since the nonlinear load draws the harmonic current from the voltage source, the nonlinear current will flow through the line impedance and the voltage distortion across the line, V_{ln} is obtained as follows:

$$I_{ln} = I_{ln1} + I_{lnh} \tag{3.3}$$

$$V_{ln} = V_{ln1} + V_{lnh} \tag{3.4}$$

$$V_{ln} = Z_{ln} \cdot I_{ln} = Z_{ln} \cdot (I_{ln1} + I_{lnh}) = Z_{ln} \cdot I_{ln1} + Z_{ln} \cdot I_{lnh} \tag{3.5}$$

where I_{ln1} and I_{lnh} are the fundamental and harmonic component of the line current respectively, V_{ln1} and V_{lnh} are the fundamental and harmonic component of the line

voltage respectively.

The source current and the voltage at the PCC are expressed as:

$$I_s = I_{ln} = I_{ld} = I_{ln1} + I_{lnh} = I_{ld1} + I_{ldh} = I_{s1} + I_{sh} \tag{3.6}$$

$$\therefore \quad I_{s1} = I_{ln1} = I_{ld1} \tag{3.7}$$

$$and \quad I_{sh} = I_{lnh} = I_{ldh} \tag{3.8}$$

$$V_{pcc} = V_s - V_{ln} = V_{s1} - (V_{ln1} + V_{lnh}) = (V_{s1} - V_{ln1}) - V_{lnh} = V_{pcc1} + V_{pcch} \tag{3.9}$$

$$\therefore \quad V_{pcc1} = V_{s1} - V_{ln1} \tag{3.10}$$

$$and \quad V_{pcch} = -V_{lnh} \tag{3.11}$$

where I_{ld1} and I_{ldh} are the fundamental and harmonic component of the load current respectively, V_{pcc1} and V_{pcch} are the fundamental and harmonic component of the voltage at the PCC respectively.

In order to remove the harmonic components of I_s, the compensation injection of the CCS, i.e. I_c, should be equal to the presumed current distortion I_{sh}. Similarly, the compensation injection of the VCS, i.e. V_c, should be equal to the measured voltage distortion V_{pcch} to maintain V_{pcc} free of harmonics. After the VCS and the CCS are applied into the circuit, the source current and the voltage at the PCC are given by:

$$I_s = I_{ln} - I_c = (I_{ln1} + I_{lnh}) - I_c = I_{ln1} + (I_{lnh} - I_c) = I_{s1} + I_{sh} \tag{3.12}$$

$$\begin{aligned} V_{pcc} &= V_s - V_{ln} - V_c = V_{s1} - (V_{ln1} + V_{lnh}) - V_c = (V_{s1} - V_{ln1}) - (V_{lnh} + V_c) \\ &= V_{pcc1} + V_{pcch} \end{aligned} \tag{3.13}$$

$$\therefore \quad I_{sh} = I_{lnh} - I_c = 0 \rightarrow I_c = I_{lnh} \tag{3.14}$$

$$and \quad V_{pcch} = -(V_{lnh} + V_c) = 0 \rightarrow V_c = -V_{lnh} \tag{3.15}$$

Equations (3.14) and (3.15) define which signals should be sensed using the RANN and also show the relationship between the reference signals and the output signals of the CCS and the VCS. According to (3.5) and (3.15), V_c can be derived from I_{lnh} without the extra sensing of line voltage, which can greatly simplify the structure of the whole series-shunt compensation system. However, the dependence on the line impedance restricts the flexibility of this application.

3.2 Performance of the Series-Shunt Compensation System under Various Conditions

The series-shunt compensation system has more complicated structure than the single VCS or CCS subsystem does, which leads to a more limited range for the parameter tuning. Hence the effect of harmonic order and sampling frequency on the compensation results would be investigated. The series-shunt compensation system is capable of mitigating voltage distortions and current harmonics regardless of its being single-phase system or three-phase system. Since the compensation of the three-phase system is achieved via three single-phase systems, the functionality of the three-phase system would effectively reflect the functionality of each single-phase subsystem. Therefore, the three-phase series-shunt compensation system would be investigated to illustrate the capability of the proposed algorithm and control method. The simpler load model was

used in obtaining the compensation results in order to reduce the number of equations to be solved and to speed up the simulation procedure. The more complex load model was then used to present a more realistic view of the system performance.

3.2.1 Effects of harmonic order and sampling frequency

The efficiency and accuracy of the RANN method depends on how close the estimated total harmonic components match the real values of the sensed signals. According to the algorithm in which the total harmonic components are calculated by subtracting the fundamental from the sensed signals, the precision of the fundamental component determines the precision of the complete compensation system. Another parameter considered to have impact on the compensation effect is the sampling frequency which defines how the source signals are sensed and discretized. The smaller sampling time should give more accurate and smoother estimation of the sensed signals, as well as harmonic replicas.

In order to verify these statements, the following three cases are considered:

- Case I: Up to 13^{th} harmonic order is used in the RANN and the sampling frequency is 7680 Hz
- Case II: Up to 13^{th} harmonic order is used in the RANN and the sampling frequency is 76800 Hz
- Case III: Up to 25^{th} harmonic order is used in the RANN and the sampling

frequency is 76800 Hz

The results are shown in Figures 3.3 to 3.5. Each figure shows the estimated fundamental component, the sampled line current and the error between the summation of all harmonic components and the total harmonic components derived from the subtraction method. The error is estimated in terms of the ratio to the fundamental magnitude of the line current.

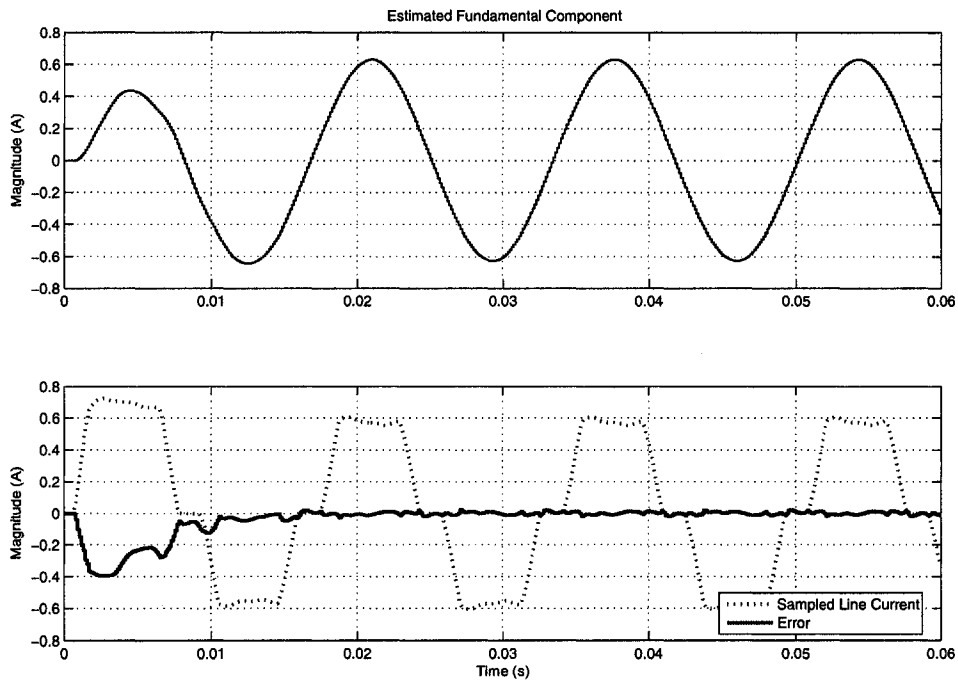

Figure 3.3: Case I: 13th harmonic order and sampling frequency of 7680 Hz (Phase A)

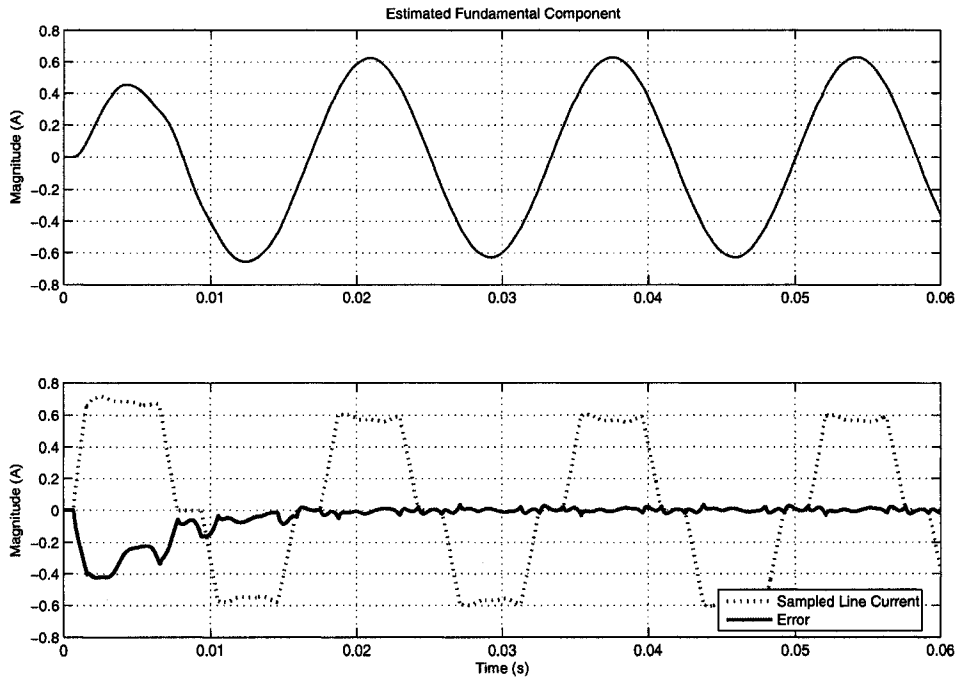

Figure 3.4: Case II: 13th harmonic order and sampling frequency of 76800 Hz (Phase A)

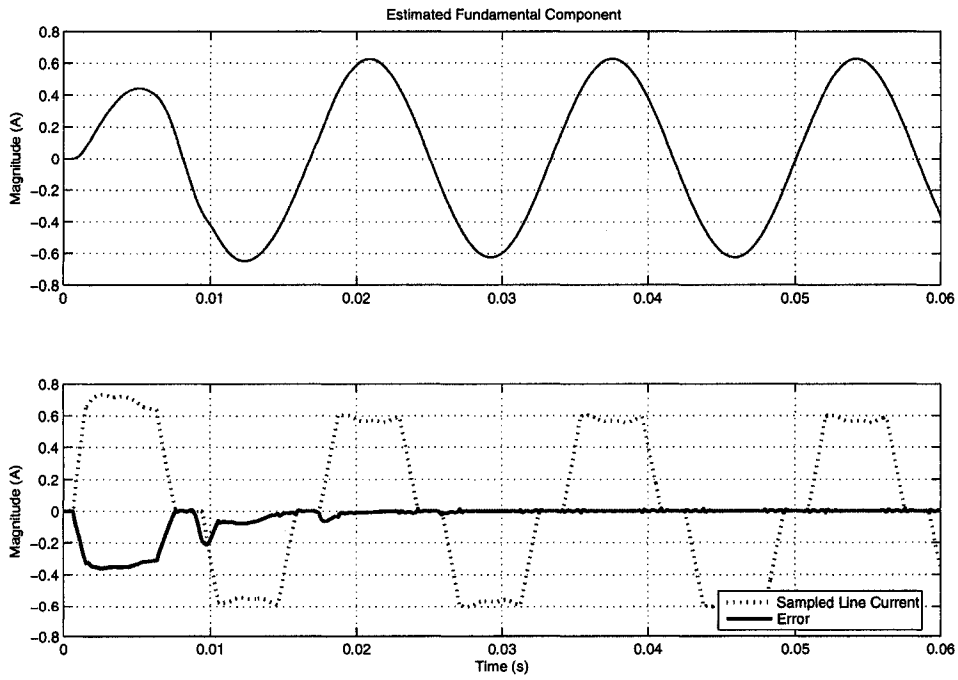

Figure 3.5: Case III: 25th harmonic order and sampling frequency of 76800 Hz (Phase A)

Compared with the Cases II and III, the fundamental component of Case I has the poorest quality due to the lower sampling frequency which causes the larger error at every discretized sampling step. When the sampling frequency increased ten times from 7680 Hz to 76800 Hz in Cases II and III, both estimated fundamental components are nearly pure sinusoidal waves and the error is decreased from the value of 0.40% of Case I to the value of 0.32% and 0.19% of Case II and Case III, respectively.

Certainly there is still some difference between Case II and Case III because of the changed maximum harmonic order. Compared with Cases I and II, Case III has the smallest error between the summation of all harmonic components and the total harmonic components derived from the subtraction method, which is shown in these figures. Given that the calculation of the fundamental component in the RANN is influenced by the interconnections among harmonic coefficients, the higher the harmonic order adopted in the RANN, the more accurate the fundamental estimation and the smaller the error between the total harmonic assessment and the real value.

In a word, the higher harmonic order estimation in the RANN and the smaller sampling time can lead to better harmonic extraction results and less errors, which is the cornerstone of the whole compensation system. However, the sampling frequency of 76800 Hz is high enough for power systems which are operated at the line frequency of 60 Hz. Adoption of the higher sampling frequency than 76800 Hz would not provide the

significant improvement in the harmonic extraction, it will greatly deteriorate the system response performance instead. The issue of computation workload of the RANN method with respect to harmonic order and sampling frequency needs further investigation. For the subsequent tests, the harmonic order and sampling frequency are selected as 25^{th} and 76800 Hz respectively.

3.2.2 Performance of the series-shunt compensation system with non-sinusoidal reference

A computer simulation model of the series-shunt compensation system is constructed in MATLAB using SIMULINK and SimPowerSystems blockset (see Appendix A) to verify its performance under various operating conditions. The nonlinear harmonic source is a current source three-phase diode bridge rectifier with an inductive load. The system specification and circuit parameters used in the simulation are presented in Table 3.1.

Table 3.1: System specification and circuit parameters (One phase)

AC Source Voltage, V_s	100 V (Peak)
DC Inverter Voltage, V_{DC}	250 V
Fundamental Frequency	60 Hz
Sampling Frequency	76,800 Hz
PWM Carrier Frequency	50 kHz
Load Resistance, R_L	100 Ω
Load Inductance, L_L	95 mH
Line Resistance, R_l	100 Ω
Line Inductance, L_l	2 mH
Outer Loop Gain for VCS Controller, k_{1V}	4
Inner Loop Gain for VCS Controller, k_{2V}	2
Outer Loop Gain for CCS Controller, k_{1C}	100
Inner Loop Gain for CCS Controller, k_{2C}	10

The performance of the series-shunt compensation system under normal operation was first investigated, i.e. there is no system disturbance of any form and the system is loaded by the balanced nonlinear load. Figures 3.6 and 3.7 show the waveforms and harmonic spectra of the three-phase line voltage and voltage at the PCC. Figures 3.11 and 3.12 show the waveforms and harmonic spectra of the three-phase line current and source current. The given spectra results in Figures 3.6(b), 3.7(b), 3.11(b) and 3.12(b) by SIMULINK include the interharmonics and subharmonics. VRANN and VAPF, CRANN and CAPF are the harmonic extraction unit and harmonic regeneration unit for voltage and current components respectively.

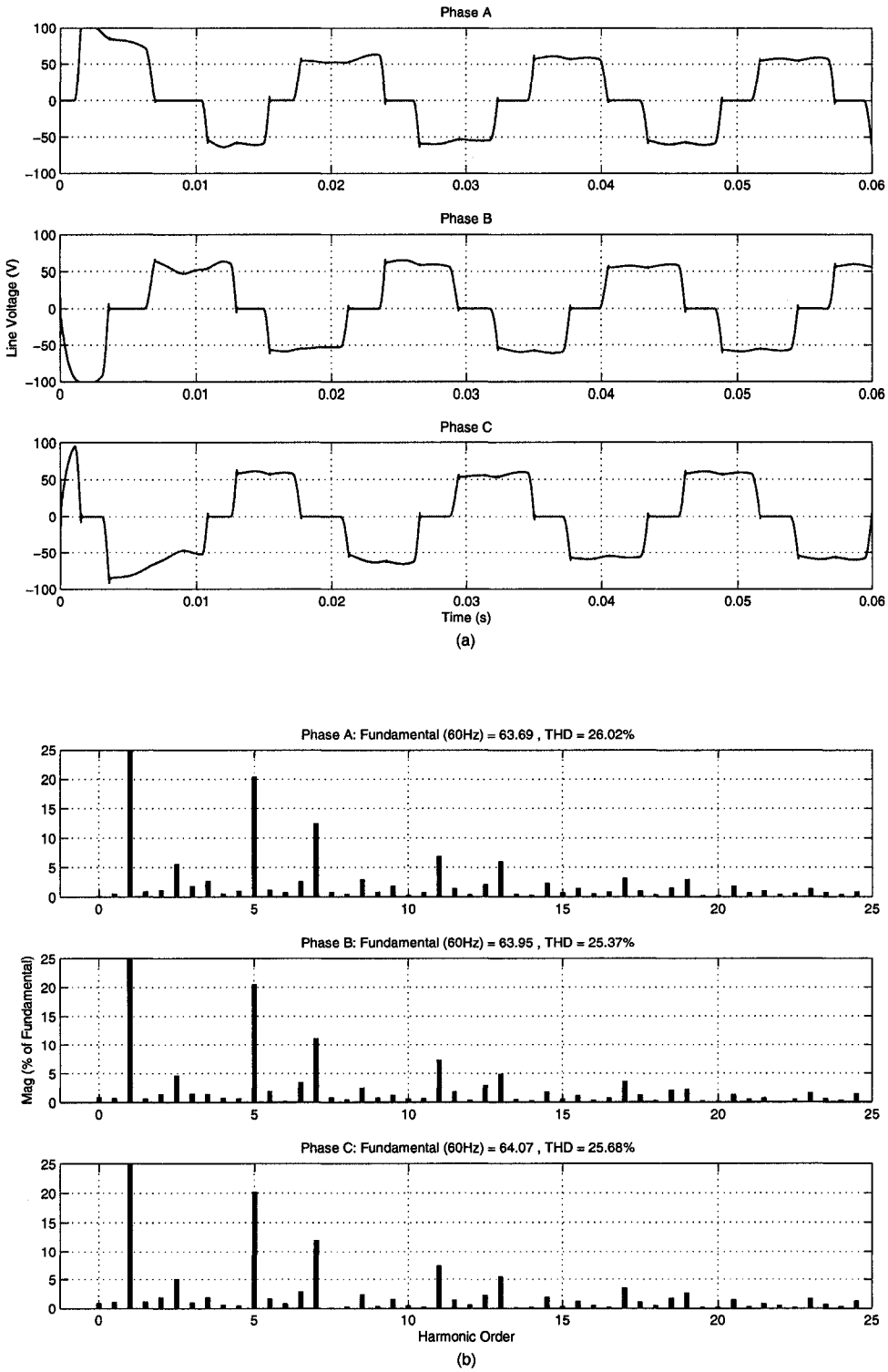

Figure 3.6: Performance of the system (a) Line voltage; (b) Harmonic spectra

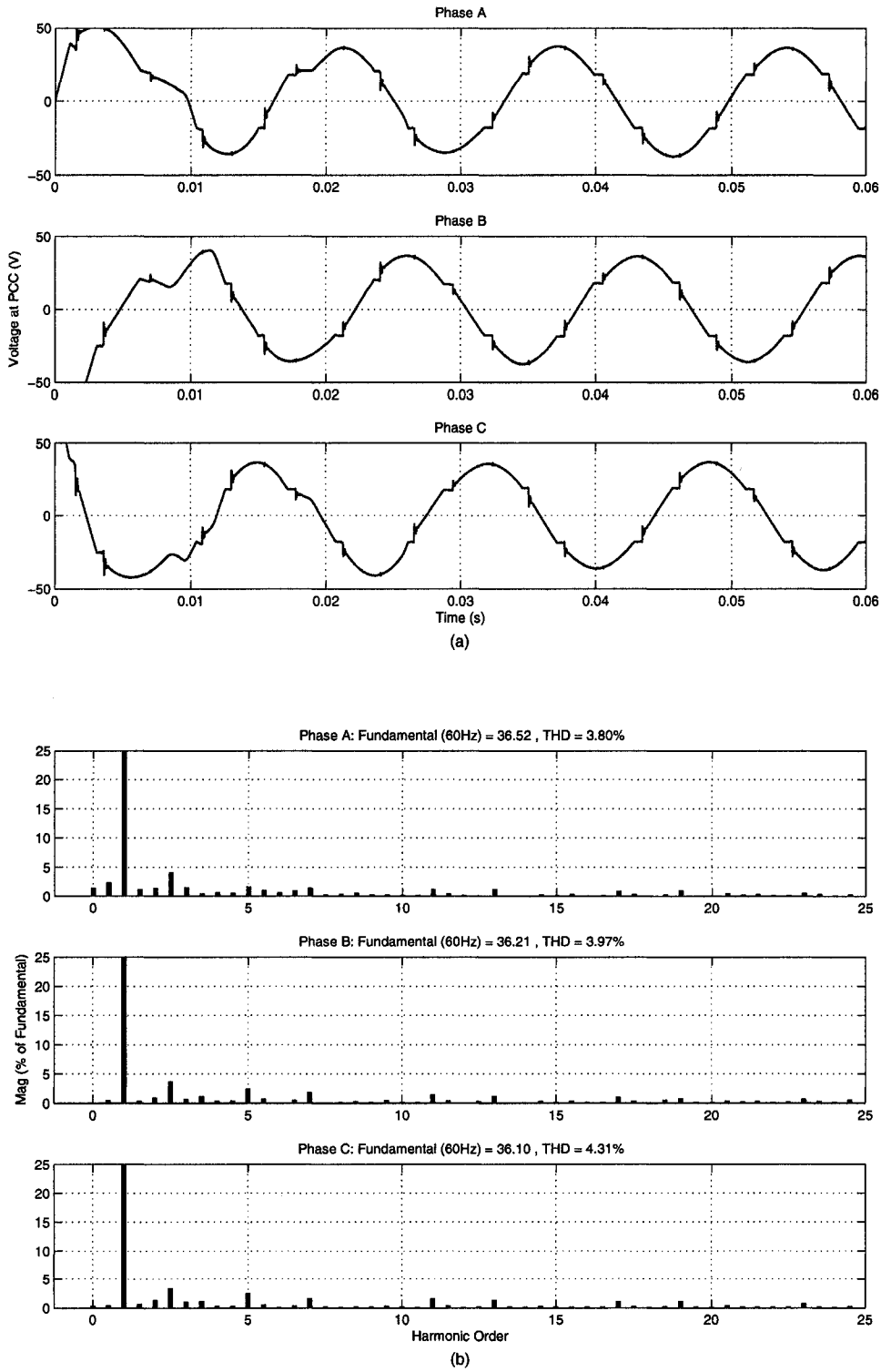

Figure 3.7: Performance of the system (a) Voltage at PCC; (b) Harmonic spectra

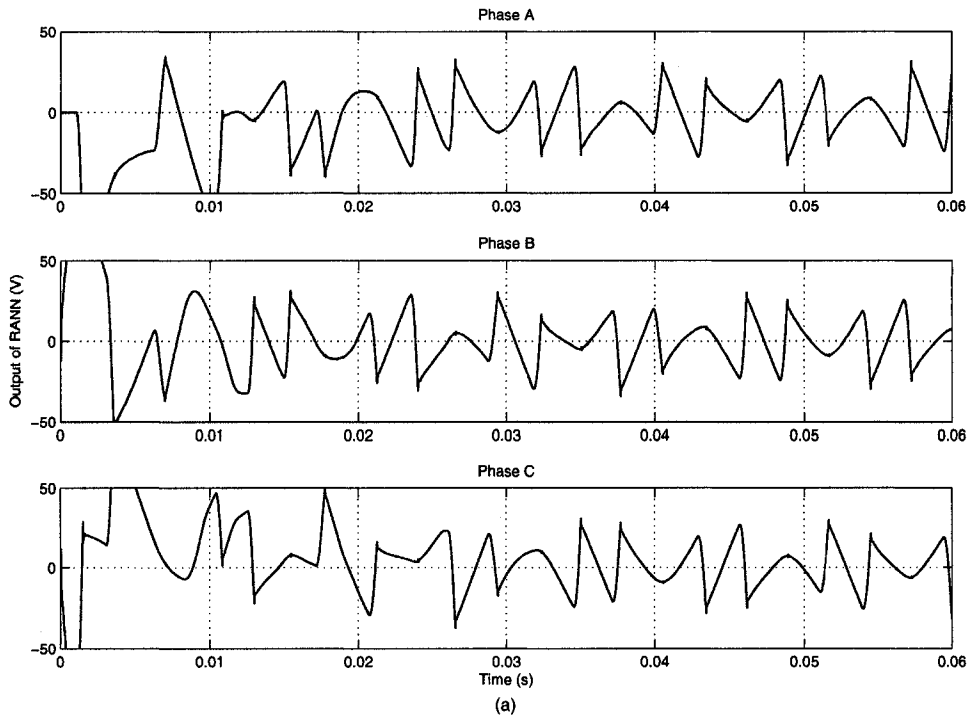

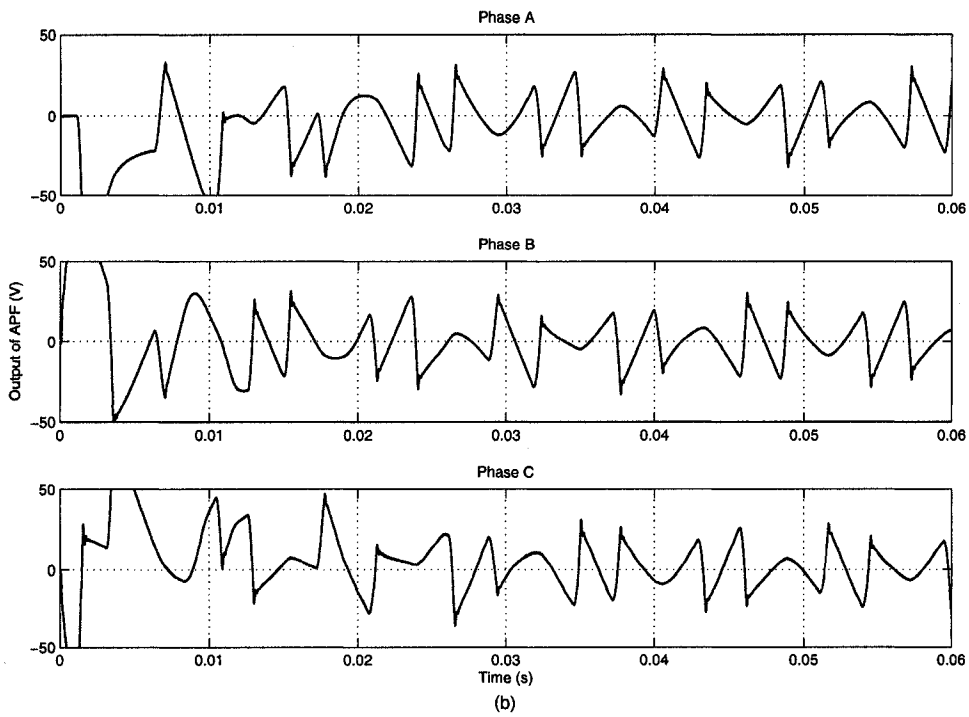

Figure 3.8: Performance of the system (a) Output of VRANN; (b) Output of VAPF

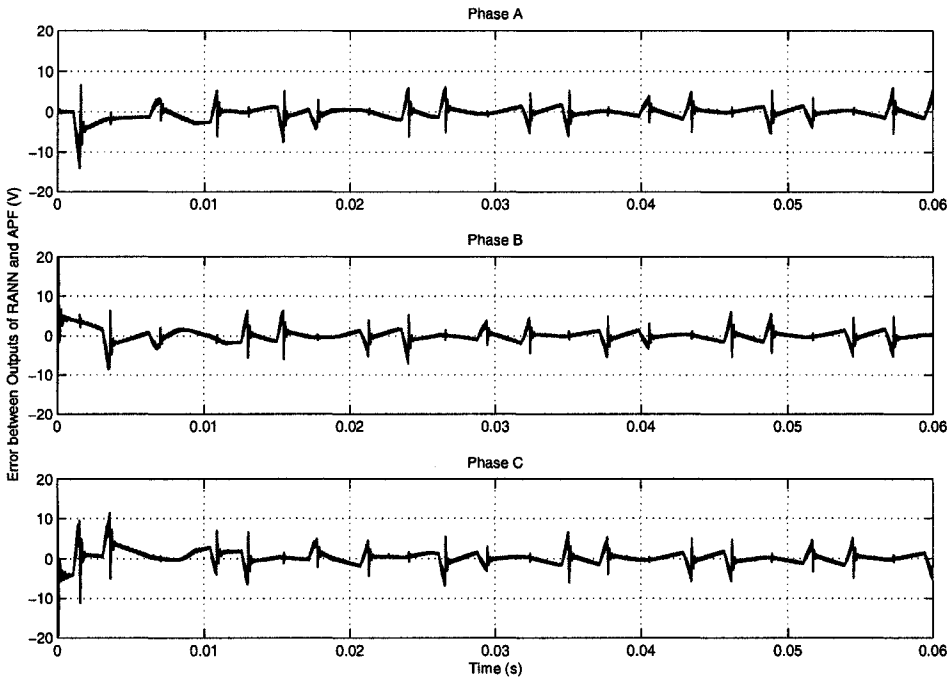

Figure 3.9: Error between the outputs of VRANN and VAPF

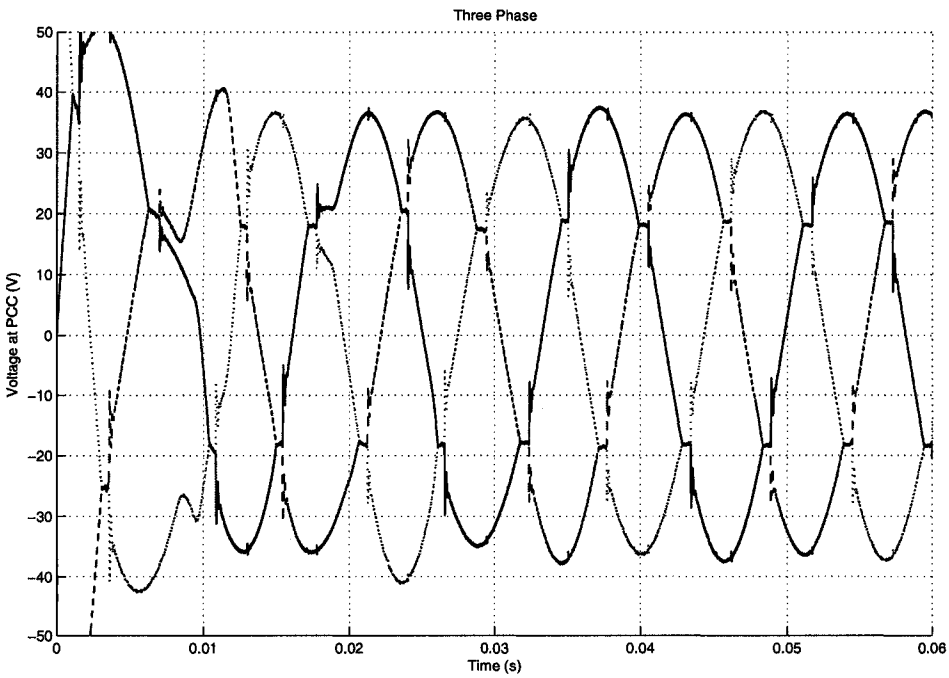

Figure 3.10: Compensated three-phase voltage at PCC

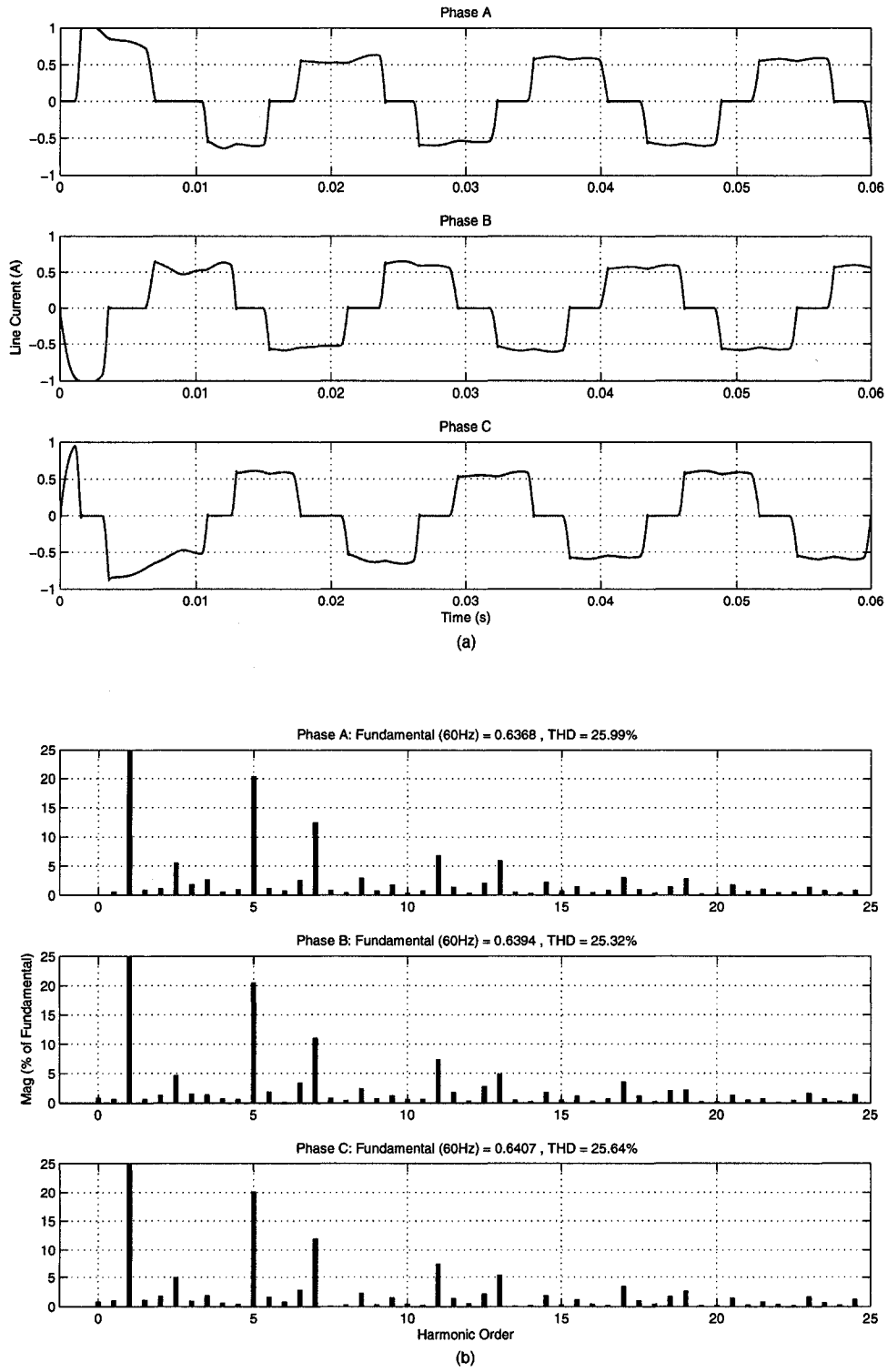

Figure 3.11: Performance of the system (a) Line current; (b) Harmonic spectra

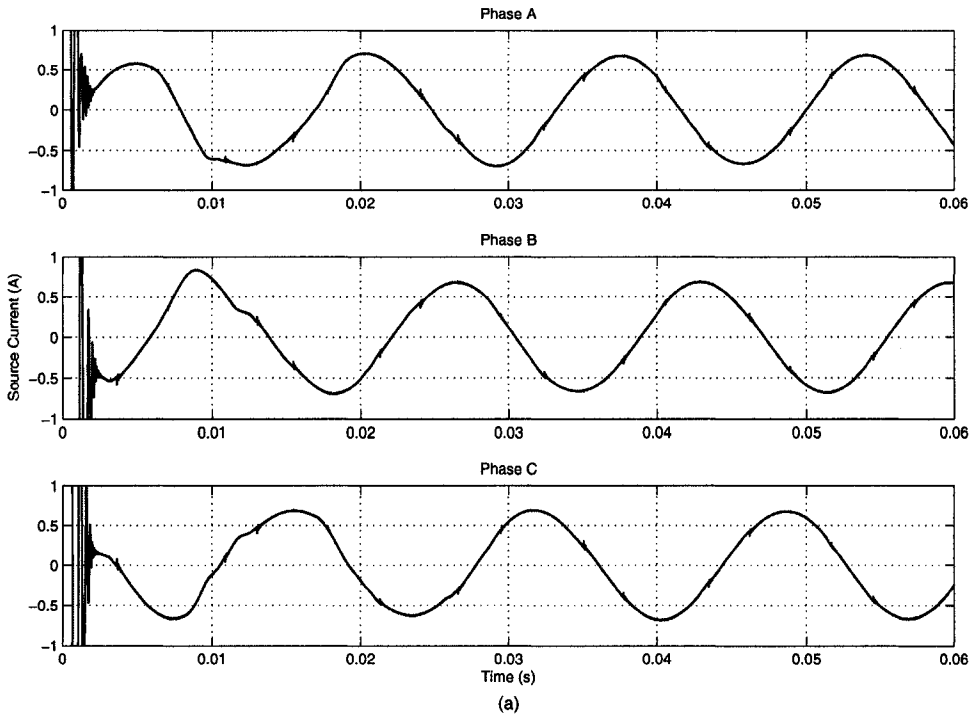

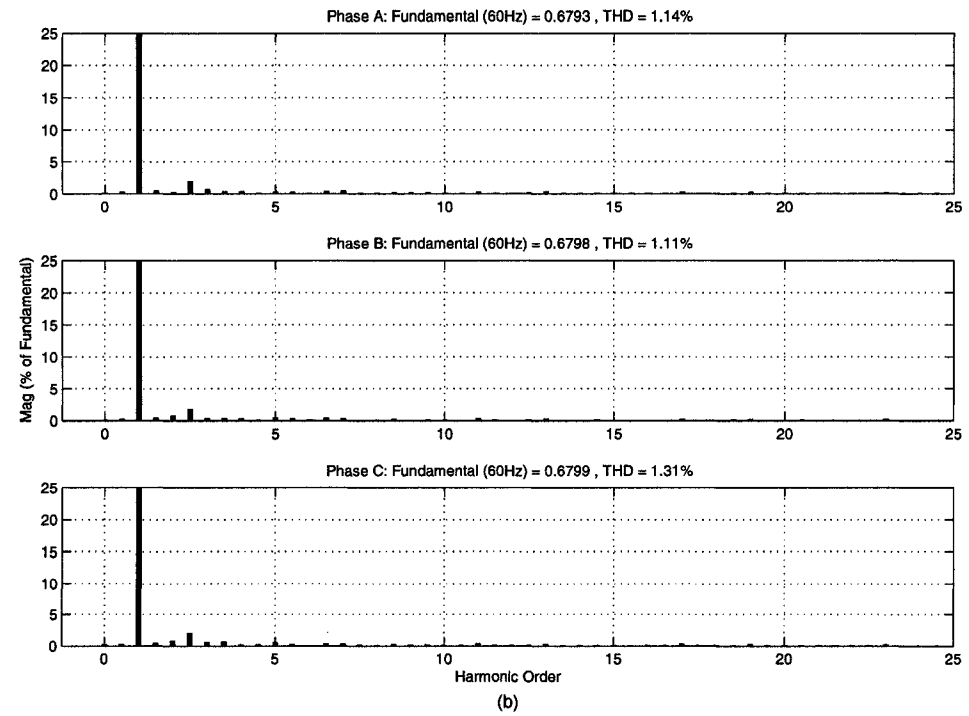

Figure 3.12: Performance of the system (a) Source current; (b) Harmonic spectra

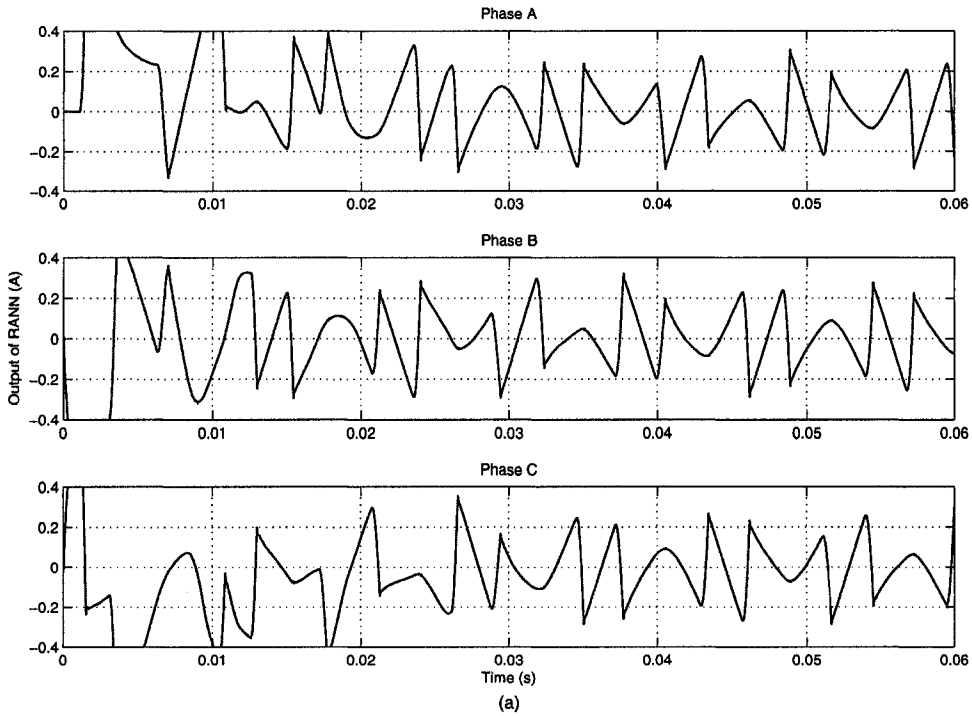

Figure 3.13: Performance of the system (a) Output of CRANN; (b) Output of CAPF

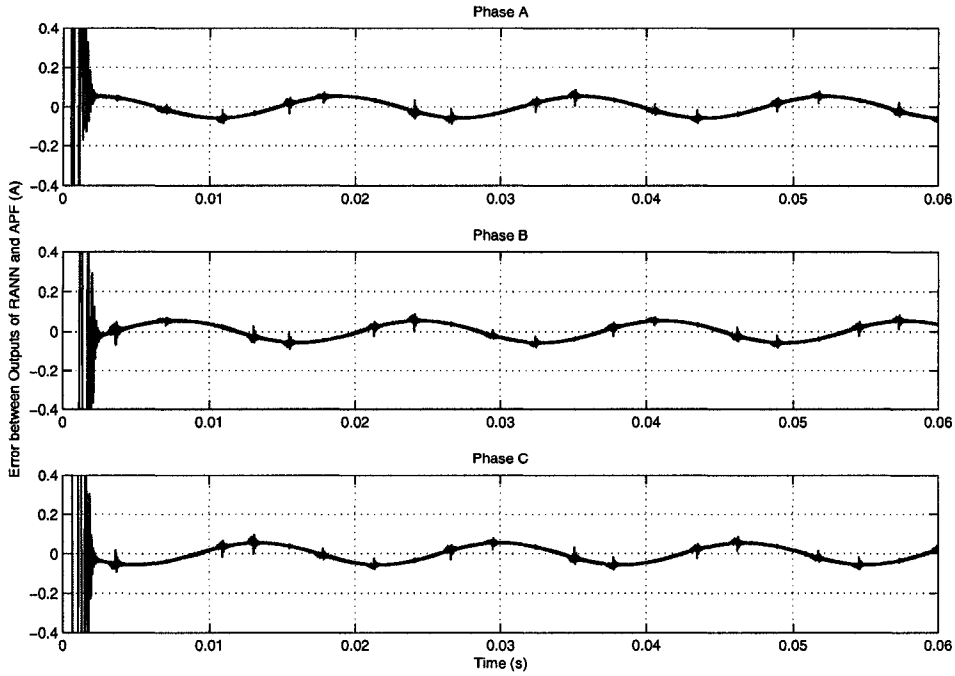

Figure 3.14: Error between the outputs of CRANN and CAPF

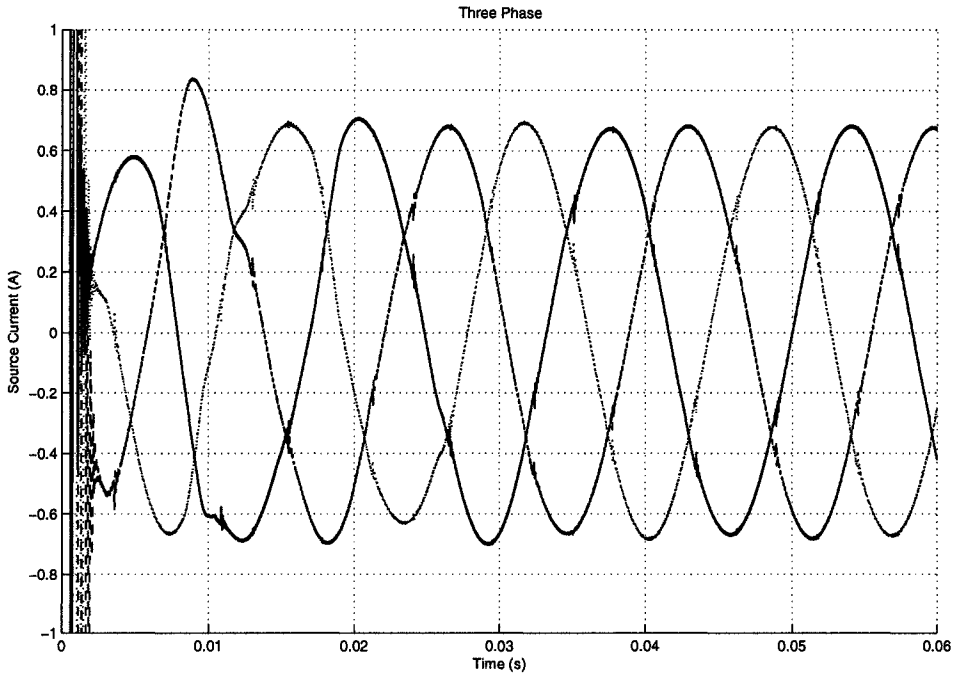

Figure 3.15: Compensated three-phase source current

Since the results of phase A, phase B and phase C are similar and evenly phase-shifted by 120 degrees under normal operation, the following analysis will be focused on phase A only. For phase A, the total line voltage harmonic distortion is determined as 26.02% from Figure 3.6(b) while the total line current harmonic distortion is determined as 25.99% from Figure 3.11(b). On the other hand, the THD of the voltage at the PCC is obtained from Figure 3.7(b) as 3.80% and the THD of the source current is obtained from Figure 3.12(b) as 1.14%. Both figures successfully meet the recommended harmonic specifications of IEEE Standard 519-1992 [2]. The results of phase B and phase C fulfill this mandatory requirements as well. Figure 3.7(a) and Figure 3.12(a) show that the series-shunt compensation system can remove the harmonics from the voltage at the PCC and the source current successfully within about one-and-half fundamental cycles which verifies the system has very fast dynamic response.

From the obtained results, the series-shunt compensation system has the capability of compensating for nonlinear line voltage and line current distortions, and maintaining the voltage at the PCC and the source current almost sinusoidal at the same time. This could be predicted from the series-shunt system's structure. From the point of view of the VCS, the presence of the CCS does not change the way of sensing and injecting signals because the CCS is placed in front of the VCS. From the point of view of the CCS, the presence of the VCS does not alter the low-impedance byway for the harmonic components

generated by the nonlinear loads due to the fact that the VCS is treated as an ideal voltage source. The system is thus able to prevent the voltage harmonic distortion from spreading beyond the point of common coupling and the source current from being contaminated by current harmonics.

Figure 3.8(a) shows the compensating voltage reference signals and Figure 3.13(a) shows the compensating current reference signals, which are generated by the VRANN and the CRANN harmonic extraction unit respectively. Figure 3.8(b) and Figure 3.13(b) illustrates the compensation voltage and current signals regenerated by the VAPF and CAPF respectively, which are then injected into the main grid by the coupling transformer. Figure 3.9 and Figure 3.14 show the error signals between the references and outputs of the series-shunt compensation system. The figures show that the output signals follow the reference signals closely to guarantee the satisfactory compensation performance. Certainly the more complicated structure increases the computation workload that has been reflected by the slightly increasing settling time. Moreover, adding more subsystems makes it more difficult to tune the control parameters to reach the feasible and reliable solution.

3.2.3 Performance of the series-shunt compensation system with more complex loads

The simpler load was used in obtaining the simulation results of the previous section in order to reduce the number of equations to be solved and to speed up the simulation time. The more complex loads were then used in this section to present a more realistic view of the system performance. The nonlinear load consists of two components which are connected in shunt with each other. The first component is a three-phase six-pulse full-bridge thyristor-based rectifier with a RL load and the second component is a three-phase back-to-back full-wave thyristor-based voltage controller with RL loads. The typical industrial applications of thyristor-based controlled rectifiers include DC motor speed control systems, electrochemical and electrometallurgical processes, magnet power supplies and converters at the input end of DC transmission lines. The applications of thyristor-based voltage controllers include industrial heating, lighting controls, transformer tap changing and speed control of induction-motor driven pumps and fans. The details of the loads are given in Appendix A. The simulation results are presented in Figures 3.16 to 3.25.

The given spectra results in Figures 3.16(b), 3.17(b), 3.21(b) and 3.22(b) by SIMULINK include the interharmonics and subharmonics.

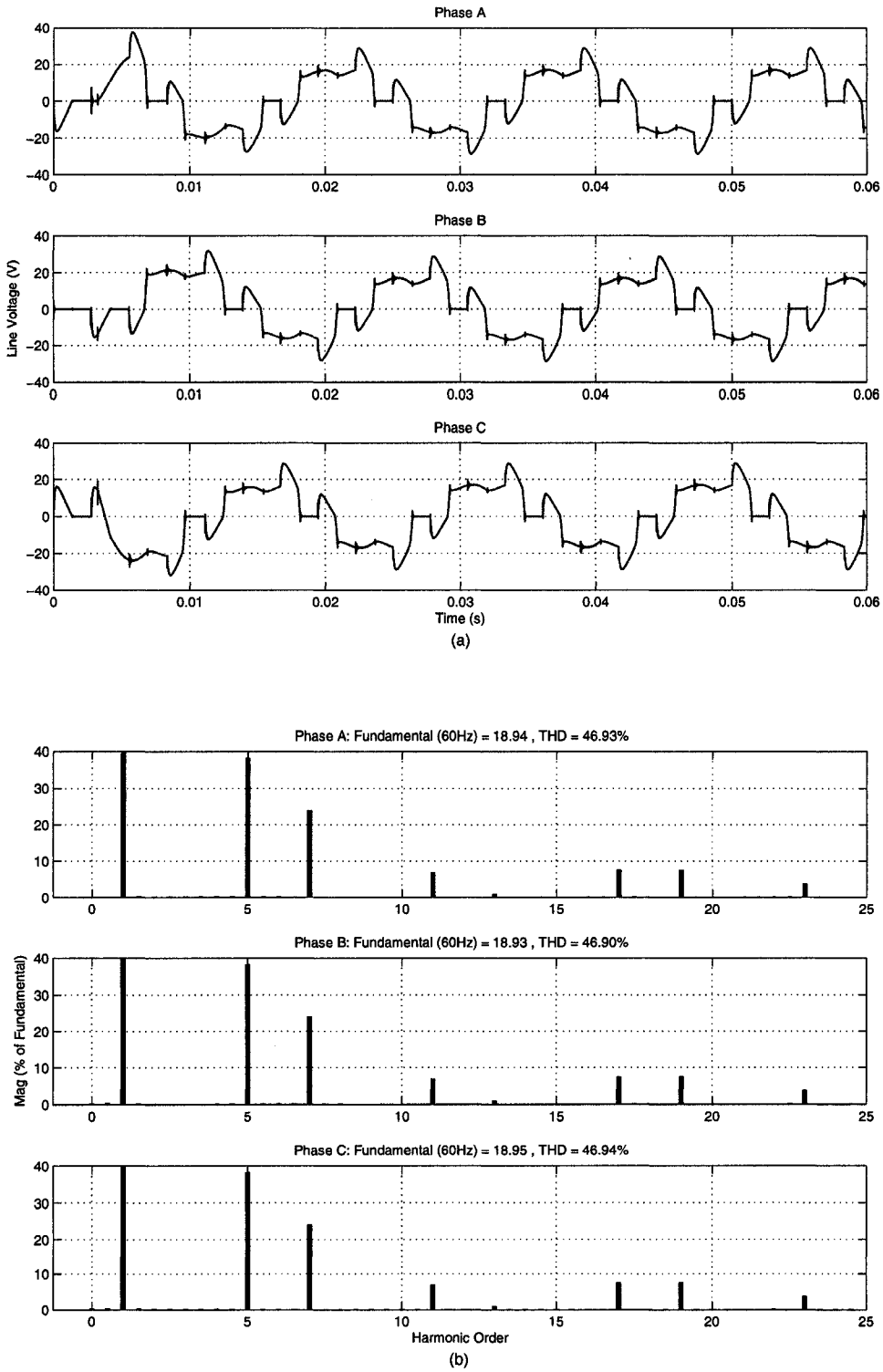

Figure 3.16: Performance of the system (a) Line voltage; (b) Harmonic spectra

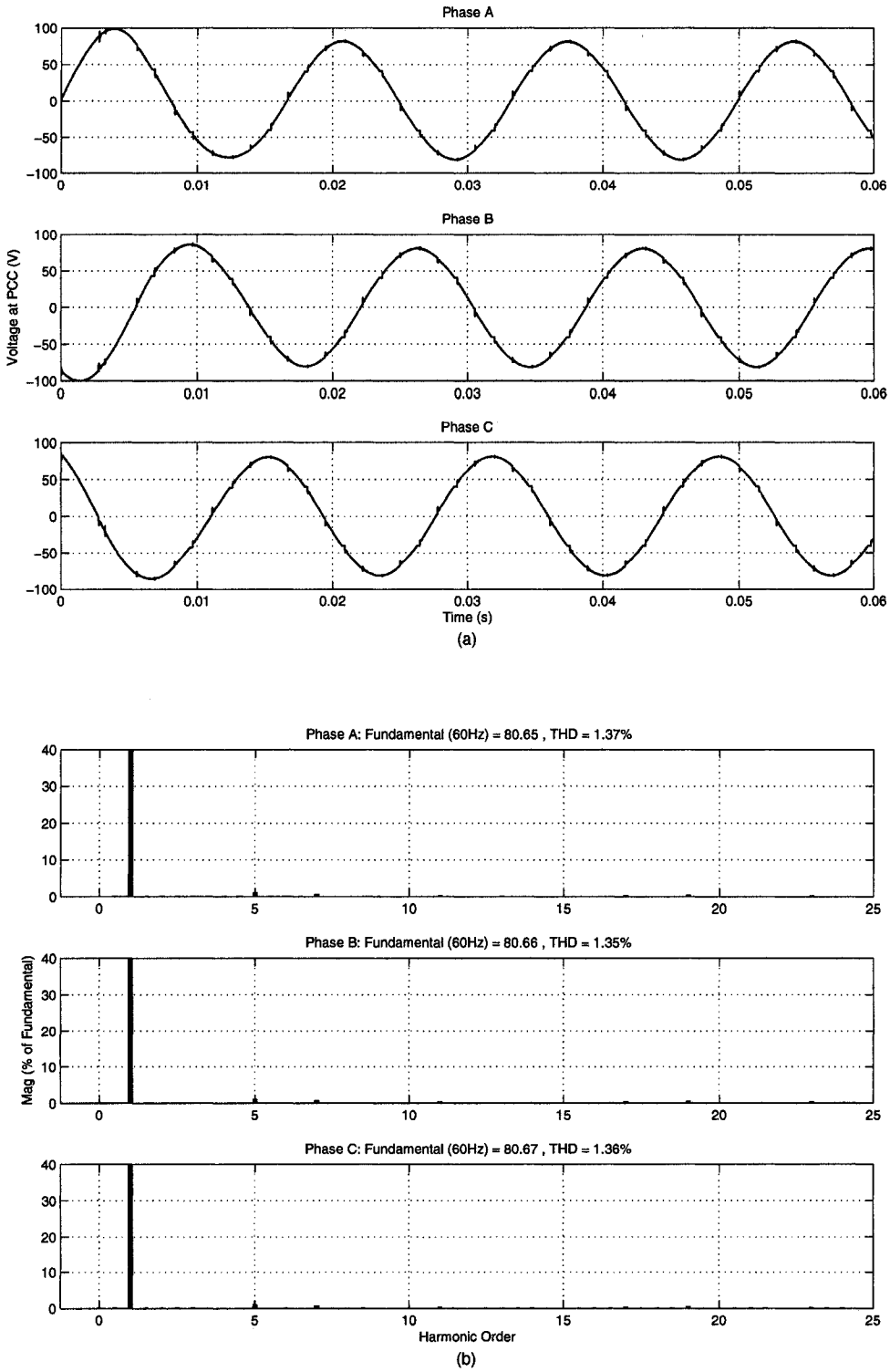

Figure 3.17: Performance of the system (a) Voltage at PCC; (b) Harmonic spectra

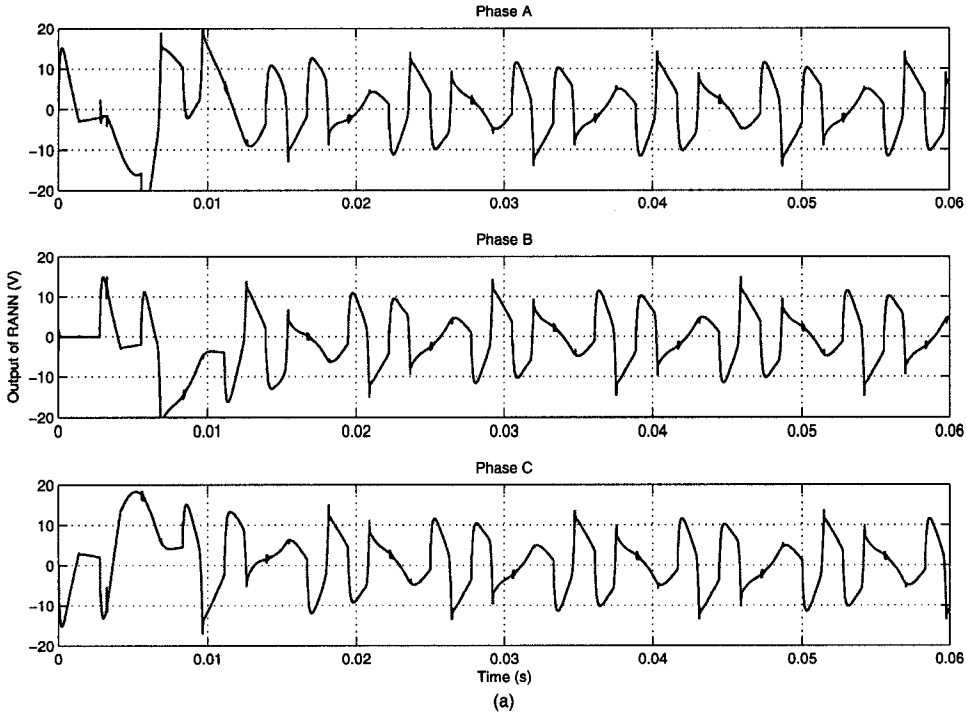

Figure 3.18: Performance of the system (a) Output of VRANN; (b) Output of VAPF

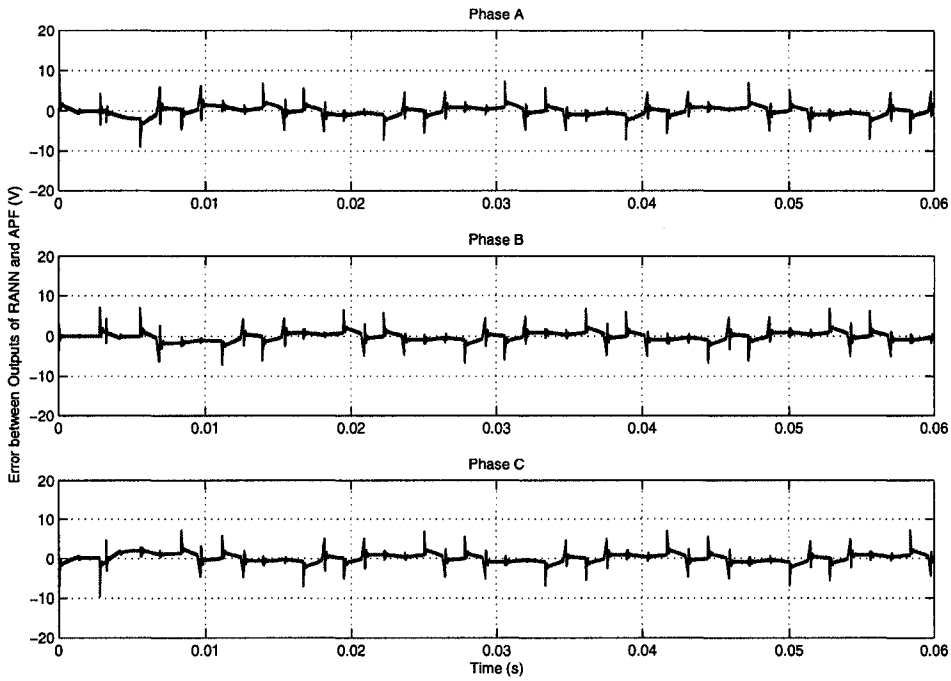

Figure 3.19: Error between the outputs of VRANN and VAPF

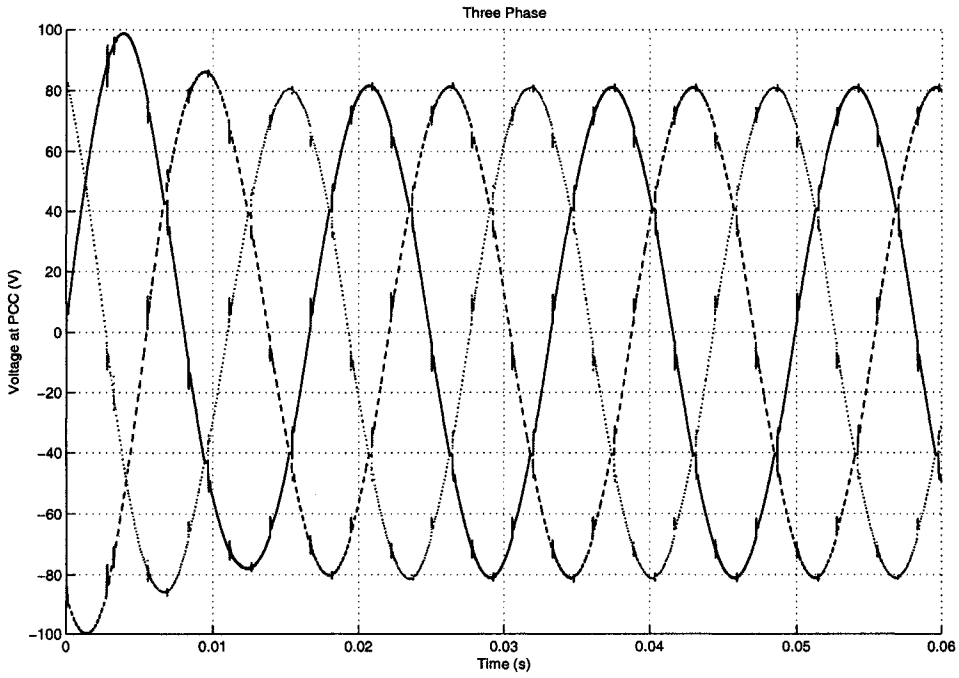

Figure 3.20: Compensated three-phase voltage at PCC

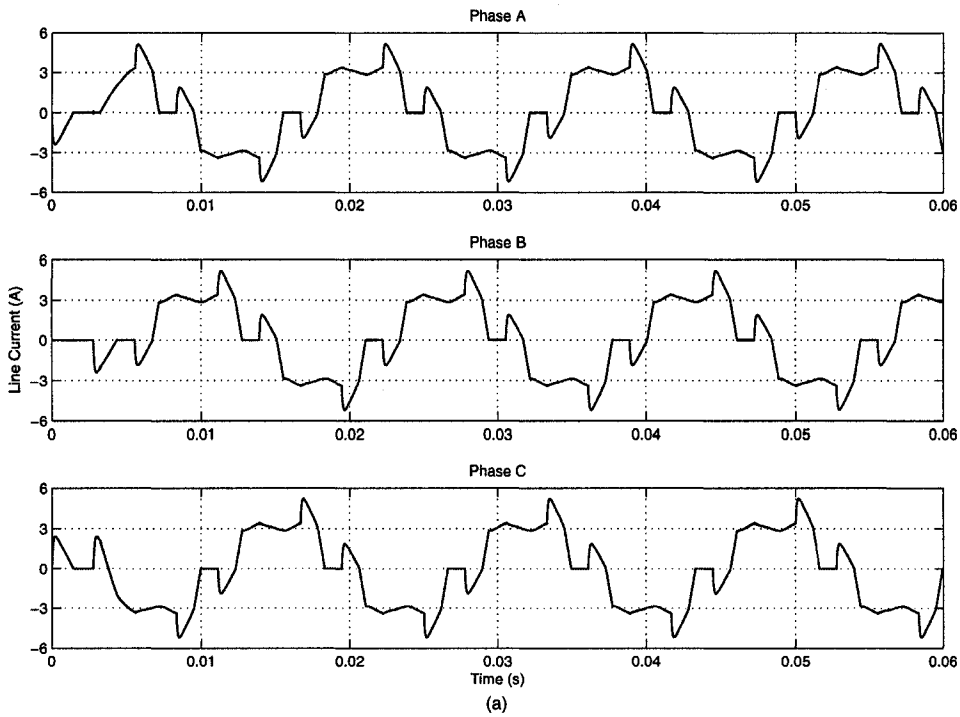

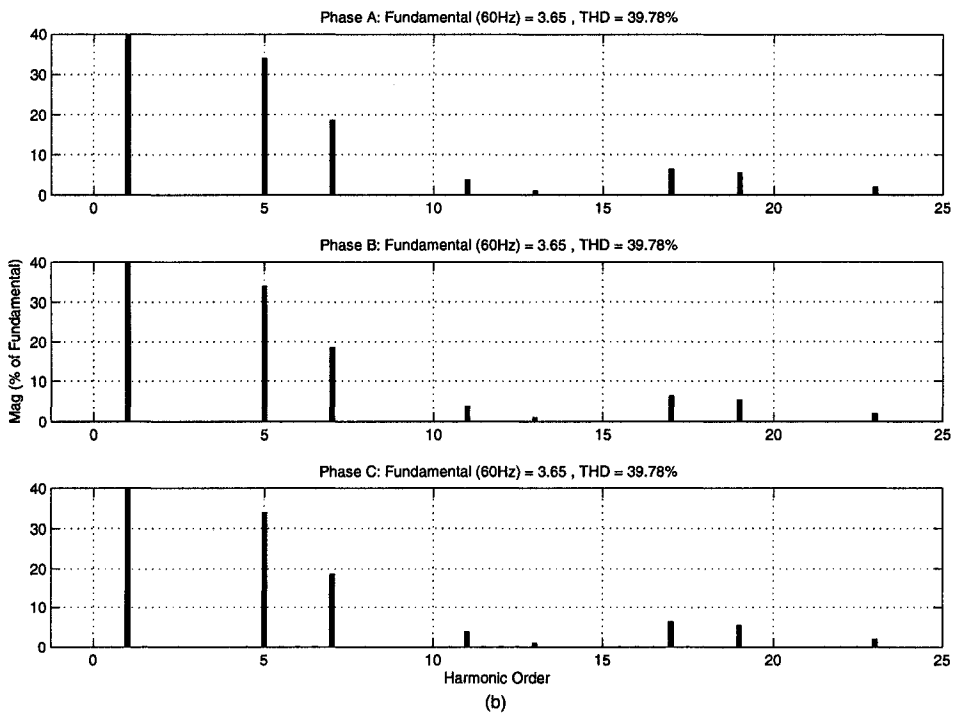

Figure 3.21: Performance of the system (a) Line current; (b) Harmonic spectra

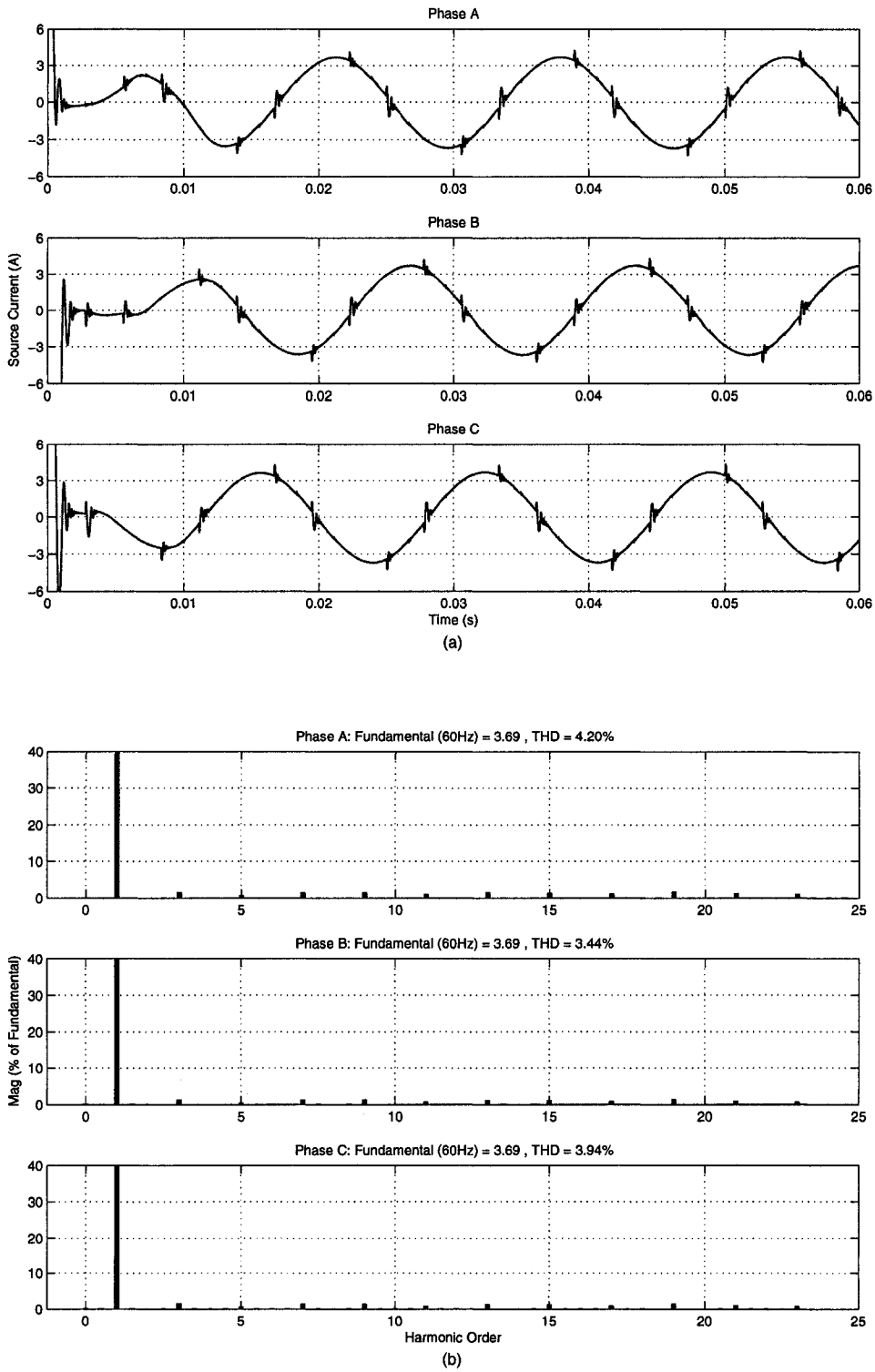

Figure 3.22: Performance of the system (a) Source current; (b) Harmonic spectra

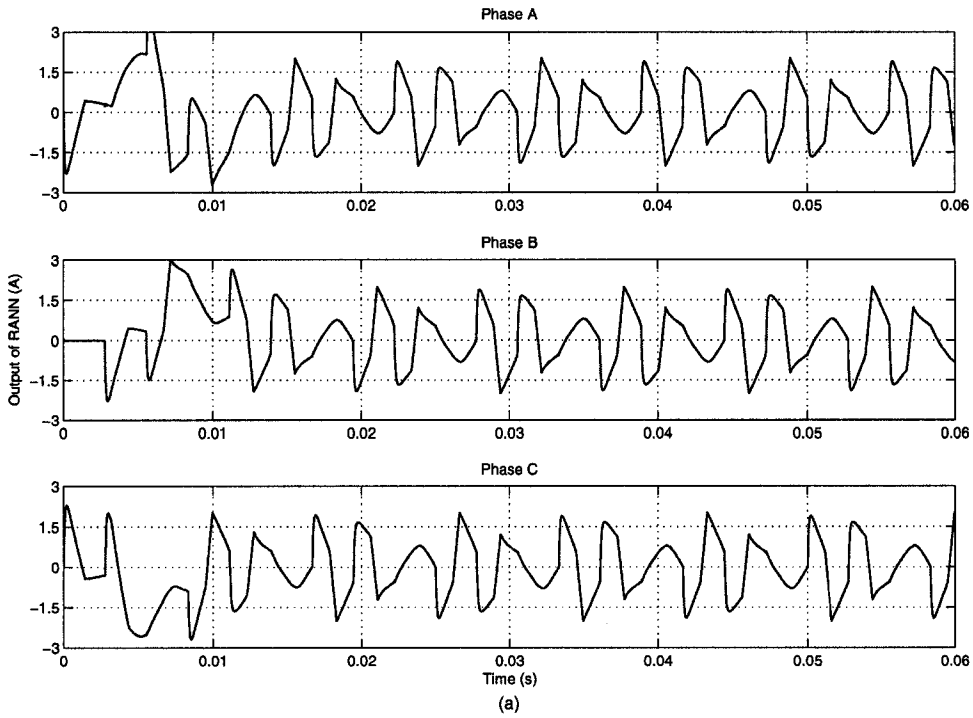

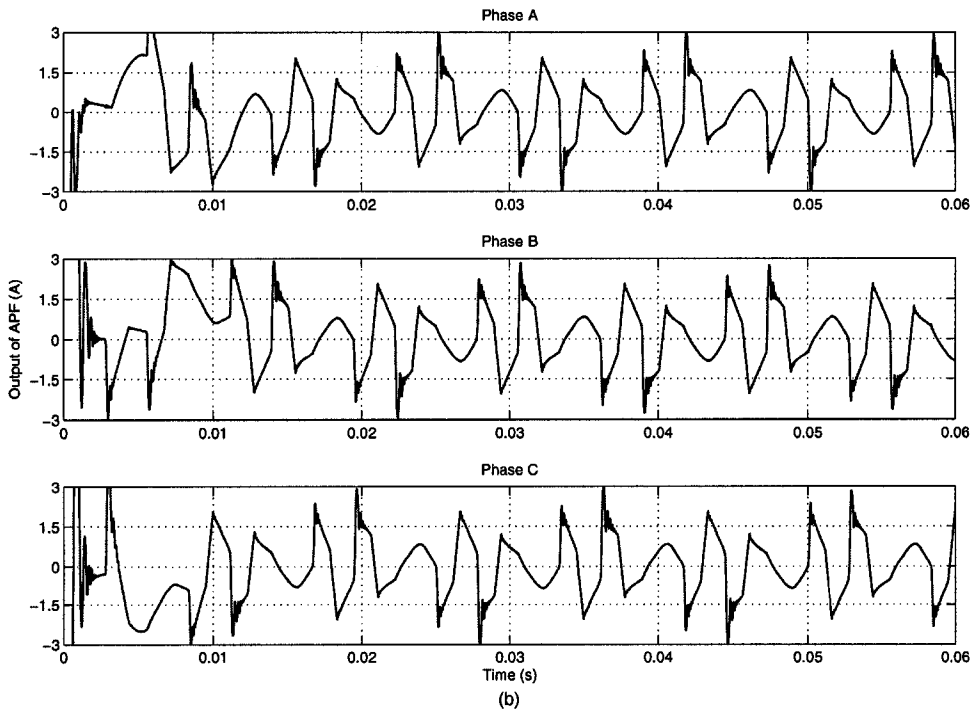

Figure 3.23: Performance of the system (a) Output of CRANN; (b) Output of CAPF

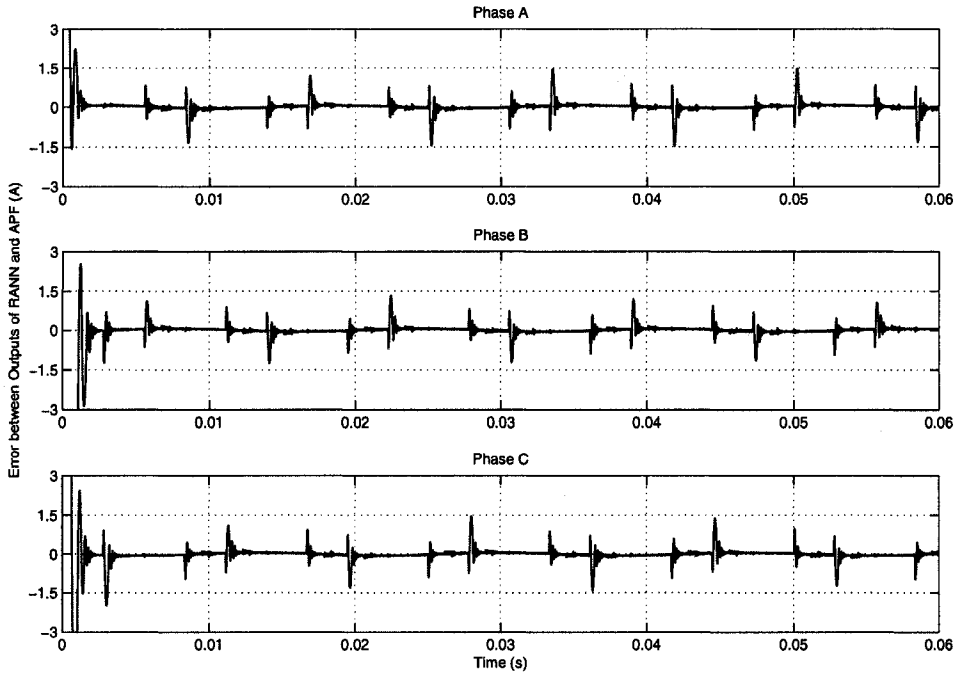

Figure 3.24: Error between the outputs of CRANN and CAPF

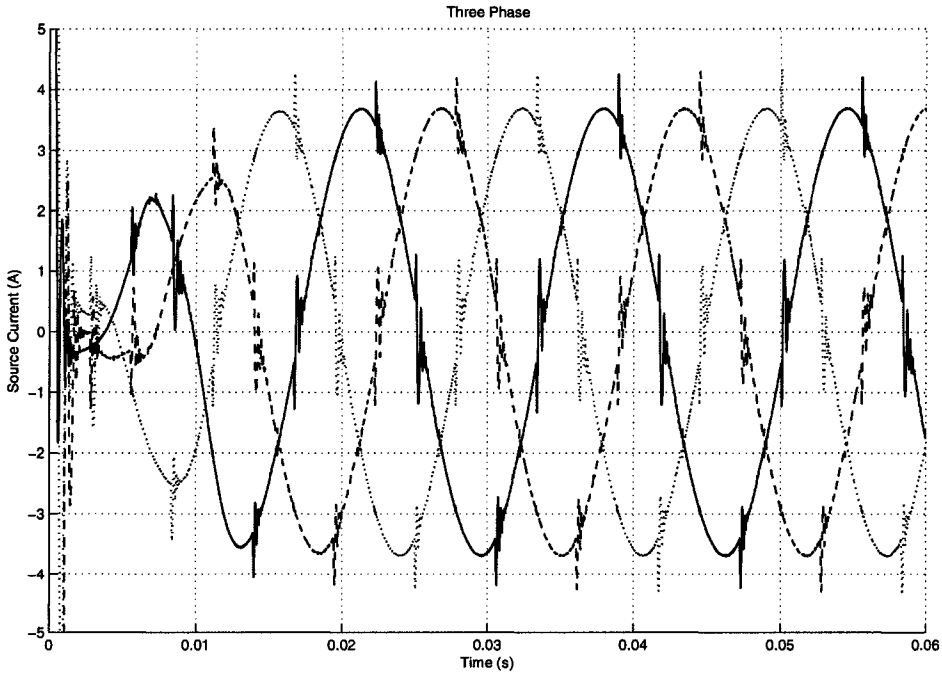

Figure 3.25: Compensated three-phase source current

For phase A, the total line voltage harmonic distortion is determined as 46.93% from Figure 3.16(b) while the total line current harmonic distortion is determined as 39.78% from Figure 3.21(b). On the other hand, the THD of the voltage at the PCC is obtained from Figure 3.17(b) as 1.37% and the THD of the source current is obtained from Figure 3.22(b) as 4.20%. Although the THD levels before compensation are around 1.5 times higher than those of the case with simpler load, both figures after compensation still successfully meet the recommended harmonic specifications of IEEE Standard 519-1992 [2]. These results illustrate that the proposed series-shunt compensation system is quite effective and efficient with more complex load models, which verifies the feasibility of the compensation method in more realistic applications.

3.3 Performance of Preprocessing Unit

In Chapter 2, the simulation results showed that the simple VCS and CCS cannot compensate for the source-end distortions such as voltage sag, voltage swell or voltage flicker without additional assistance. The worse situation is that the power supply may sustain some imbalance interference as well. Compared to three-phase balanced voltage sources which have equal magnitudes and an equal 120 degree phase difference between any two phases, three-phase unbalanced voltage sources have unequal magnitudes or have unequal phase difference between any two phases. In the unbalanced case, the unbalanced voltage source will affect the electrical quantities in the system, including the

fundamental component and the harmonic components in both magnitude and phase angle.

Under the conditions of source-end imbalance and distortion, the RANN method will lose the proper reference signals, and while the compensated signals would be harmonic free they would remain unbalanced. One feasible approach is to introduce a preprocessing unit between the unbalanced power supply and the main power grid. This unit will sense the source voltage and then compare it to the preset standard reference value to determine if the preprocessing unit needs to be launched to correct the imbalance in the source voltage before it is applied to the main power grid. The preprocessing unit uses the same control scheme as the VCS and CCS to generate the required compensation signals. There is no need to facilitate the RANN in this pre unit due to the absence of harmonics, which would greatly reduce the preprocessing time to a negligible level. More generally, if the power supply is some kind of sub supply such as the secondary side of the step-down transformer which might be contaminated by the primary side harmonics, the RANN could be insert into the preprocessing unit to handle the source-end harmonic problem. Figure 3.26 illustrates the single-phase schematic configuration of this preprocessing unit. The unbalanced conditions are given in Table 3.2.

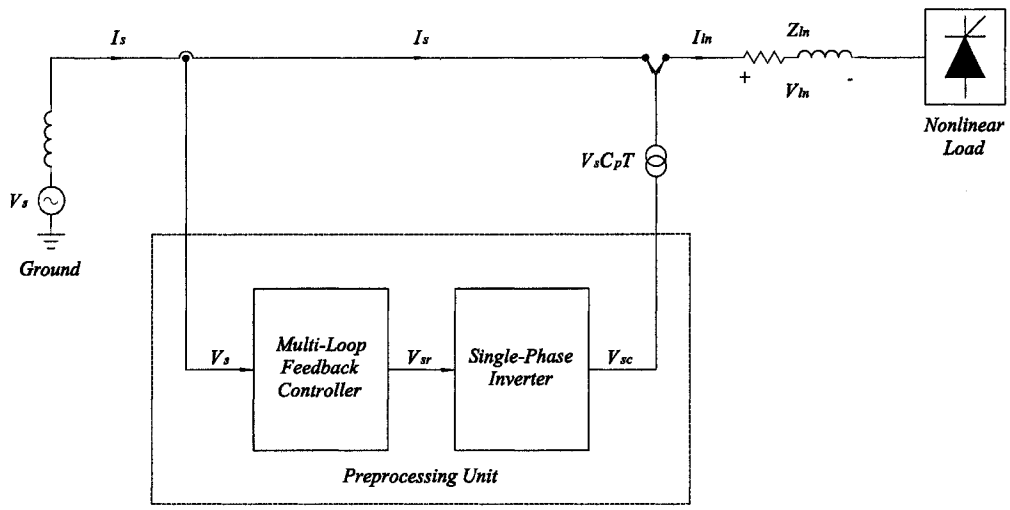

Figure 3.26: The single-phase schematic configuration of the preprocessing unit

Figure 3.27(a) and Figure 3.27(b) show three-phase unbalanced source voltages and three-phase compensated source voltages respectively. It is seen that the unbalanced potions are completely removed from the power supply after the pretreatment, which resulting in pure sinusoidal balanced source voltages that are then applied to the main grid. The preprocessing unit is totally tuning-free regardless of the degree of imbalance as long as the desired balanced source voltages are unchanged and the fast dynamic response guarantees the transient could be ignored. Figures 3.28 to 3.30 give more detailed comparison between the input signals and output signals of the preprocessing unit.

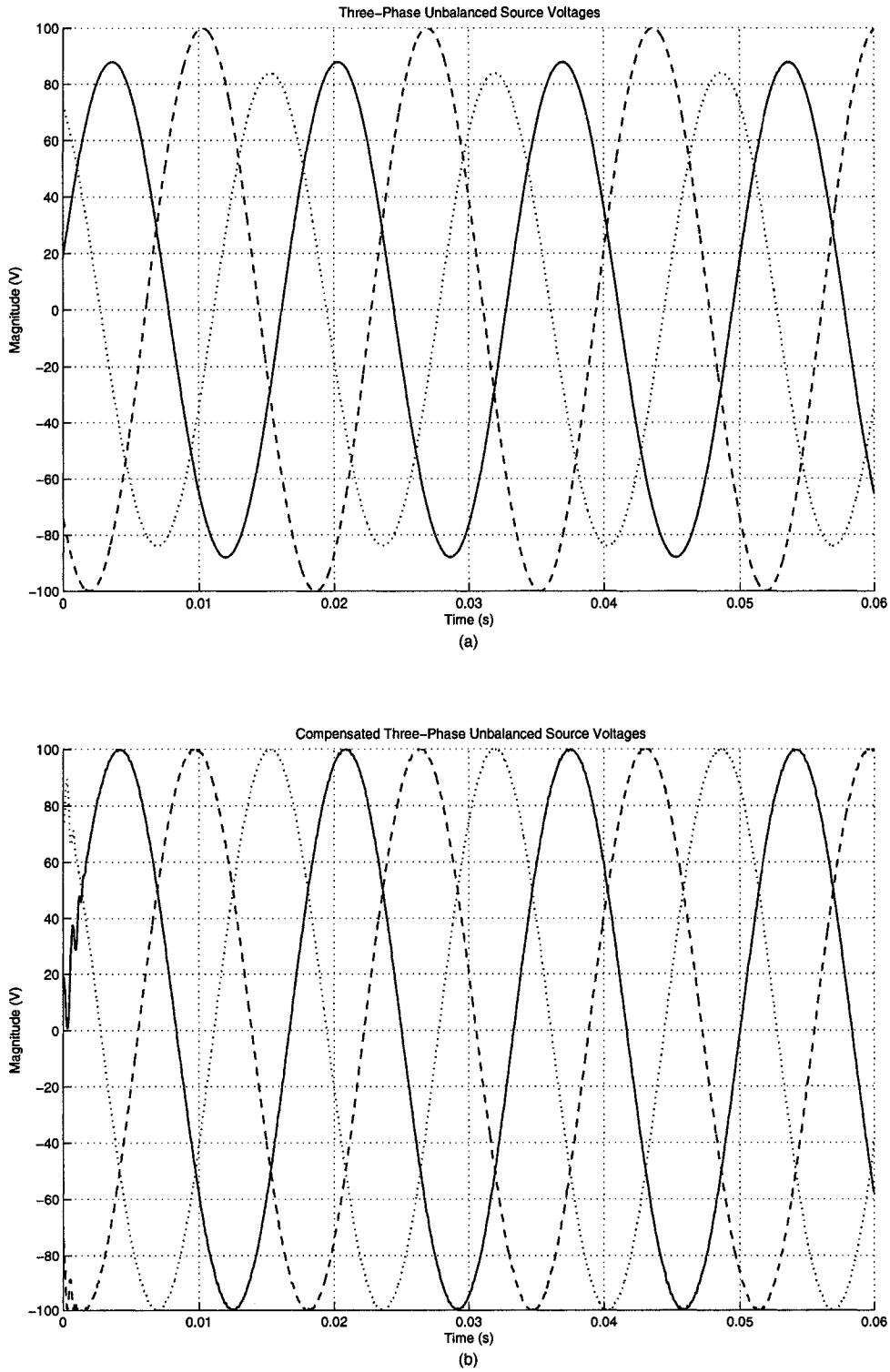

Figure 3.27: Three-phase source voltages (a) Unbalanced; (b) Compensated

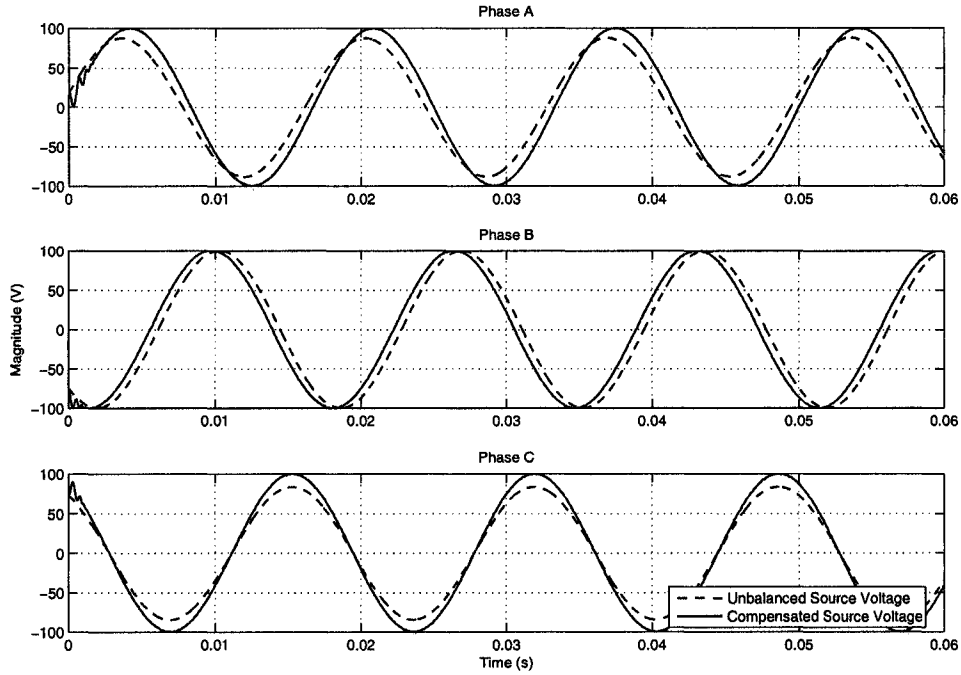

Figure 3.28: Three-phase unbalanced and compensated source voltages

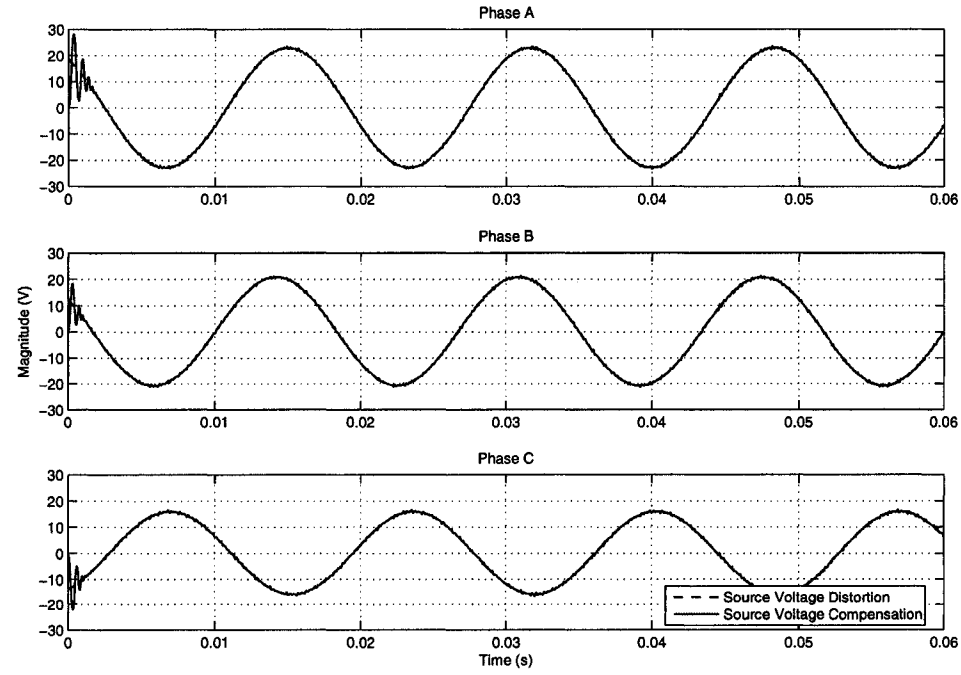

Figure 3.29: Three-phase source voltage distortion and compensation

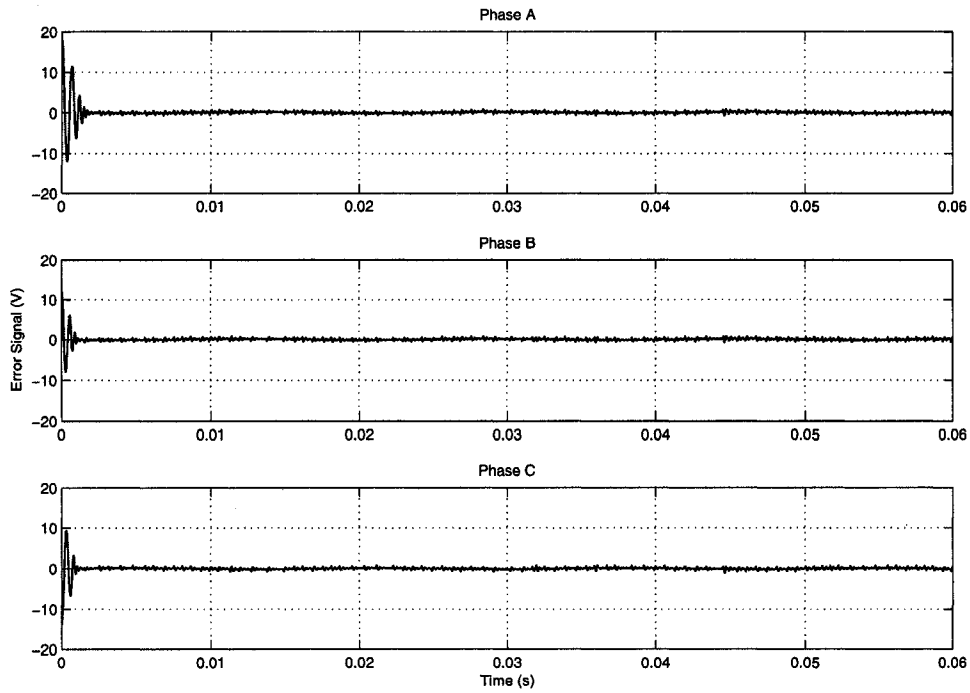

Figure 3.30: Error between the distorted and compensated signals

Table 3.2: Unbalanced voltage source parameters

Voltage Source	Magnitude (V)	Phase Angle (degree)
Normal Values (A/B/C)	100/100/100	0/-120/120
Phase A	88	12
Phase B	100	-132
Phase C	84	120

According to the principle of the preprocessing unit, the source-end distortion problem such as voltage sag, voltage swell or voltage flicker could be fully solved as well as the imbalance problem. For comparison with the abnormal operation in Chapter 2, the same

configurations for the source-end distortion are applied to the power supply to verify the compensation results. The disturbance conditions are given in Table 3.3.

Table 3.3: Distorted voltage source parameters

Type of Distortion	Depth (%)	Duration (s)
Voltage Sag	30	1/15 to 2/15
Voltage Swell	20	2/15 to 3/15
Voltage Flicker	30 @ 10 Hz	0 to 0.3

Figures 3.31 and 3.32 show the detailed compensation results of the preprocessing unit under the source-end disturbances. Similar to the unbalanced case, the distorted source voltages are instantaneously compensated, resulting in the desired sinusoidal balanced waveforms, whatever the type of distortion. The parameters of the control scheme used in the preprocessing unit are unchanged with these three different cases and produce similar negligible errors, which shows the versatility of the scheme.

From the point of view of the main power grid, the disturbed power supply would be the ideal three-phase sinusoidal balanced voltage source after the pretreatment. Therefore all conclusions given by the normal operations of the single VCS, the single CCS or the series-shunt compensation system, which are presented in Chapters 2 and 3, can be directly applied into the abnormal operations of the system.

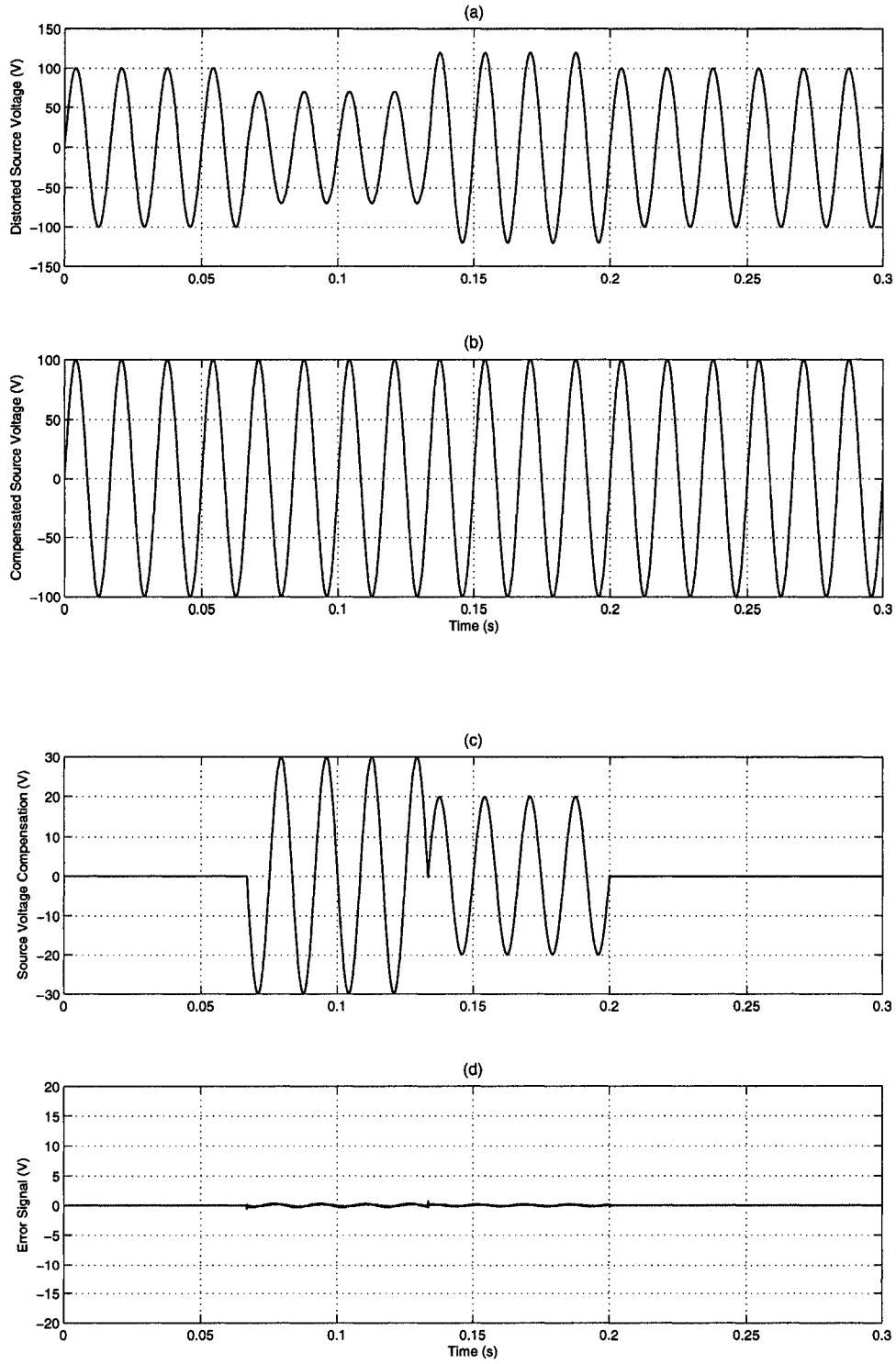

Figure 3.31: Performance of the preprocessing unit under voltage sag and voltage swell

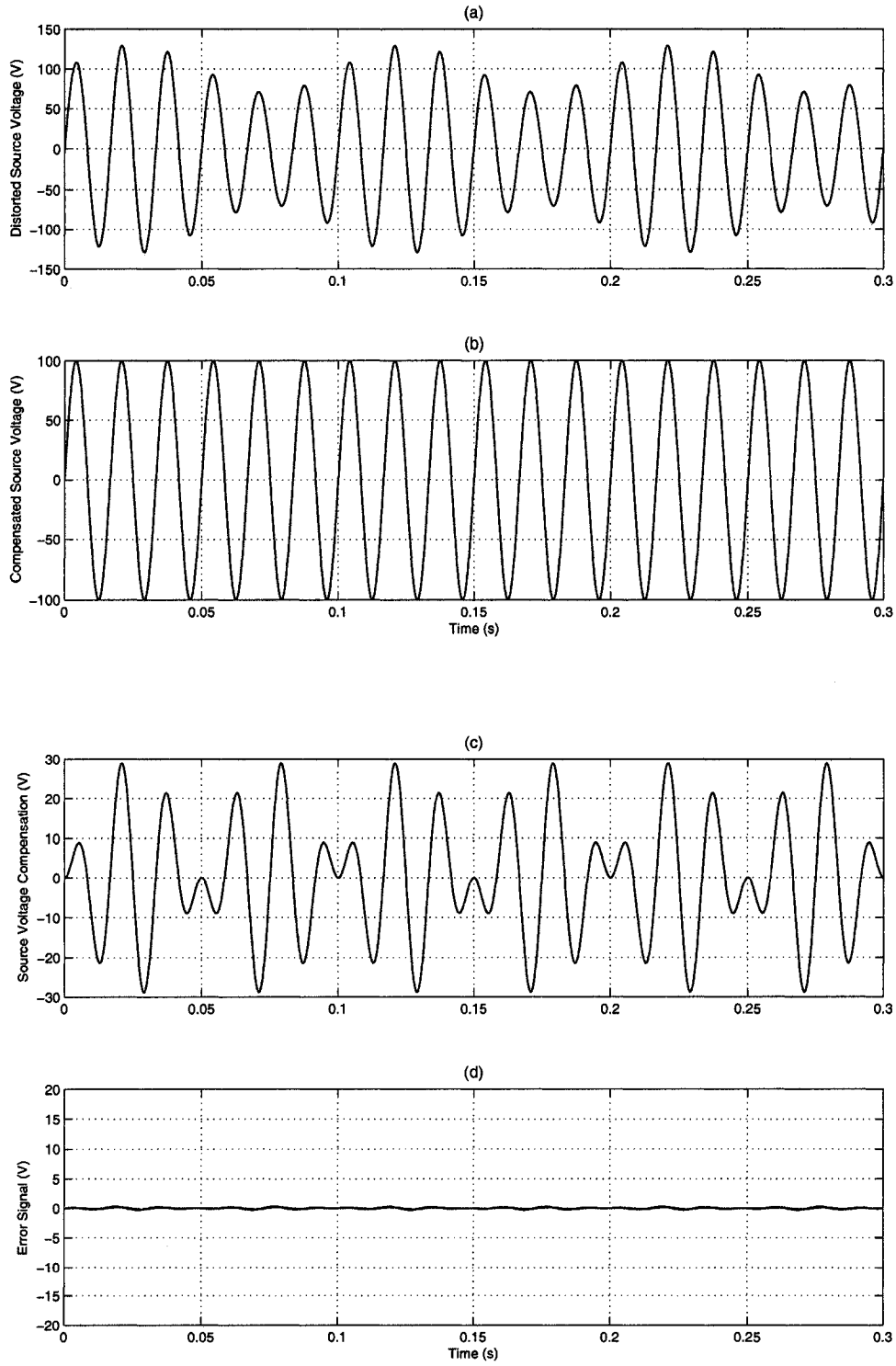

Figure 3.32: Performance of the preprocessing unit under voltage flicker

3.4 Summary

In this chapter , the model and the function of the series-shunt compensation system were introduced and analyzed. The performance of the series-shunt compensation system which is suitable for the simpler or more complex nonlinear loads were investigated. The whole compensation system combines the VCS and the CCS together to compensate for the voltage at the PCC and the source current simultaneously. The parameter settings of the RANN in harmonic extraction unit and the APF in harmonics regeneration unit are identical with those of the single VCS and the single CCS applications.

The effects of harmonic order and sampling frequency on the performance of the series-shunt compensation system were investigated. The higher harmonic order estimation in the RANN and the smaller sampling time can lead to better harmonic extraction results and less errors. However, the issue of computation workload of the RANN method with respect to harmonic order and sampling frequency needs further investigation. The performance of the whole system under various load conditions was investigated. Whether the nonlinear load is the simpler load, such as a diode bridge rectifier or the more complex load such as the combination of a thyristor bridge rectifier and a thyristor back-to-back controller, the presented series-shunt compensation system was effective and efficient in maintaining the voltage at the PCC almost sinusoidal and in keeping the source current from being contaminated by the current harmonics.

The preprocessing unit was introduced into the compensation system to solve the problems caused by the abnormal source conditions such as voltage imbalance, voltage sag, voltage swell and voltage flicker. The performance of the preprocessing unit under these source-end disturbances were investigated. The tuning-free pretreating unit is capable of compensating for any type of source-end distortions to any desired extent before the source voltages are applied to the main grid. The abnormal operation of the system is converted to the normal operation with the aid of this unit and the fast dynamic response would not have any visible influence upon the subsequent voltage and current compensation procedure.

Chapter 4
Optimization of Design Parameters Using Response Surface Method (RSM)

According to the algorithm of the RANN harmonic extraction method and the model of the APF, which employs the multi-loop feedback control scheme, the performance of the whole compensation system is considerably dependent on the parameters in the system. The maximum harmonic order used in the estimation, the sampling frequency of the RANN, the inclusion of triplen harmonics, the outer and inner loop gains of the multi-loop feedback structure, the carrier frequency of the PWM controller and the values of the output low-pass filter components affect the effectiveness and quality of the compensation. How to tune these parameters is a pivotal issue in the compensation system.

One intuitional method is to establish the differential equations that describe the circuit structure and to determine the optimal value of the objective function. However, in consideration of the complex interconnections between these parameters, it would be

laborious and difficult to achieve a theoretical solution to the large differential equations. Another approach often used in scientific researches is to adjust the parameters through trial and error. In trial and error method, some different possible configurations are generated to test their fitness to the problem. The ones that satisfy the preset criterion could be retained and the others are eliminated. The trial and error method can proceed where there is little or no knowledge of the subject. In an optimization problem, the trial and error method is unacceptable since it makes attempts to find a solution, neither all solutions nor the best solution. In the context of the present work, the computation time involved in the trial and error method would be longer than the simulation time, which means an exhaustive investigation would be virtually unacceptable.

Since the computer simulation could be treated as one particular kind of experiment, the theory of design and analysis of experiments is capable of dealing with this optimization task.

4.1 Introduction to Response Surface Method (RSM)

The response surface method (RSM) is a collection of mathematical and statistical techniques that are useful for the modeling and analysis of problems in which a response of interest is influenced by several variables and the objective is to optimize this response [35]. The advantage of RSM is that the procedure can help engineers and designers to identify the predominant variables and to obtain a better understanding of the overall

system.

4.1.1 Basic concept of RSM

For example, suppose that an electrical engineer wishes to find the values of frequency (x_1) and inductance (x_2) that maximize the output power (y) of a circuit. The circuit output power is expressed as function of the values of frequency and inductance as

$$y = f(x_1, x_2) + \varepsilon \tag{4.1}$$

where ε represents the noise or error observed in the response y. If the expected response is denoted by $E(y) = f(x_1, x_2) = \eta$, then the surface represented by $\eta = f(x_1, x_2)$ is called a response surface.

The response surface is usually represented by the three dimensional graph, such as in Figure 4.1, where η is plotted versus the values of x_1 and x_2. To help visualize the shape of a response surface, the contours of the response surface are often plotted as shown in Figure 4.1. In the contour plot, lines of constant response are drawn in the x_1, x_2 plane. Each contour corresponds to a particular height of the response surface.

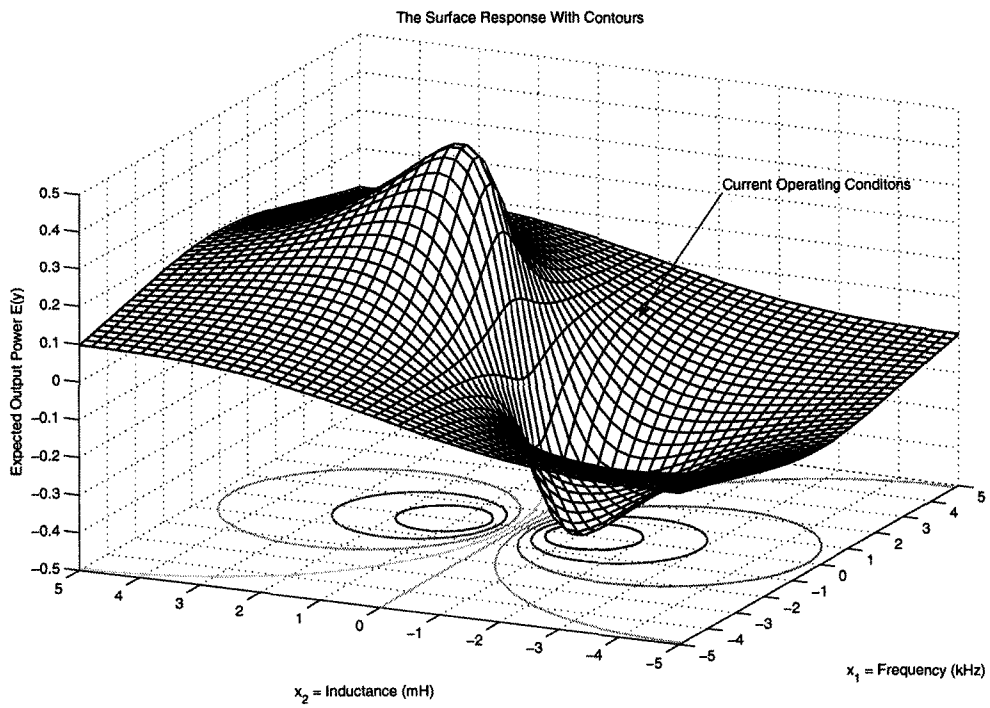

Figure 4.1: The response surface with contours

4.1.2 Approximate model of RSM

In most RSM problems, the form of the relationship between the response and the independent variables is unknown. Thus, the first step in RSM is to find a suitable approximation for the true functional relationship between y and the set of independent variables. Usually, a low-order polynomial in some region of the independent variables is employed. If the response is well modeled by a linear function of the independent variables, then the approximating function is the first-order model [35]

$$y = \beta_0 + \beta_1 x_1 + \beta_2 x_2 + \cdots + \beta_k x_k + \varepsilon \tag{4.2}$$

If there is curvature in the system, then a polynomial of higher degree must be used, such as the second-order model [35]

$$y = \beta_0 + \sum_{i=1}^{k} \beta_i x_i + \sum_{i=1}^{k} \beta_{ii} x_i^2 + \sum\sum_{i<j} \beta_{ij} x_i x_j + \varepsilon \qquad (4.3)$$

Almost all RSM problems utilize one or both of these models. Of course, it is unlikely that a polynomial model will be a reasonable approximation of the true functional relationship over the entire space of the independent variables, but for a relatively small region they usually work quite well.

The method of least squares is used to estimate the parameters in the approximating polynomials. The response surface analysis is then done in terms of the fitted surface. If the fitted surface is an adequate approximation of the true response function, then the analysis of the fitted surface will be approximately equivalent to the analysis of the actual system. The model parameters can be estimated most effectively if proper experimental designs are used to collect the data. Designs for fitting response surfaces are called response surface designs.

4.1.3 Design objective of RSM

RSM is a sequential procedure. Often, when a point on the response surface is remote from the optimum, such as the current operating conditions in Figure 4.1, there is little curvature in the system and the first-order model will be appropriate. The objective here is to lead the experiment rapidly and efficiently along a path of improvement towards the

general vicinity of the optimum. Once the region of the optimum has been found, a more elaborate model, such as the second-order model, may be employed, and an analysis may be performed to locate the optimum. The analysis of a response surface can be thought of as climbing a hill, where the top of the hill represents the point of maximum response. If the true optimum is a point of minimum response, then it could be thought of as descending into a valley.

The eventual objective of RSM is to determine the optimum operating conditions for the system or to determine a region of the factor space in which operating requirements are satisfied.

4.2 Analysis of APF Compensation System Using RSM

The independent variables in the APF compensation system can be roughly divided into two categories according to their locations. The parameters in the harmonic extraction unit have been discussed in Chapter 3 and the parameters in the harmonic regeneration unit will be investigated in detail in this chapter. By conducting a factorial experiment, the results of the experiment are analyzed, and the parameters of the design unit and parameter interactions that affect the performance of APF compensation system are identified and quantified. From the analysis, the optimum combination of the design parameters can be determined.

In order to obtain the optimum operating conditions to improve the compensation system,

the contribution of the parameters of APF that independently or simultaneously affect the system performance should be investigated. For this purpose, Design-Expert [36], a software that systematically applies the statistics to experimentation, is used to determine the relationship between the important parameters and the system so that this design can work well to accommodate a wide variety of application cases.

4.2.1 Design of experiment

In consideration of the similarity and complexity of the compensation system, the three-phase VCS is chosen to perform the RSM analysis. The VCS system is operated in a three-phase power system with ideal voltage source and a three-phase diode bridge rectifier with an inductive load as the nonlinear harmonic source. A computer simulation model of this VCS system is developed in MATLAB using SIMULINK and SimPowerSystems blockset. The following experiments are based on this computer simulation model.

4.2.1.1 Factors and response of experiment

All adjustable parameters of the VCS system would be considered as the design factors. Based on previous experiments and professional experience, six factors ($k=6$) with their levels given in Table 4.1 are selected.

Table 4.1: Design factors

Factor Name	Low Level	High Level
Outer Loop Gain, k_1	1.0	8.0
Inner Loop Gain, k_2	1.0	4.0
Carrier Frequency of PWM, f_c (kHz)	50.0	100.0
LPF Resistance, R (ohm)	0.0	10.0
LPF Capacitance, C (μF)	80.0	320.0
LPF Inductance, L (mH)	0.9	3.6

In this case, the total harmonic distortion (THD) level of the voltage at the PCC that measures the performance of the VCS system would be taken as the design response. It is defined as the ratio of the portion of total harmonic distortion to the compensated voltage at the PCC. The smaller the THD value, the better the performance of the compensation system.

4.2.1.2 Choice of design of experiment

In order to collect the data that are required to conduct the 2^k factorial design, the simulation was run in randomized order with different parameters in the range given in Table 4.1. Since this experiment is a computer simulation, only one replication of the experiment need to be executed. The first step is to apply the technique of 2^6 full factorial with center point design to estimate the contribution of the main effects and their interactions. It is anticipated that a quadratic model will need to be employed to account for the curvature. For this reason, the second step is to apply the technique of face-centered central composite design (CCD), which adds some axial and center points to

augment the 2^k design, to describe the response surface more accurately and smoothly.

4.2.2 The 2^6 full factorial with center point design

The data collection and design table is shown in Table 4.2. The results of the effects of estimation and the analysis of variance (ANOVA) given by Design-Expert are presented and interpreted.

Table 4.2: Data collection and simulation runs

Std	R	Block	A: k_1	B: k_2	C: f_c	D: R	E: C	F: L	Response: *THD*
1	41	Block 1	1.0	1.0	50	0	80	0.90	**10.08**
2	46	Block 1	8.0	1.0	50	0	80	0.90	**3.75**
3	48	Block 1	1.0	4.0	50	0	80	0.90	**4.35**
4	59	Block 1	8.0	4.0	50	0	80	0.90	**4.13**
5	19	Block 1	1.0	1.0	100	0	80	0.90	**10.11**
6	33	Block 1	8.	1.0	100	0	80	0.90	**3.72**
7	10	Block 1	1.0	4.0	100	0	80	0.90	**4.33**
8	60	Block 1	8.0	4.0	100	0	80	0.90	**4.25**
9	52	Block 1	1.0	1.0	50	10	80	0.90	**14.92**
10	37	Block 1	8.0	1.0	50	10	80	0.90	**6.34**
11	61	Block 1	1.0	4.0	50	10	80	0.90	**9.93**
12	22	Block 1	8.0	4.0	50	10	80	0.90	**4.35**
13	24	Block 1	1.0	1.0	100	10	80	0.90	**14.99**
14	39	Block 1	8.0	1.0	100	10	80	0.90	**6.33**
15	25	Block 1	1.0	4.0	100	10	80	0.90	**9.94**
16	45	Block 1	8.0	4.0	100	10	80	0.90	**4.35**
17	27	Block 1	1.0	1.0	50	0	320	0.90	**10.02**
18	57	Block 1	8.0	1.0	50	0	320	0.90	**11.78**
19	50	Block 1	1.0	4.0	50	0	320	0.90	**7.28**
20	1	Block 1	8.0	4.0	50	0	320	0.90	**8.82**
21	53	Block 1	1.0	1.0	100	0	320	0.90	**11.08**
22	51	Block 1	8.0	1.0	100	0	320	0.90	**11.77**
23	18	Block 1	1.0	4.0	100	0	320	0.90	**9.37**
24	28	Block 1	8.0	4.0	100	0	320	0.90	**8.81**
25	65	Block 1	1.0	1.0	50	10	320	0.90	**20.70**
26	63	Block 1	8.0	1.0	50	10	320	0.90	**13.96**
27	2	Block 1	1.0	4.0	50	10	320	0.90	**19.92**
28	55	Block 1	8.0	4.0	50	10	320	0.90	**9.77**

Table 4.2: Data collection and simulation runs (Continued)

Std	R	Block	A: k_1	B: k_2	C: f_c	D: R	E: C	F: L	Response: *THD*
29	54	Block 1	1.0	1.0	100	10	320	0.90	**20.71**
30	8	Block 1	8.0	1.0	100	10	320	0.90	**13.92**
31	13	Block 1	1.0	4.0	100	10	320	0.90	**19.92**
32	35	Block 1	8.0	4.0	100	10	320	0.90	**9.77**
33	49	Block 1	1.0	1.0	50	0	80	3.60	**19.23**
34	3	Block 1	8.0	1.0	50	0	80	3.60	**19.84**
35	30	Block 1	1.0	4.0	50	0	80	3.60	**14.21**
36	29	Block 1	8.0	4.0	50	0	80	3.60	**34.57**
37	36	Block 1	1.0	1.0	100	0	80	3.60	**19.36**
38	21	Block 1	8.0	1.0	100	0	80	3.60	**20.66**
39	64	Block 1	1.0	4.0	100	0	80	3.60	**14.20**
40	5	Block 1	8.0	4.0	100	0	80	3.60	**30.99**
41	43	Block 1	1.0	1.0	50	10	80	3.60	**19.49**
42	17	Block 1	8.0	1.0	50	10	80	3.60	**10.91**
43	58	Block 1	1.0	4.0	50	10	80	3.60	**13.77**
44	34	Block 1	8.0	4.0	50	10	80	3.60	**8.84**
45	32	Block 1	1.0	1.0	100	10	80	3.60	**19.59**
46	56	Block 1	8.0	1.0	100	10	80	3.60	**10.81**
47	42	Block 1	1.0	4.0	100	10	80	3.60	**13.76**
48	20	Block 1	8.0	4.0	100	10	80	3.60	**9.02**
49	15	Block 1	1.0	1.0	50	0	320	3.60	**24.37**
50	62	Block 1	8.0	1.0	50	0	320	3.60	**38.76**
51	4	Block 1	1.0	4.0	50	0	320	3.60	**22.31**
52	14	Block 1	8.0	4.0	50	0	320	3.60	**39.75**
53	26	Block 1	1.0	1.0	100	0	320	3.60	**24.42**
54	11	Block 1	8.0	1.0	100	0	320	3.60	**35.89**
55	47	Block 1	1.0	4.0	100	0	320	3.60	**22.31**
56	16	Block 1	8.0	4.0	100	0	320	3.60	**46.20**
57	23	Block 1	1.0	1.0	50	10	320	3.60	**21.48**
58	38	Block 1	8.0	1.0	50	10	320	3.60	**18.54**
59	40	Block 1	1.0	4.0	50	10	320	3.60	**19.85**
60	6	Block 1	8.0	4.0	50	10	320	3.60	**13.63**
61	9	Block 1	1.0	1.0	100	10	320	3.60	**21.51**
62	44	Block 1	8.0	1.0	100	10	320	3.60	**18.53**
63	31	Block 1	1.0	4.0	100	10	320	3.60	**19.84**
64	7	Block 1	8.0	4.0	100	10	320	3.60	**13.58**
65	12	Block 1	4.5	2.5	75	5	200	2.25	**11.20**

4.2.2.1 Analysis of the results of the effects estimation

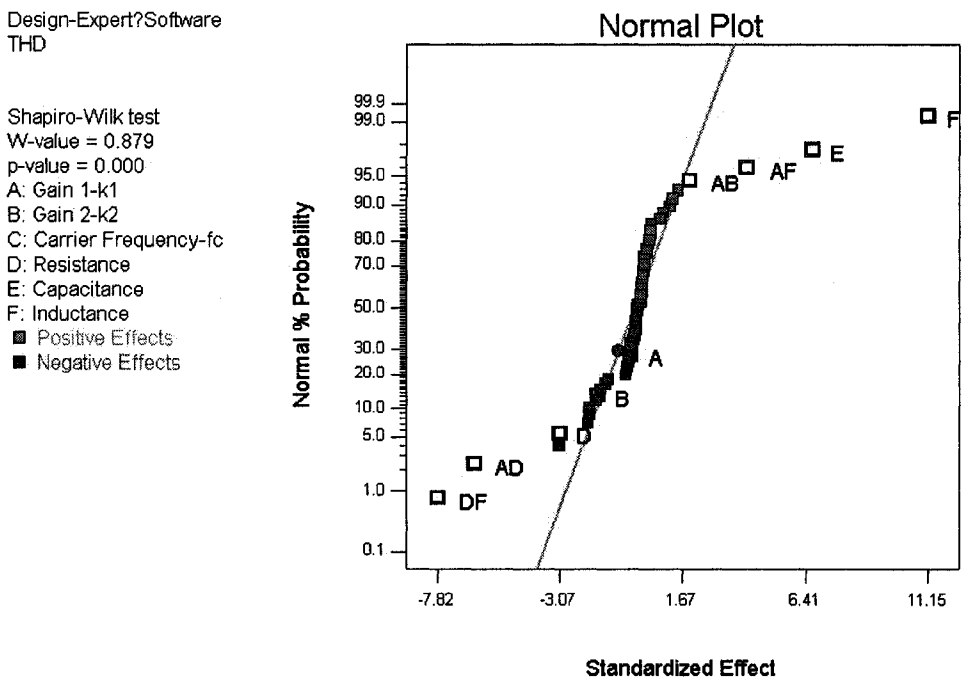

Figure 4.2: Normal plot of standardized effects

Figure 4.2 shows the normal plot of standardized effects. The model factors that are not on the straight line in Figure 4.2 are important and should be taken into account in designing the experiment. The farther away the factor is from the straight line, the more significant the effect. In this experiment, the most important factor is F. Other major factors are D, E, AB, AD, AF and DF. Among the interactions between two factors, DF contributes most to the response. Furthermore, all interactions among three or more factors are not significant at all for this design and can be neglected during the analysis.

In order to avoid the hierarchy problem, the negligible factors A and B should be included in the consideration due to the involvement of factor AB. The detailed factor effects obtained from Design-Expert are listed in Figure 4.3.

Term	Stdized Effects	Sum of Squares	% Contribution
Intercept			
A-Gain 1-k1	-0.34	1.89	0.034
B-Gain 2-k2	-1.61	41.36	0.75
C-Carrier Frequency-fc	0.14	0.30	5.479E-003
D-Resistance	-3.05	149.30	2.72
E-Capacitance	6.67	711.89	12.95
F-Inductance	11.15	1988.60	36.19
AB	1.94	60.24	1.10
AC	-0.083	0.11	2.027E-003
AD	-6.39	652.36	11.87
AE	1.49	35.69	0.65
AF	4.15	274.94	5.00
BC	0.19	0.55	9.998E-003
BD	-1.67	44.77	0.81
BE	-0.037	0.021	3.892E-004
BF	1.20	22.96	0.42
CD	-0.13	0.26	4.664E-003
CE	0.28	1.26	0.023
CF	-0.067	0.072	1.314E-003
DE	-0.53	4.45	0.081
DF	-7.82	977.27	17.78
EF	0.94	14.05	0.26
ABC	0.15	0.36	6.524E-003
ABD	-1.91	58.56	1.07
ABE	-1.90	57.67	1.05
ABF	1.30	27.03	0.49
ACD	0.069	0.076	1.389E-003
ACE	0.098	0.15	2.785E-003
ACF	0.12	0.22	4.084E-003
ADE	-1.29	26.74	0.49
ADF	-3.09	153.23	2.79
AEF	0.80	10.34	0.19
BCD	-0.18	0.52	9.532E-003
BCE	0.46	3.32	0.060
BCF	0.12	0.22	3.913E-003
BDE	0.43	3.01	0.055
BDF	-1.49	35.45	0.65
BEF	-0.31	1.51	0.027
CDE	-0.30	1.44	0.026
CDF	0.073	0.085	1.544E-003
CEF	0.098	0.15	2.785E-003
DEF	-1.98	62.98	1.15
ABCD	-0.12	0.22	4.041E-003
ABCE	0.37	2.25	0.041
ABCF	0.19	0.60	0.011
ABDE	0.21	0.67	0.012
ABDF	-1.19	22.48	0.41
ABEF	-0.23	0.83	0.015
ACDE	-0.100	0.16	2.893E-003
ACDF	-0.12	0.21	3.871E-003
ACEF	0.30	1.43	0.026
ADEF	0.074	0.088	1.597E-003
BCDE	-0.47	3.47	0.063
BCDF	-0.11	0.19	3.463E-003
BCEF	0.39	2.46	0.045
BDEF	0.19	0.59	0.011
CDEF	-0.10	0.18	3.191E-003
ABCDE	-0.40	2.56	0.047
ABCDF	-0.18	0.50	9.141E-003
ABCEF	0.45	3.28	0.060
ABDEF	0.14	0.31	5.681E-003
ACDEF	-0.31	1.49	0.027
BCDEF	-0.41	2.73	0.050
ABCDEF	-0.48	3.62	0.066
Curvature	-3.76	19.79	0.36
Lenth's ME		0.80	
Lenth's SME		1.13	

Figure 4.3: Detailed factor effects and contribution

4.2.2.2 Analysis of the results of ANOVA

The calculated results of ANOVA are listed in Figure 4.4. According to the theory of ANOVA, the model term whose "p-value" is less than 0.05 would be a significant factor. In this experiment, factors D, E, F, AB, AD, AF and DF are significant model terms while

factors A and B are not. From an overall point of view, the whole model is also significant and the "p-value" of curvature is not significant, which means the model might be quite linear. However, for purposes of improving the accuracy and precision of the model, a second-order quadratic model should be identified by RSM.

ANOVA for selected factorial model

Analysis of variance table [Partial sum of squares - Type III]

Source	Sum of Squares	df	Mean Square	F Value	p-value Prob > F	
Model	4857.84	9	539.76	47.17	< 0.0001	significant
A-Gain 1-k1	*1.89*	*1*	*1.89*	*0.17*	*0.6857*	
B-Gain 2-k2	*41.36*	*1*	*41.36*	*3.61*	*0.0626*	
D-Resistance	*149.30*	*1*	*149.30*	*13.05*	*0.0007*	
E-Capacitance	*711.89*	*1*	*711.89*	*62.21*	*< 0.0001*	
F-Inductance	*1988.60*	*1*	*1988.60*	*173.79*	*< 0.0001*	
AB	*60.24*	*1*	*60.24*	*5.26*	*0.0257*	
AD	*652.36*	*1*	*652.36*	*57.01*	*< 0.0001*	
AF	*274.94*	*1*	*274.94*	*24.03*	*< 0.0001*	
DF	*977.27*	*1*	*977.27*	*85.41*	*< 0.0001*	
Curvature	19.79	1	19.79	1.73	0.1941	not significant
Residual	617.91	54	11.44			
Cor Total	5495.53	64				

Std. Dev.	3.38	R-Squared	0.8872
Mean	15.61	Adj R-Squared	0.8683
C.V. %	21.66	Pred R-Squared	N/A
PRESS	N/A	Adeq Precision	24.157

Case(s) with leverage of 1.0000: Pred R-Squared and PRESS statistic not defined

Figure 4.4: Detailed analysis of ANOVA for selected factorial model

4.2.3 The face-centered central composite design (CCD)

A central composite design (CCD) is an experimental design which contains an embedded factorial or fractional factorial design with center points [37]. The CCD

improves the estimation of the curvature by augmenting the number of experiment points. The face-centered CCD adds the extra points to the center of each face of the factorial space and this variety requires three levels of each factor.

The data collection and design table is shown in Table 4.3. The results of the diagnosis and the analysis of variance (ANOVA) given by Design-Expert are presented and interpreted.

Table 4.3: Data collection and simulation runs

Std	R	Block	A: k_1	B: k_2	C: f_c	D: R	E: C	F: L	Response: *THD*
1	32	Block 1	1.0	1.0	50	0	80	0.90	**10.08**
2	14	Block 1	8.0	1.0	50	0	80	0.90	**3.75**
3	18	Block 1	1.0	4.0	50	0	80	0.90	**4.35**
4	30	Block 1	8.0	4.0	50	0	80	0.90	**4.13**
5	27	Block 1	1.0	1.0	100	0	80	0.90	**10.11**
6	52	Block 1	8.	1.0	100	0	80	0.90	**3.72**
7	60	Block 1	1.0	4.0	100	0	80	0.90	**4.33**
8	25	Block 1	8.0	4.0	100	0	80	0.90	**4.25**
9	43	Block 1	1.0	1.0	50	10	80	0.90	**14.92**
10	11	Block 1	8.0	1.0	50	10	80	0.90	**6.34**
11	49	Block 1	1.0	4.0	50	10	80	0.90	**9.93**
12	13	Block 1	8.0	4.0	50	10	80	0.90	**4.35**
13	4	Block 1	1.0	1.0	100	10	80	0.90	**14.99**
14	42	Block 1	8.0	1.0	100	10	80	0.90	**6.33**
15	37	Block 1	1.0	4.0	100	10	80	0.90	**9.94**
16	65	Block 1	8.0	4.0	100	10	80	0.90	**4.35**
17	81	Block 1	1.0	1.0	50	0	320	0.90	**10.02**
18	75	Block 1	8.0	1.0	50	0	320	0.90	**11.78**
19	7	Block 1	1.0	4.0	50	0	320	0.90	**7.28**
20	39	Block 1	8.0	4.0	50	0	320	0.90	**8.82**
21	6	Block 1	1.0	1.0	100	0	320	0.90	**11.08**
22	59	Block 1	8.0	1.0	100	0	320	0.90	**11.77**
23	20	Block 1	1.0	4.0	100	0	320	0.90	**9.37**
24	46	Block 1	8.0	4.0	100	0	320	0.90	**8.81**
25	31	Block 1	1.0	1.0	50	10	320	0.90	**20.70**
26	73	Block 1	8.0	1.0	50	10	320	0.90	**13.96**

Table 4.3: Data collection and simulation runs (Continued)

Std	R	Block	A: k_1	B: k_2	C: f_c	D: R	E: C	F: L	Response: *THD*
27	15	Block 1	1.0	4.0	50	10	320	0.90	**19.92**
28	72	Block 1	8.0	4.0	50	10	320	0.90	**9.77**
29	44	Block 1	1.0	1.0	100	10	320	0.90	**20.71**
30	53	Block 1	8.0	1.0	100	10	320	0.90	**13.92**
31	33	Block 1	1.0	4.0	100	10	320	0.90	**19.92**
32	67	Block 1	8.0	4.0	100	10	320	0.90	**9.77**
33	8	Block 1	1.0	1.0	50	0	80	3.60	**19.23**
34	5	Block 1	8.0	1.0	50	0	80	3.60	**19.84**
35	34	Block 1	1.0	4.0	50	0	80	3.60	**14.21**
36	36	Block 1	8.0	4.0	50	0	80	3.60	**34.57**
37	3	Block 1	1.0	1.0	100	0	80	3.60	**19.36**
38	51	Block 1	8.0	1.0	100	0	80	3.60	**20.66**
39	29	Block 1	1.0	4.0	100	0	80	3.60	**14.20**
40	23	Block 1	8.0	4.0	100	0	80	3.60	**30.99**
41	66	Block 1	1.0	1.0	50	10	80	3.60	**19.49**
42	69	Block 1	8.0	1.0	50	10	80	3.60	**10.91**
43	64	Block 1	1.0	4.0	50	10	80	3.60	**13.77**
44	24	Block 1	8.0	4.0	50	10	80	3.60	**8.84**
45	21	Block 1	1.0	1.0	100	10	80	3.60	**19.59**
46	50	Block 1	8.0	1.0	100	10	80	3.60	**10.81**
47	48	Block 1	1.0	4.0	100	10	80	3.60	**13.76**
48	38	Block 1	8.0	4.0	100	10	80	3.60	**9.02**
49	70	Block 1	1.0	1.0	50	0	320	3.60	**24.37**
50	47	Block 1	8.0	1.0	50	0	320	3.60	**38.76**
51	41	Block 1	1.0	4.0	50	0	320	3.60	**22.31**
52	40	Block 1	8.0	4.0	50	0	320	3.60	**39.75**
53	68	Block 1	1.0	1.0	100	0	320	3.60	**24.42**
54	2	Block 1	8.0	1.0	100	0	320	3.60	**35.89**
55	76	Block 1	1.0	4.0	100	0	320	3.60	**22.31**
56	79	Block 1	8.0	4.0	100	0	320	3.60	**46.20**
57	63	Block 1	1.0	1.0	50	10	320	3.60	**21.48**
58	77	Block 1	8.0	1.0	50	10	320	3.60	**18.54**
59	62	Block 1	1.0	4.0	50	10	320	3.60	**19.85**
60	78	Block 1	8.0	4.0	50	10	320	3.60	**13.63**
61	17	Block 1	1.0	1.0	100	10	320	3.60	**21.51**
62	10	Block 1	8.0	1.0	100	10	320	3.60	**18.53**
63	71	Block 1	1.0	4.0	100	10	320	3.60	**19.84**
64	74	Block 1	8.0	4.0	100	10	320	3.60	**13.58**
65	16	Block 1	1.0	2.5	75	5	200	2.25	**19.54**

Table 4.3: Data collection and simulation runs (Continued)

Std	R	Block	A: k_1	B: k_2	C: f_c	D: R	E: C	F: L	Response: *THD*
66	80	Block 1	8.0	2.5	75	5	200	2.25	**11.24**
67	56	Block 1	4.5	1.0	75	5	200	2.25	**14.77**
68	35	Block 1	4.5	4.0	75	5	200	2.25	**10.42**
69	45	Block 1	4.5	2.5	50	5	200	2.25	**11.25**
70	54	Block 1	4.5	2.5	100	5	200	2.25	**11.22**
71	57	Block 1	4.5	2.5	75	0	200	2.25	**14.74**
72	55	Block 1	4.5	2.5	75	10	200	2.25	**11.77**
73	61	Block 1	4.5	2.5	75	5	80	2.25	**6.35**
74	9	Block 1	4.5	2.5	75	5	320	2.25	**13.35**
75	12	Block 1	4.5	2.5	75	5	200	0.90	**8.91**
76	58	Block 1	4.5	2.5	75	5	200	3.60	**14.70**
77	1	Block 1	4.5	2.5	75	5	200	2.25	**11.20**
78	28	Block 1	4.5	2.5	75	5	200	2.25	**11.20**
79	26	Block 1	4.5	2.5	75	5	200	2.25	**11.20**
80	19	Block 1	4.5	2.5	75	5	200	2.25	**11.20**
81	22	Block 1	4.5	2.5	75	5	200	2.25	**11.20**

4.2.3.1 Analysis of the first phase design

The diagnostic plots are presented in Figure 4.5. ANOVA was checked to find out the necessity of the transformation of the model. Although ANOVA shows the model is significant, there is a quite apparent outlier in all diagnostic plots which indicates a power transformation is required. The suggestion of transformation given by the Box-Cox plot is a square root transformation. Consequently, the second phase design would be based on the square root transformation model.

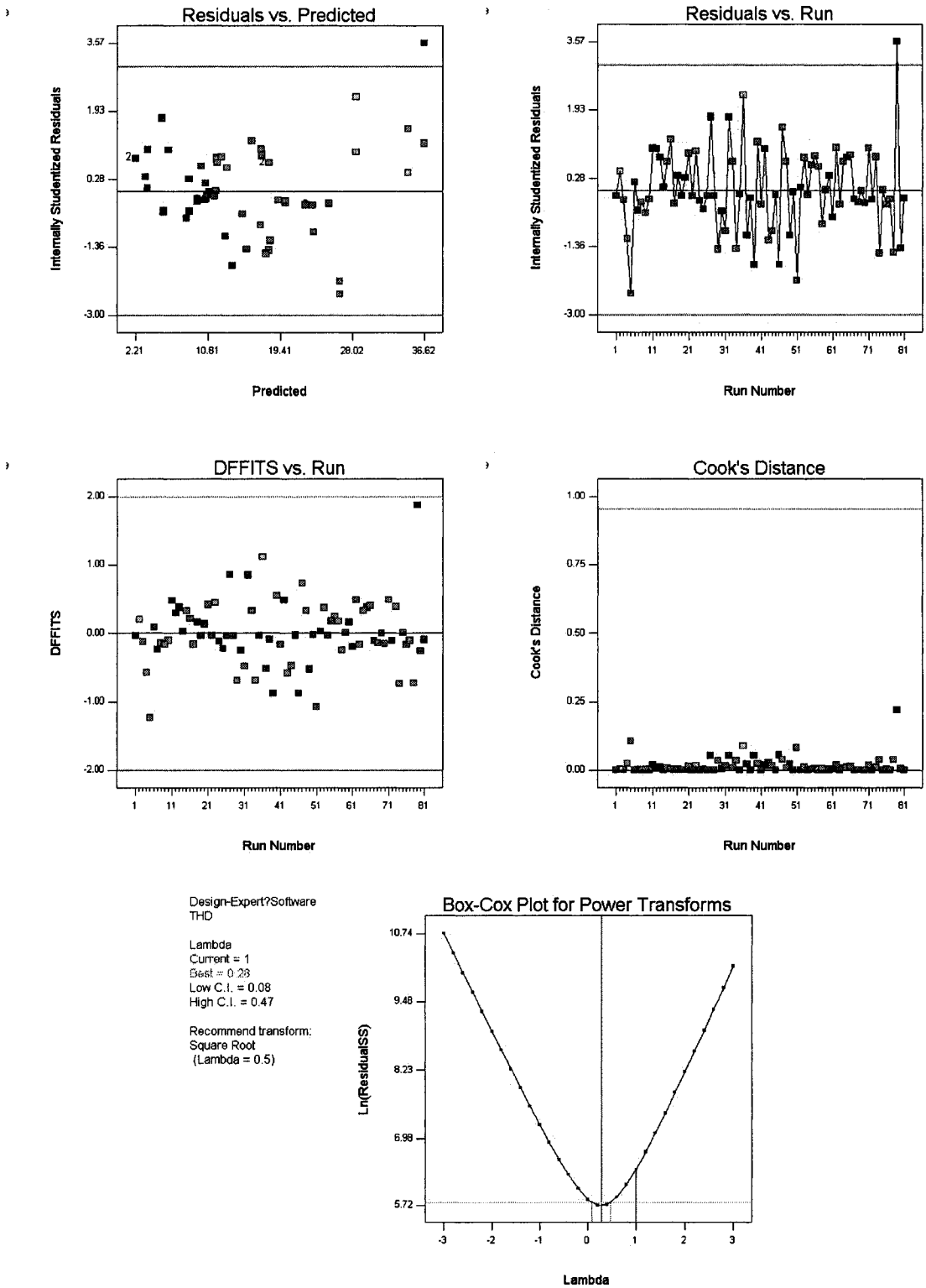

Figure 4.5: Diagnostic plots of the first phase of CCD

4.2.3.2 Analysis of the second phase design

Sequential Model Sum of Squares [Type I]

Source	Sum of Squares	df	Mean Square	F Value	p-value Prob > F	
Mean vs Total	1122.08	1	1122.08			
Linear vs Mean	49.49	6	8.25	16.78	< 0.0001	
2FI vs Linear	28.46	15	1.90	14.15	< 0.0001	
Quadratic vs 2FI	2.45	6	0.41	3.96	0.0024	Suggested
Cubic vs Quadra	5.04	26	0.19	12.44	< 0.0001	Aliased
Residual	0.42	27	0.016			
Total	1207.95	81	14.91			

Lack of Fit Tests

Source	Sum of Squares	df	Mean Square	F Value	p-value Prob > F
Linear	36.37	70	0.52		
2FI	7.91	55	0.14		
Quadratic	5.46	49	0.11		
Cubic	0.42	23	0.018		
Pure Error	0.000	4	0.000		

Model Summary Statistics

Source	Std. Dev.	R-Squared	Adjusted R-Squared	Predicted R-Squared	PRESS	
Linear	0.70	0.5764	0.5421	0.4794	44.70	
2FI	0.37	0.9079	0.8751	0.8289	14.69	
Quadratic	0.32	0.9364	0.9040	0.8435	13.44	Suggested
Cubic	0.12	0.9951	0.9855	0.8810	10.22	Aliased

Figure 4.6: Detailed fit summary of transformed model

The detailed analysis of the second phase design, which is based on the square root transformed model, is presented in Figure 4.6. According to the theory of design of experiments (DOE), the model which maximizes the values of "Adjusted R-Squared" and

"Predicted R-Squared" and is not aliased should be chosen as the starting model, which is a quadratic model in this experiment.

4.2.3.3 Analysis of the results of ANOVA and the predictive model

Using the method of backward elimination regression with "Alpha to Exit" = 0.05 to remove the insignificant factors, the results of ANOVA are calculated and listed in Figure 4.7. The "f-value" of 69.51 implies that the model is significant and there is only a 0.01% chance that this value is caused by noise signal. The model term whose "p-value" is less than 0.05 is the significant term. In this case, factors A, B, D, E, F, AB, AD, AE, AF, BD, BF, DF and A^2 are significant model terms with the consideration of hierarchy. All other insignificant model terms are removed to improve the design, which doesn't count those required to support hierarchy.

Adding terms generally increases the model's fit to existing data, but may not improve its ability to predict values for new observations. In contrast to "R-Squared" and "Adjusted R-Squared" which measure the goodness-of-fit, "Predicted R-Squared" measures the goodness-of-prediction. It indicates how well the model will fit unknown future data and safeguards against overfitting. The "Predicted R-Squared" value of 0.8969 means the analysis of the reduced model relating to design variables can account for 89.69% of total variability of the response, which is in reasonable agreement with the value of "Adjusted R-Squared" of 0.9176.

Transform: Square root Constant: 0

Backward Elimination Regression with Alpha to Exit = 0.050

Forced Terms Intercept

Removed	Coefficient Estimate	t for H_0 Coeff=0	Prob > |t|	R-Squared	MSE
F^2	-7.545E-003	-0.036	0.9712	0.9364	0.10
CF	-7.430E-003	-0.19	0.8524	0.9364	0.099
AC	-8.040E-003	-0.20	0.8391	0.9363	0.098
BC	8.603E-003	0.22	0.8265	0.9363	0.096
CD	-8.988E-003	-0.23	0.8173	0.9362	0.094
DE	-9.458E-003	-0.25	0.8064	0.9361	0.093
C-Carrier Freq.	9.359E-003	0.25	0.8039	0.9361	0.091
C^2	-0.067	-0.35	0.7300	0.9359	0.090
BE	0.014	0.37	0.7108	0.9358	0.089
CE	0.015	0.39	0.6985	0.9356	0.088
B^2	0.10	0.55	0.5818	0.9353	0.087
EF	-0.029	-0.79	0.4326	0.9347	0.086
D^2	0.23	1.35	0.1819	0.9329	0.087
E^2	-0.21	-1.36	0.1777	0.9310	0.088

ANOVA for Response Surface Reduced Quadratic Model

Analysis of variance table [Partial sum of squares - Type III]

Source	Sum of Squares	df	Mean Square	F Value	p-value Prob > F	
Model	79.94	13	6.15	69.51	< 0.0001	significant
A-Gain 1-k1	*0.97*	*1*	*0.97*	*10.95*	*0.0015*	
B-Gain 2-k2	*1.48*	*1*	*1.48*	*16.77*	*0.0001*	
D-Resistance-R	*0.82*	*1*	*0.82*	*9.30*	*0.0033*	
E-Capacitance-	*13.12*	*1*	*13.12*	*148.30*	*< 0.0001*	
F-Inductance-L	*33.10*	*1*	*33.10*	*374.10*	*< 0.0001*	
AB	*0.70*	*1*	*0.70*	*7.93*	*0.0064*	
AD	*8.36*	*1*	*8.36*	*94.51*	*< 0.0001*	
AE	*0.77*	*1*	*0.77*	*8.66*	*0.0045*	
AF	*3.70*	*1*	*3.70*	*41.80*	*< 0.0001*	
BD	*0.45*	*1*	*0.45*	*5.05*	*0.0279*	
BF	*0.44*	*1*	*0.44*	*5.01*	*0.0286*	
DF	*13.94*	*1*	*13.94*	*157.58*	*< 0.0001*	
A^2	*2.09*	*1*	*2.09*	*23.66*	*< 0.0001*	
Residual	5.93	67	0.088			
Lack of Fit	5.93	63	*0.094*			
Pure Error	*0.000*	*4*	*0.000*			
Cor Total	85.87	80				

Std. Dev.	0.30	R-Squared	0.9310
Mean	3.72	Adj R-Squared	0.9176
C.V. %	7.99	Pred R-Squared	0.8969
PRESS	8.86	Adeq Precision	34.671

Figure 4.7: Detailed analysis of ANOVA for transformed model

The predictive model in terms of coded factors and actual factors are given in (4.4) and (4.5) respectively.

$$\begin{aligned}\sqrt{THD} = {} & 3.38 - 0.12 \cdot A - 0.15 \cdot B - 0.11 \cdot D + 0.45 \cdot E + 0.71 \cdot F \\ & + 0.10 \cdot A \cdot B - 0.36 \cdot A \cdot D + 0.11 \cdot A \cdot E + 0.24 \cdot A \cdot F \\ & - 0.084 \cdot B \cdot D + 0.083 \cdot B \cdot F - 0.47 \cdot D \cdot F + 0.41 \cdot A^2\end{aligned} \tag{4.4}$$

$$\begin{aligned}\sqrt{THD} = {} & 2.486 - 0.452 \cdot k_1 - 0.226 \cdot k_2 + 0.254 \cdot R + 2.543 \times 10^{-3} \cdot C + 0.539 \cdot L \\ & + 0.020 \cdot k_1 \cdot k_2 - 0.021 \cdot k_1 \cdot R + 2.606 \times 10^{-4} \cdot k_1 \cdot C + 0.051 \cdot k_1 \cdot L \\ & - 0.011 \cdot k_2 \cdot R + 0.041 \cdot k_2 \cdot L - 0.069 \cdot R \cdot L + 0.034 \cdot k_1^2\end{aligned} \tag{4.5}$$

4.2.3.4 Analysis of the diagnostic plots

It is important to check for normality of residuals, constant error, influential values and power transformations using the diagnostic plots, which are illustrated in Figure 4.8 and 4.9. The following comments relate to the individual plots.

- Normal Plot of Residuals: This plot shows an excellent straight line that indicates the model's residuals are as normal as desired.
- Residuals vs. Predicated: This plot does not demonstrate any systematic distribution, which implies the assumption of constant variance is satisfied and the model is correct.
- Residuals vs. Run: This plot is generally used to detect correlation between the residuals, which would occur where there is the influence of lurking variables in the experiment. In this case, there is no positive or negative correlation found between the residuals, which means the assumption of independence on random

errors is satisfied as well.

- Predicted vs. Actual: The relationship between the predicted response values and the actual response values shown in this plot is approximately linear, especially in low-THD region.
- Residuals vs. Factor: The random scatter of this plot indicates that there is no systematic distribution of independent factors that could not be accounted for by the model.
- Leverage vs. Run: The value of leverage of 0.2 shown in this plot defines how much each run affects the model's fitness. The strong clustering indicates that the model is close to the actual response.
- DFFITS vs. Run: The outlier may be caused by mistake in calculations, data coding or copying error, which could be determined by analyzing the externally Studentized residuals. A residual bigger than 3 or 4 standard deviation from zero is a potential outlier. The fact that the biggest residual is 2.971 indicates no data should cause concern.
- Cook's Distance: This plot illustrates that few points have moderate values compared to the majority, which reflects how well the model fits the observation.

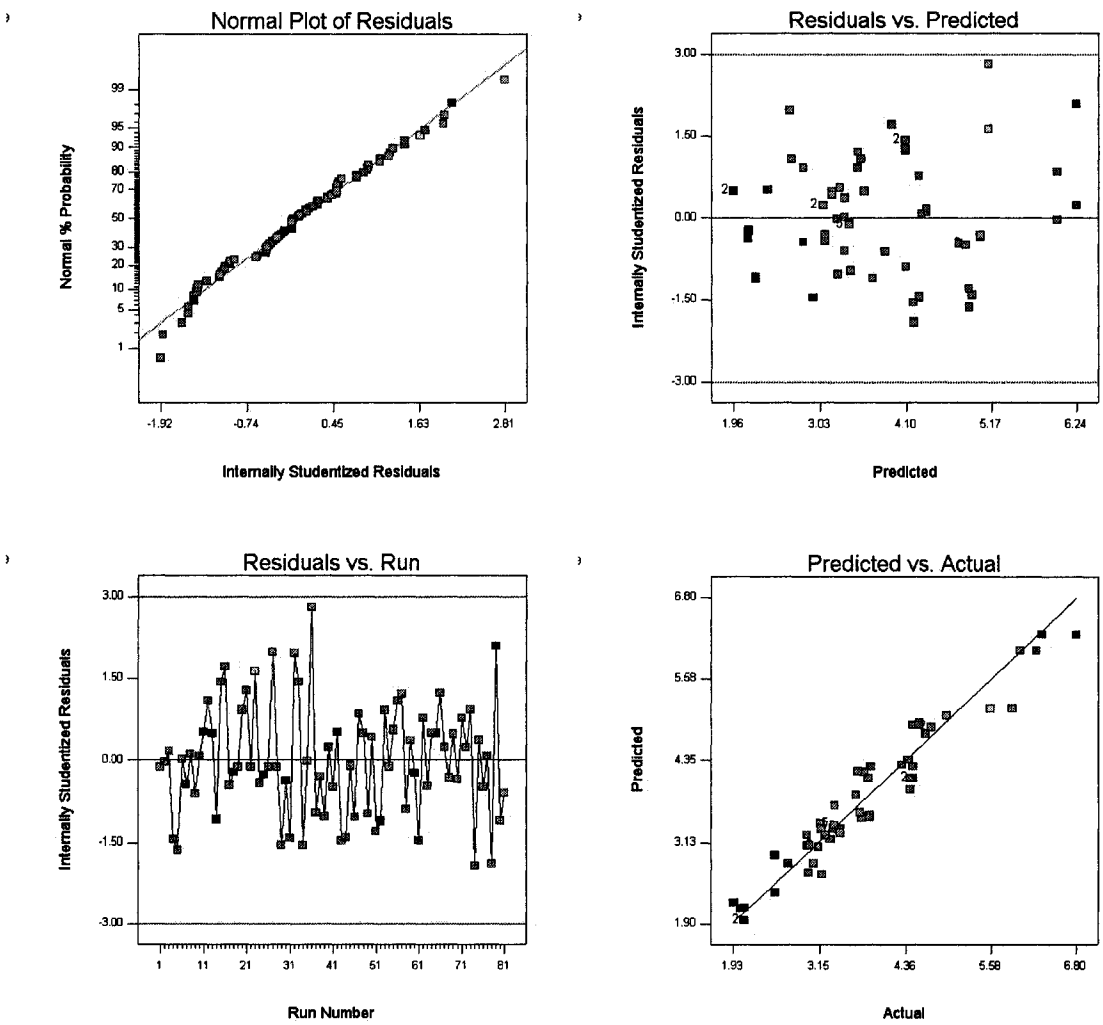

Figure 4.8: Diagnostic plots of the second phase of CCD

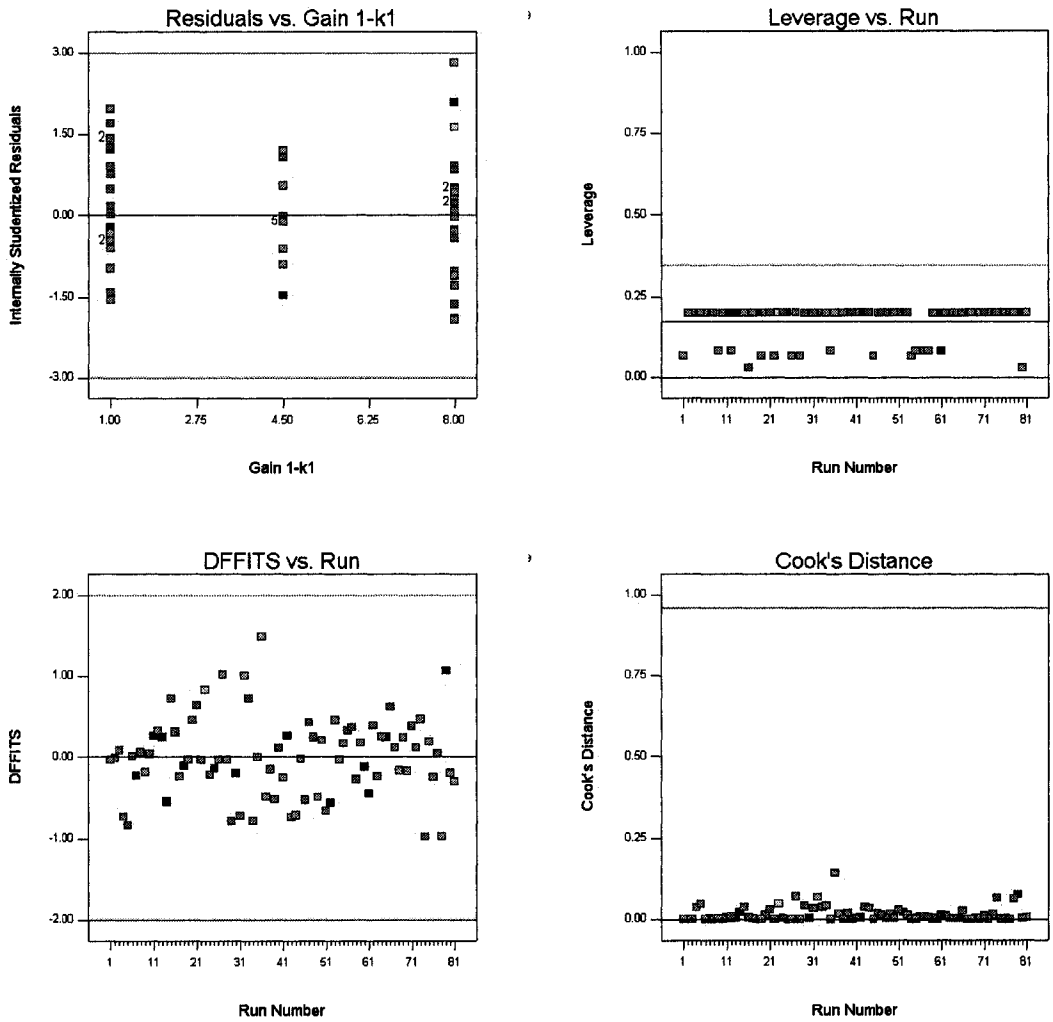

Figure 4.9: Diagnostic plots of the second phase of CCD (Continued)

4.2.3.5 Analysis of the model graphs

Compared to other factors, model terms AB, AD, AE, AF, BD, BF and DF have significant interactions. The interactions of AD, AF and DF that contribute most to the response are demonstrated in Figure 4.10.

- A (Outer Loop Gain, k_I) vs. D (LPF Resistance, R):

  When the resistance is at the low level, the square root of THD increases slightly as the gain increases. On the other hand, the square root of THD decreases as the gain increases when the resistance is at the high level. There is an obvious curvature in the response surface.

- A (Outer Loop Gain, k_I) vs. F (LPF Inductance, L):

  When the inductance is at the low level, the square root of THD decreases as the gain increases. However, the square root of THD increases little as the gain increases when the inductance is at the high level. An obvious curvature in the response surface is presented.

- D (LPF Resistance, R) vs. F (LPF Inductance, L):

  When the inductance is at the low level, the square root of THD increases as the resistance increases. On the contrary, the square root of THD apparently decreases as the resistance increases when the inductance is at the high level. No obvious curvature in the response surface can be observed.

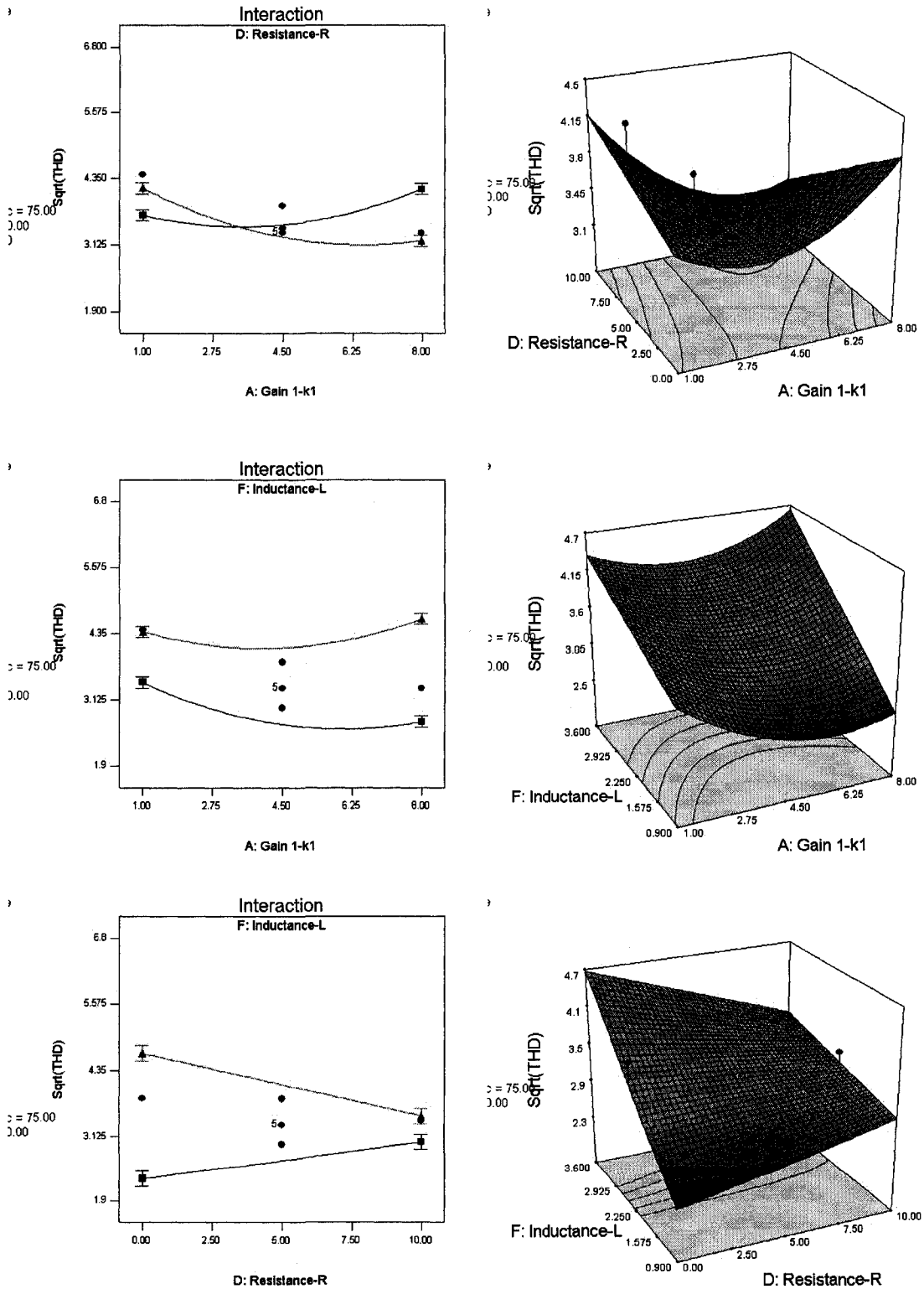

Figure 4.10: Interaction and 3D surface plots of AD, AF and DF

4.2.3.6 Numerical optimization and point prediction

The objective function, the design variables, the preassigned parameters and the constraints describe an optimization problem. In most practical cases, an infinite number of feasible solutions exist. In order to find the best one, it is necessary to form a function of the variables and use it for comparison of solution alternatives. The objective function is the function whose least, or greatest value is sought in an optimization procedure. The quantities, which describe a structural system, can be divided into two groups: design variables and preassigned parameters. The quantities, which determine the behaviour of a system, usually form two kinds of constraints: explicit and implicit ones. The form of the feasible region, determined by the constraints indicates if a local optimum is also a global one or not.

Explicit constraints which restrict the range of design variables may be called size constraints or technological constraints. Constraints derived from behaviour requirements are called behavioural constraints. There are six size constraints and no behavioural constraints in the proposed case study.

The predictive model in terms of actual factors is able to be used to perform the numerical optimization. The iterative solutions are presented in Figure 4.11.

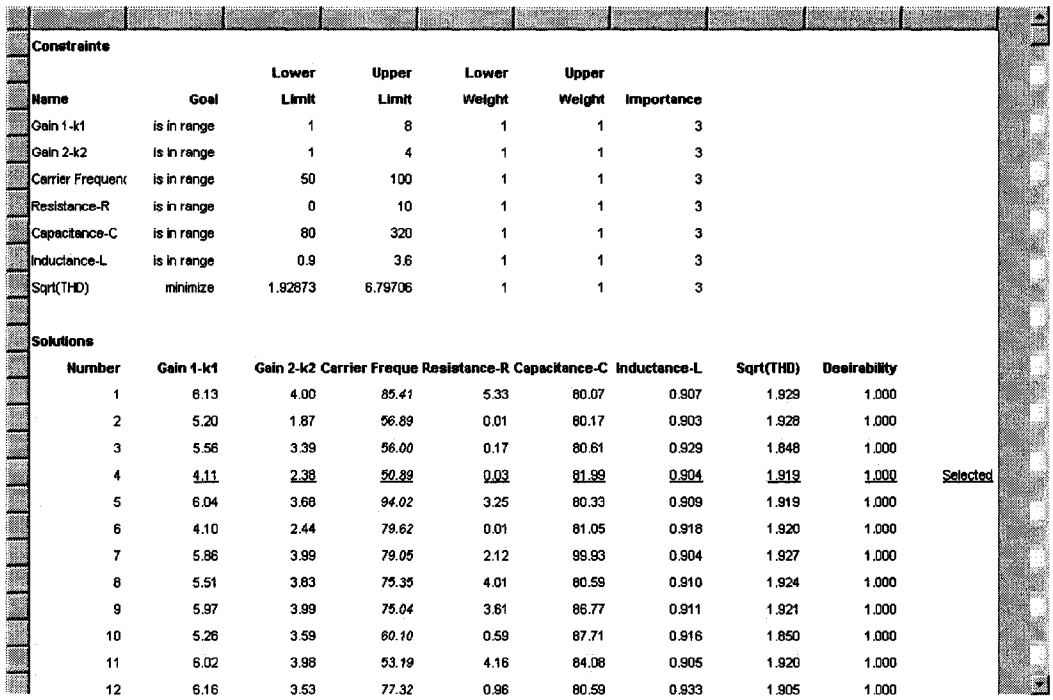

Constraints

Name	Goal	Lower Limit	Upper Limit	Lower Weight	Upper Weight	Importance
Gain 1-k1	is in range	1	8	1	1	3
Gain 2-k2	is in range	1	4	1	1	3
Carrier Frequenc	is in range	50	100	1	1	3
Resistance-R	is in range	0	10	1	1	3
Capacitance-C	is in range	80	320	1	1	3
Inductance-L	is in range	0.9	3.6	1	1	3
Sqrt(THD)	minimize	1.92873	6.79706	1	1	3

Solutions

Number	Gain 1-k1	Gain 2-k2	Carrier Freque	Resistance-R	Capacitance-C	Inductance-L	Sqrt(THD)	Desirability	
1	6.13	4.00	*85.41*	5.33	80.07	0.907	1.929	1.000	
2	5.20	1.87	*56.89*	0.01	80.17	0.903	1.928	1.000	
3	5.56	3.39	*56.00*	0.17	80.61	0.929	1.848	1.000	
4	4.11	2.38	*50.89*	0.03	81.99	0.904	1.919	1.000	Selected
5	6.04	3.66	*94.02*	3.25	80.33	0.909	1.919	1.000	
6	4.10	2.44	*79.62*	0.01	81.05	0.918	1.920	1.000	
7	5.86	3.99	*79.05*	2.12	99.93	0.904	1.927	1.000	
8	5.51	3.83	*75.35*	4.01	80.59	0.910	1.924	1.000	
9	5.97	3.99	*75.04*	3.61	86.77	0.911	1.921	1.000	
10	5.26	3.59	*60.10*	0.59	87.71	0.916	1.850	1.000	
11	6.02	3.98	*53.19*	4.16	84.08	0.905	1.920	1.000	
12	6.16	3.53	*77.32*	0.96	80.59	0.933	1.905	1.000	

Figure 4.11: Constraints and results of numerical optimization

If the ranges of the design factors are too limited, the constructed response surface may not reflect the whole operating space correctly. On the other hand, if the ranges of the design factors are too broad, the optimal points obtained from the constructed response surface may not have practical and feasible corresponding experiments. The selected optimal operating point in Figure 4.11 has a THD value of 3.68 while the minimal THD value in the raw experimental data is 3.72, even though they are obtained in different operating conditions. It indicates the coverage area of the starting data is quite suitable for this design.

The accuracy of the predictive model is checked by comparing the predicted value with

the simulated value at some randomly chosen experimental points. The results are presented in following Table 4.4.

Table 4.4: Point prediction and comparison

Factor and Response	Experimental Point					
	P_1	P_2	P_3	P_4	P_{Opt}	P_{Pra}
Outer Loop Gain, k_1	8.00	1.00	8.00	4.50	4.11	4.00
Inner Loop Gain, k_2	1.00	1.00	4.00	2.50	2.38	2.00
Carrier Freq of PWM, f_c (kHz)	100.00	100.00	50.00	100.00	50.89	50.00
LPF Resistance, R (ohm)	0.00	10.00	0.00	5.00	0.03	5.00
LPF Capacitance, C (μF)	80.00	320.00	320.00	200.00	81.99	40.00
LPF Inductance, L (mH)	0.90	0.90	3.60	2.25	0.90	0.45
Predicted Response *THD*	**4.95**	**24.27**	**38.98**	**11.46**	**3.68**	**4.12**
Simulated Response *THD*	**3.72**	**20.71**	**39.75**	**11.22**	**3.84**	**3.93**

In Table 4.4, P_1 to P_4 are randomly picked points where P_1 has the minimum simulated response value. P_{Opt} and P_{Pra} are the optimal point and the practical parameter used in the voltage and current compensation system, respectively. The comparison demonstrates the good fitness between the predicted values and the actual values, which verifies the predictive model is accurate and effective enough to be utilized to analyze the compensation system. Although the value of P_{Pra} is obtained from trial and error method, the fact that it is close to the theoretical optimal value confirms that the analysis in previous chapters is reasonable and well-founded.

4.3 Summary

The experiment of the three-phase VCS system was designed and analyzed to investigate the performance of the compensation system with the guidance of DOE method. Some diagnostic plots and data tables were presented to illustrate the interconnections and interactions among the design factors and response.

According to the analysis in Section 4.2, the capacitance and inductance are the most important parameters in this system while other parameters did not influence the response too much, with no consideration of their interactions. Especially, the carrier frequency of PWM in the selected range does not affect the response at all, including its interactions with other factors. Therefore, the capacitance and inductance of the output low-pass filter should be given more attention than other parameters in future design of different application cases and the carrier frequency of PWM might not be considered as an influential factor.

With consideration of the interactions, the interaction between the resistance and inductance contributes most to the response surface, although the resistance is not a significant single factor. The reason is that the resistance and inductance have to be adjusted simultaneously to perform the compensation while changing the resistance independently does not have any significant effect on the response. Similarly, the outer loop gain also plays an important role when taking into account its interactions with the

resistance and inductance. The possible reason is that the outer loop gain directly controls the feedback of the output signal that is critical to the compensation results.

With the aid of RSM, the influence of each factor on the response becomes more visual and graphic and the search for some specific points under varied operating conditions, such as the minimum value, would be more convenient and easier. Generally, DOE is an efficient tool to identify the contribution of design parameters and their interactions. The design criteria should be chosen carefully to avoid overbrimming the operating space.

Chapter 5
Conclusions and Scope for Future Work

5.1 Summary and Conclusions

The main objective of this research work was to develop a compensation approach that could effectively compensate for voltage distortion, current harmonics and source-end disturbances such as voltage sags, voltage swells and voltage flicker. The performance characteristics were determined and quantified using the total harmonic distortion (THD) of the compensated voltage at the PCC and source current. The use of a combination of the series APF and the shunt APF, termed the series-shunt APF, was identified as a cost effective solution to voltage distortion and current harmonics.

First off, the regeneration of the distorted voltage and the harmonic current is dependent on the effectiveness of the algorithm of extracting the harmonic components from the sensed signals, which are going to be used as the reference signals for the power inverter. The principle of the recurrent artificial neural network (RANN) was introduced and discussed. The harmonic extraction method based on the RANN was adopted and

demonstrated that the method is capable of determining the harmonic contents that may be present in load current, in either single-phase or three-phase system.

The quality and performance of the compensation system is also dependent on the fulfillment of the task of regenerating the replica of the estimated distorted voltage and harmonic current which could comprise highly non-sinusoidal signals in different magnitudes, phases and frequencies. The multi-loop feedback control scheme, first developed for use in the uninterruptible power supply (UPS) applications, was investigated to determine its suitability for use in active filtering applications. The following basic features of this scheme made it attractive for harmonic compensation. The inner current loop of the control scheme has been shown to provide a peak current limit in the capacitor of the output filter, hence limiting current surges at start up. It has also been shown to be capable of predicting and correcting near future variation in the output voltage, hence resulting in fast dynamic response in the inverter. The outer voltage loop ensures that the inverter output voltage is a replica of the reference. The original capacitor-based multi-loop feedback control scheme was extended to the inductor-based dual structure to satisfy the requirement of current harmonic compensation. It was shown that this control method is capable of:

- Generating non-sinusoidal voltages and currents for harmonic compensation in the line

- Generating sinusoidal voltages at the line frequency for injection into the main grid for compensation of voltage sags, voltage swells and voltage flicker

Having developed the harmonic extraction method and inverter control scheme for active filtering applications, three compensation topologies were investigated to verify the functionality of the system. The capacity of the compensation system to mitigate the harmonic and distortion caused by the operation of two kinds of nonlinear loads was the subject of the investigation. The considered complex nonlinear loads consisted of the current source type and voltage source type nonlinear load. The simulation results demonstrated that the voltage compensation scheme (VCS) utilizing the series APF was effective in minimizing the THD level of the line voltage and in maintaining the voltage at the PCC almost sinusoidal. Meanwhile, the current compensation scheme (CCS) employing the shunt APF was capable of supplying a low-impedance harmonic component bypass for the nonlinear loads and of keeping the source current from being contaminated. The whole series-shunt compensation system which combines the VCS and the CCS together was proven to be effective and efficient in compensating for the voltage at the PCC and the source current simultaneously with the simple or complex nonlinear loads.

The effects of harmonic order and sampling frequency on the performance of the series-shunt compensation system were investigated. The higher harmonic order estimation in

the RANN and the smaller sampling time can lead to better harmonic extraction results and less errors. However the issue of computation workload of the RANN method with respect to harmonic order and sampling frequency needs further investigation.

Due to the inherent limitations of the algorithm, the VCS and CCS are unable to sufficiently compensate for the relevant voltages and currents under the source-end disturbances such as voltage sags, voltage swells and voltage flicker. The preprocessing unit was then introduced into the whole compensation system to solve the problems caused by the abnormal source conditions such as voltage imbalance and voltage distortion. The tuning-free pretreating unit is capable of compensating for any type of source-end distortions to any desired extent before the source voltages are applied into the main grid. The abnormal operation of the system is switched into the normal operation with the aid of this unit and the fast dynamic response would not have any visible influence upon the subsequent voltage and current compensation procedure.

With the aid of response surface method (RSM), the experiment of the three-phase VCS system was designed and analyzed to investigate the performance of the compensation system with the guidance of design of experiments (DOE) method. The interconnections and interactions among the design factors and response shown in diagnostic plots and data tables illustrated that the capacitance and inductance of the output low-pass filter should be paid more attention than other parameters in future design of different

application cases and the carrier frequency of PWM might not be considered as an influential factor. The resistance and the outer loop gain are also important roles when taking into account their interactions with the inductance and resistance, respectively.

The contribution of this work can be summarized as follows:

- An investigation of the performance of the compensation system that incorporates voltage compensation and harmonic isolation together in both single-phase and three-phase systems in the case of voltage imbalance and more complicated non-linear loads. This is significant because it allows the designers to make an informed choice regarding the type of compensation system depending on the loads in the system.
- An investigation of the influence of the controlling parameters such as inverter controller gains and low-pass filter specification on the performance of the overall system using the response surface method (RSM). This is also necessary since it make the search of some specific points under varied operating conditions, such as the minimum value, more convenient and easier.
- The development of a reliable and high efficient harmonic extraction scheme that provides an accurate measure of the harmonics in the presence of source-end disturbances. It eliminates the need for complicated extraction circuits and long computation time.

- An investigation of the decoupled voltage and current compensation processes that adopt the modified multi-loop feedback control strategy. A preprocessing unit was introduced to solve the problems caused by the abnormal source-end conditions.

The applications of active power filters including the current harmonic compensator, the cancellation of zero-sequence current and the static VAR compensator have been widely exploited and developed in power industry. The high demand in industry stimulates the emergence of some novel methods and technologies applied in the active power filters. The proposed schemes may not be very easy to implement but generates knowledge on the possible application of active power filters.

5.2 Scope for Future Work

The effectiveness of any compensation system depends upon the capability of the harmonic extraction subsystem which is utilized to accurately estimate the harmonics. The control scheme used here is the RANN based method which works well in the case of single-phase system and unbalanced system with the aid of preprocessing unit. However, the presence of high order harmonics in the distorted signals would require much more complicated circuit structure and much longer computation time, which greatly deteriorate the real-time compensation. Simplification of the harmonic extraction scheme and integration of the preprocessing unit into the strategy, without compromising its desired features, will be a worthwhile challenge.

The active power filtering is essentially a task of nonlinear control application. It may be advantageous to investigate other nonlinear control methods, such as one-cycle method and fuzzy logic based controllers, for power inverter operation.

Since the compensation is dependent on the filter response in the control path and sensor gains, it is important to track and compensate any filter nonlinearities, low-pass output filter parameter variations or sensor gain variations. A combination of feedback and feedforward approach with an adaptive compensation scheme can account for load fluctuations and time varying parameters.

An experimental verification of the control method and the compensation system in this work is recommended.

References

[1] Product Data Bulletin, Power System Harmonics: Causes and Effects of Variable Frequency Drives Relative to the IEEE 519-1992 Standard, Schneider Electric Corporate, 1994.

[2]. IEEE Standard 519-1992, IEEE Recommended Practices and Requirements for Harmonic Control in Electrical Power Systems, New York, NY, IEEE. 1993.

[3]. IEEE Standard 1159-1995, IEEE Recommended Practice for Monitoring Electric Power Quality, New York, NY, IEEE. 1995.

[4]. IEEE Standard 1453-2004, IEEE Recommended Practice for Measurement and Limits of Voltage Fluctuation and Associated Light Flicker on AC Power Systems, New York, NY, IEEE. 2005.

[5] T. Jauch, A. Kara, R. Mohamed, and D. Westermann, "Power quality ensured by dynamic voltage restoration," ABB Review 4, pp. 25-36, May 1998

[6] J. Alfonso, C. Couto, and J. Martins, "Active filters with control based on the p-q theory," IEEE Industrial Electronics Society Newsletter, vol. 47, pp. 5-10, Sept 2000.

[7] H. Akagi, A. Kanazawa, and A. Nabae, "Instantaneous reactive power compensation comprising switching devices without energy storage elements," IEEE Transactions on Industry Applications, vol. IA-20, pp. 625-630, May/June 1984.

[8] B. Singh, K. Al-Haddad and A. Chandra, "A review of active filters for power quality improvement," IEEE Transactions on Industrial Electronics, vol. 46, no. 5, pp. 960-971, Oct 1999.

[9] F. Z. Peng, "Harmonic sources and filtering approaches," IEEE Industry Applications Magazine, vol. 7, no. 4, pp. 18-25, July/Aug. 2001.

[10] T. Wunderlin, O. Amhof, P. Dahler and H. Gunning, "Power supply quality improvement with a dynamic voltage restorer (DVR)," in IEEE International Conference on Energy Management and Power Delivery, Singapore, pp. 518-525, March 1998.

[11] F. Z. Peng, H. Akagi and A. Nabae, "A new approach to harmonic compensation in power system – A combined system of shunt passive and series active filters," IEEE Transactions on Industry Applications, vol. 26, pp. 983-990, Nov. 1990.

[12] C. Hochgraf and R. H. Lasseter, "Statcom controls for operation with unbalanced voltages," IEEE Transactions on Power Delivery, vol. 13, no. 2, pp. 538-544, April 1998.

[13] H. Fujita and H. Akagi, "The unified power quality conditioner: the integration of

series and shunt active filters," IEEE Transactions on Power Electronics, vol.13, no. 2, pp. 315-322, March 1998

[14] H. Akagi and H. Fujita, "A new power line conditioner for harmonic compensation in power systems," IEEE Transactions on Power Delivery, vol. 10, no. 3, pp. 1570-1575, July 1995.

[15] M. Aredes, K. Heuman and E. H. Watanabe, "A universal active power line conditioner," IEEE Transactions on Power Delivery, vol. 13, no. 2, pp. 545-551, April 1998.

[16] H. Fujita, Y. Watanabe and H. Akagi, "Control and analysis of unified power flow controller," in Proceedings of the 29th annual IEEE Power Electronics Specialists Conference (PESC), Fukuoka, Japan, vol. 1, pp. 805-811, May 17-22, 1998

[17] W. M. Grady, M. J. Samotyj and A. H. Noyola, "Minimizing network harmonic voltage distortion with an active power line conditioner," IEEE Transactions on Power Delivery, vol. 6, no. 4, pp. 1690-1697, Oct. 1991.

[18] S. Mariethoz and A. C. Rufer, "Open loop and closed loop spectral frequency active filtering," IEEE Transactions on Power Electronics, vol. 17, no. 4, pp. 564-573, July 2002.

[19] A. Ametani, "Harmonic reduction in thyristor converters by harmonic current injection," IEEE Transactions on Power Apparatus and Systems, vol. 95, no. 2, pp. 441-449, Mar. 1976.

[20] S. Bhattacharya and D. Divan, "Synchronous frame based controller implementation for a hybrid series active filter system," in Proceedings of the 30th annual IEEE Industry Applications Conference (IAS), Orlando, Florida, vol. 3, pp. 2531-2540, Oct. 8-12, 1995.

[21] K. Karthik, "An improved control strategy for a hybrid series compensator," Master of Engineering thesis, Memorial University of Newfoundland, July 2001.

[22] R. Wei and Z. Li, "Approach of dynamic detecting harmonics and fundamental reactive current," in Proceedings of the International Conference of Electrical Engineering (ICEE), Hong Kong, C1-01, pp. 1-4, 1999.

[23] D. Gao and X. Sun, "Detecting approach of current based on neural network for single-phase active power filters," in Proceedings of the International Conference of Electrical Engineering (ICEE), pp. 540-543, July 2000.

[24] K. Tazune, T. Aoki, Y. Nozaki, Y. Kuwata and T. Koyashiki, "Harmonic current suppression in an interconnection inverter by using a neural network," in proceedings of the International Power Electronics Conference (IPEC), Yokohama, Japan, pp. 1260-1265, April 1995.

[25] S. D. Round and N. Mohan, "Comparison of frequency and time domain neural network controllers for an active power filter," in Proceedings of the IEEE Industrial Electronics, Control and Instrumentation Conference (IECON), Maui, Hawaii, vol. 2, pp. 1099-1104, Nov. 15-19, 1993.

[26] M. Rukonuzzaman and M. Nakaoka, "An advanced active power filter with adaptive neural network based harmonic detection scheme," in Proceedings of the 32nd annual IEEE Power Electronics Specialists Conference (PESC), Vancouver, British Columbia, vol. 3, pp. 1602-1607, June 17-21, 2001.

[27] M. Rukonuzzaman, K. Nishida and M. Nakaoka, "DSP control shunt APF with harmonic extraction by adaptive neural network," in Proceedings of the 38th annual IEEE Industry Applications Conference (IAS), Salt Lake City, Utah, vol. 2, pp. 1215-1221, Oct. 12-16, 2003.

[28] N. M. Abdel-Rahim and J. E. Quaicoe, "Analysis and design of a multiple feedback loop control strategy for single-phase voltage-source UPS inverters," IEEE Transactions on Power Electronics, vol. 11, no. 4, pp. 532-541, July 1996.

[29] O. Okogun, "A comparative study of hybrid compensation systems using a multiple feedback control scheme," Master of Engineering thesis, Memorial University of Newfoundland, Dec. 2002.

[30] M. Norgaard, O. Ravn, N. K. Poulsen and L. K. Hansen, Neural Networks for Modelling and Control of Dynamic Systems, London, Springer-Verlag, 2000.

[31] S. Osowski, "Neural network for estimation of harmonic components in a power system," IEE Proceedings C Generation, Transmission and Distribution, vol. 139, no. 2, pp. 129-135, Mar. 1992.

[32] B. Widrow and S. Stearns, Adaptive Signal Processing. Englewood Cliffs, New Jersey, Prentice Hall, 1985.

[33] M. P. Kennedy and L. O. Chua, "Neural networks for nonlinear programming," IEEE Transactions on Circuits and Systems, vol. 35, no. 5, pp. 554–562, May 1988.

[34] D. Tank and J. Hopfield, "Simple 'neural' optimization networks: An A/D converter, signal decision circuit, and a linear programming circuit," IEEE Trans. Circuits and Systems, vol. 33, no. 5, pp. 533–541, May 1986.

[35] D. C. Montgomery, Design and Analysis of Experiments, New York, John Wiley & Sons, Inc., 1997.

[36] Stat-Ease, Inc., Design-Expert version 7.0.0, Minneapolis, Minnesota, 2005.

[37] R. H. Myers, Response Surface Methodology, New York, John Wiley & Sons, Inc., 2002.

Appendix A
Simulink Models

A.1 Overall System

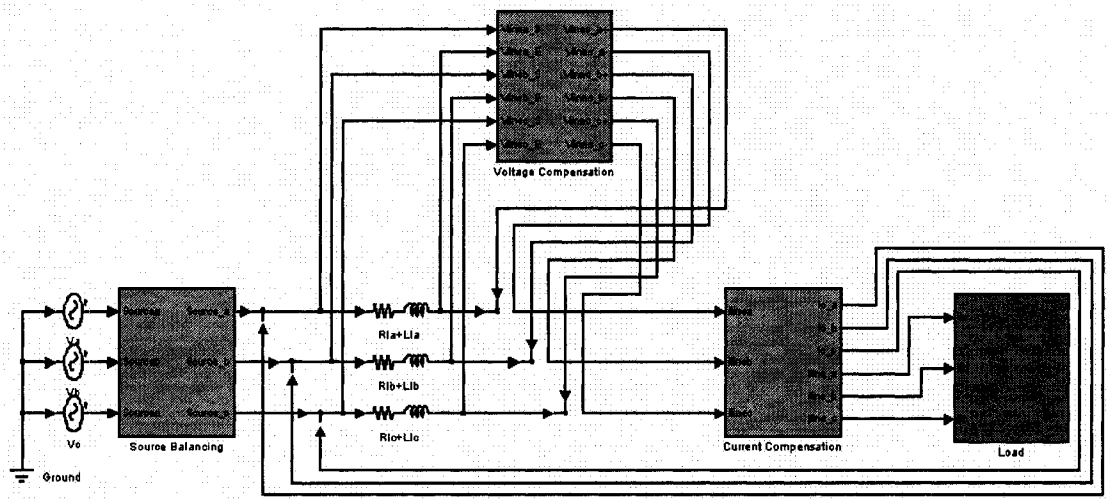

Figure A.1: Overall System

A.2 Power Supply

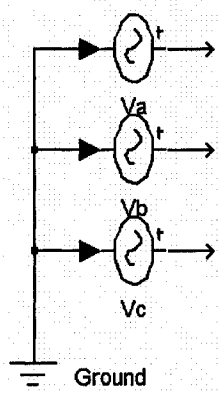

Figure A.2: Power supply without preprocessing unit

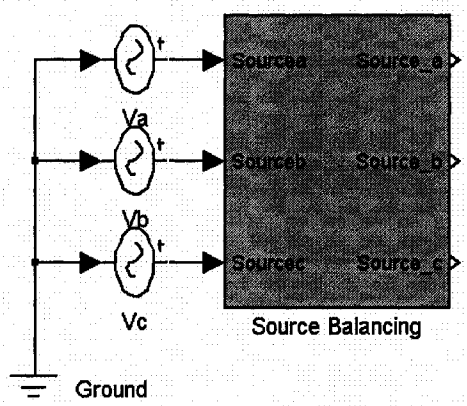

Figure A.3: Power supply with preprocessing unit

A.3 RANN Harmonic Extraction Unit

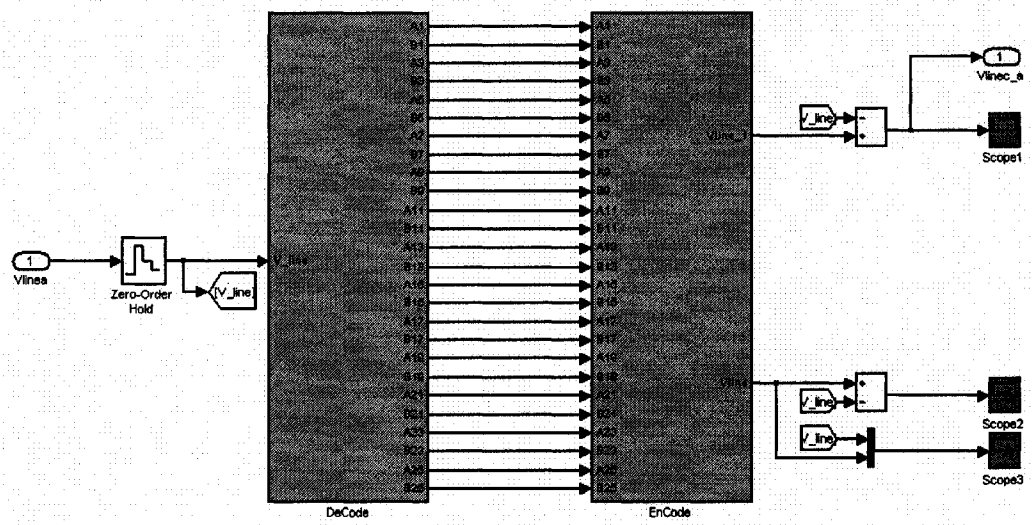

Figure A.4: Harmonic Extraction Unit

A.4 Active Power Filter Unit

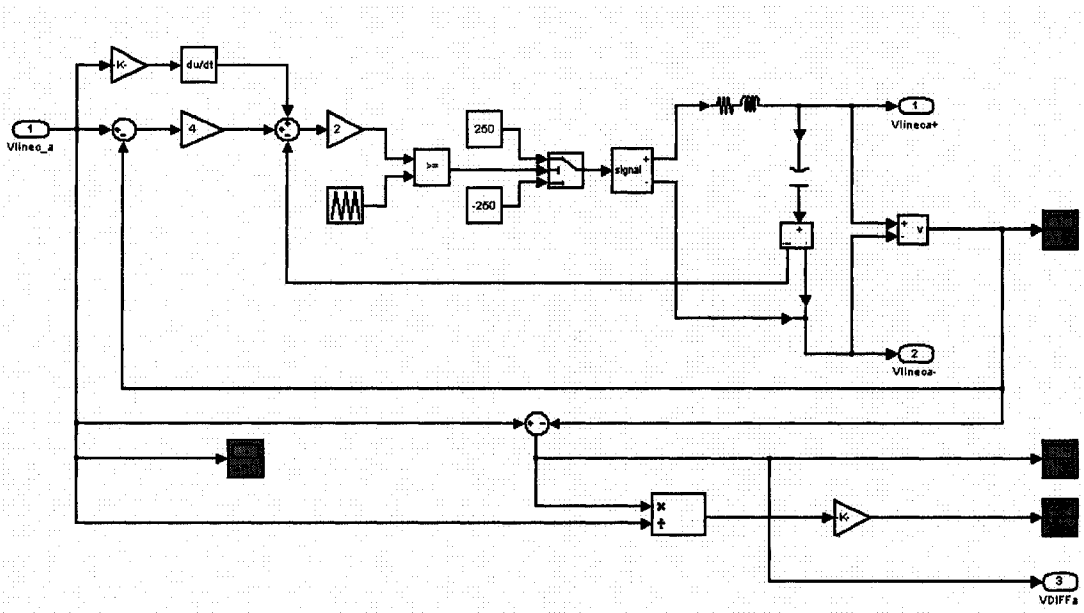

Figure A.5: Capacitor based active power filter

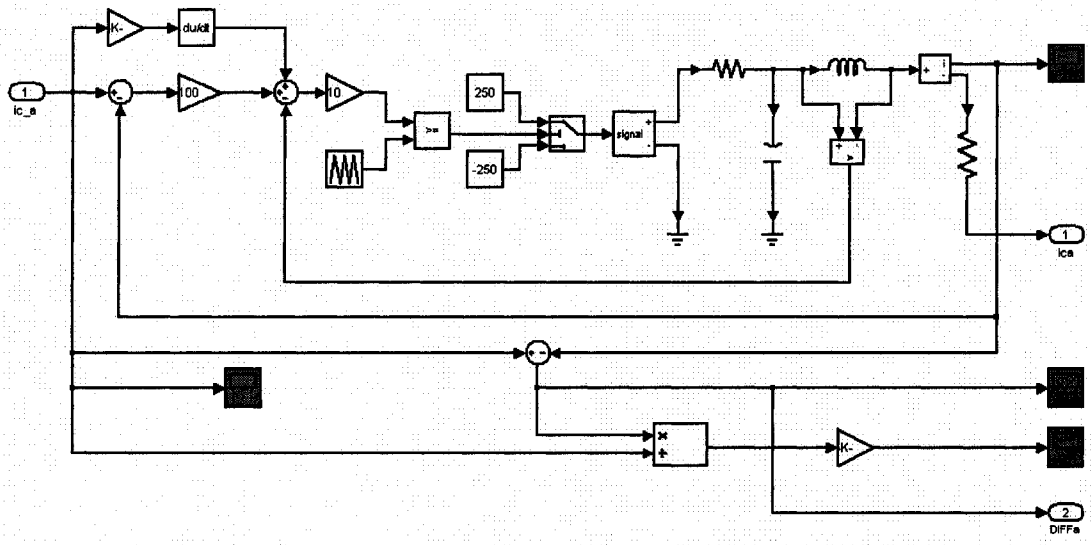

Figure A.6: Inductor based active power filter

A.5 Load Unit

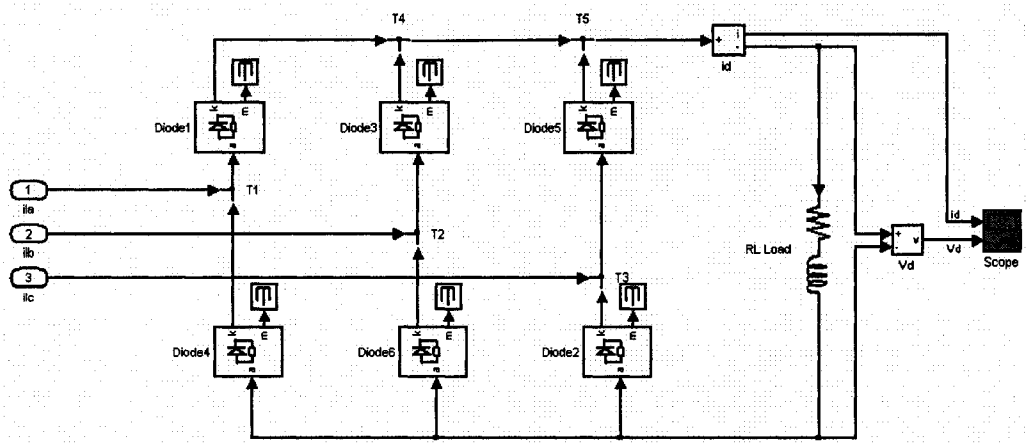

Figure A.7: Simple load

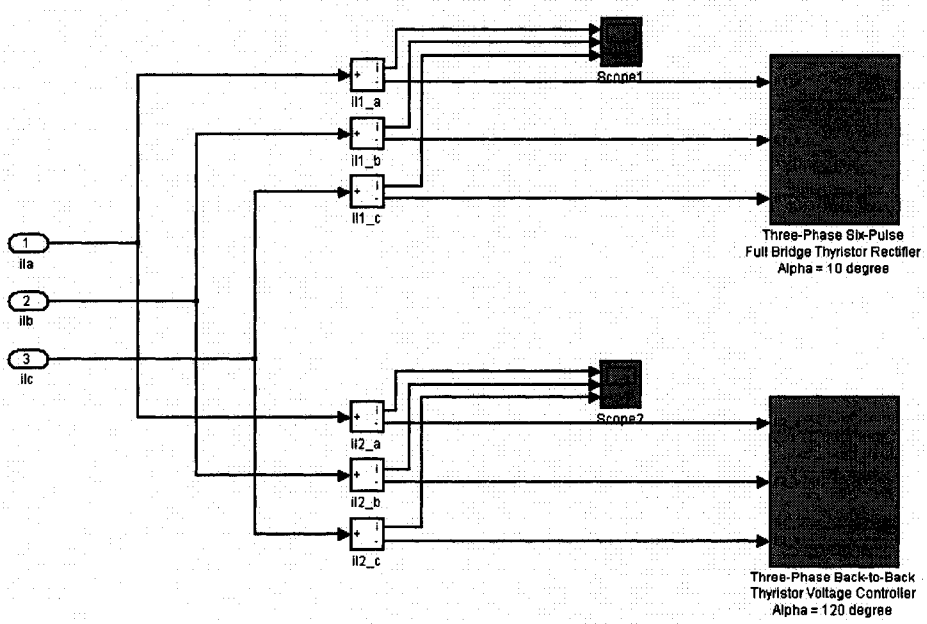

Figure A.8: Complex load

Appendix B
MATLAB Codes

B.1 MATLAB Codes for Harmonic Components Analysis

```
% This function returns the magnitude and frequency of each sinusoidal
% component which constitutes the signal s. Ts is the sampling time of FFT
% analysis.
function [ Mag, Freq ] = FFTAna( s , Ts )
MFFT = fft( s );
N = length( s );
% Judge if N is an even number
if ( fix( N/2 ) - N/2 ) < 0;
   N = N - 1;
else
   N = N;
```

```
end

% Use the first N/2+1 points to calculate the frequencies. (The other N/2-1

% points are redundant.)

Mag = abs( MFFT );

L = N/2 + 1;

Mag = Mag( 1 : L );

Freq = ( 0 : 1 : N/2 ) / ( N * Ts );
```

B.2 MATLAB Codes for Frequency Spectra Calculation

```
% This program reads the data loaded into the workspace and calculates the

% frequency spectra of the fundamental and each harmonic component of the

% signal s by calling the function FFTAna. It will computes the total

% harmonic distortion (THD) as well and plot them respectively.

clear all

clc

% This is the general version and can be appied into either voltage or

% current calculation.

load Signal.mat
```

```
Ts = 1e-5;

LN = length( Signal );

[ Sig , F ] = FFTAna( Signal , Ts );

Sig = Sig * 2 / LN;

FOrder = F / 60;

plot( FOrder , Sig );

% Calculate the THD level according to the definition

THD = 0;

for k = 109 : 72 : 5000

   THD = THD + Sig( k ) .^ 2;

end

THD = sqrt( THD ) / Sig( 37 );
```